

**Modelling changes in climate due to
enhanced CO₂, the role of atmospheric
dynamics, cloud and moisture.**

by

**C. A. Senior, J. F. B. Mitchell, H. Le Treut
and Z-X Li**

CRTN 13

July 1991

**CLIMATE
RESEARCH
TECHNICAL
NOTE**

**Hadley Centre
Meteorological Office
London Road
Bracknell
Berkshire RG12 2SY**

CLIMATE RESEARCH TECHNICAL NOTE NO. 13

MODELLING CHANGES IN CLIMATE DUE TO ENHANCED CO₂.
THE ROLE OF ATMOSPHERIC DYNAMICS, CLOUD AND MOISTURE

by

C A SENIOR, J F B MITCHELL, H LE TREUT AND Z-X LI

Hadley Centre for Climate Prediction and Research
Meteorological Office
London Road
Bracknell
Berkshire RG12 2SY
U. K.

NOTE: This paper has not been published. Permission to quote from it should be obtained from the Director of the Hadley Centre.

Final Report of CEC contract EVHC 0040 UK(H)

Modelling Changes in Climate due to enhanced CO₂, the role of atmospheric dynamics, cloud and moisture.

C A Senior^{*}, J F B Mitchell^{*}, H Le Treut⁺ and Z-X Li⁺

* At the Hadley Centre for Climate Prediction and Research,
Meteorological Office, Bracknell, Berkshire, U.K.

+ At Laboratoire de Meteorologie Dynamique du CRNS
24 rue Lhomond; 75231 Paris cedex 05; France.

CONTENTS

1. Introduction
2. CO₂ and Climate : The impact of cloud parametrization
3. A Comparison of the simulation of cloud and radiation in four versions of the UKMO model and the LMD model
4. The Impact of resolution on the simulation of cloud and radiation
5. Summary and Conclusions

CHAPTER 1

INTRODUCTION

BY

J F B MITCHELL

Introduction

This report describes research carried out under CEC contract EVHC 0040 UK(H) on the role of atmospheric dynamics, cloud and moisture in simulated changes in climate due to increased atmospheric CO_2 .

The full contract includes research on the effect of changes in water vapour on atmospheric dynamics carried out at the Department of Meteorology, University of Reading under Prof. B. J. Hoskins and on sensitivity experiments carried out at the Laboratoire de Meteorologie Dynamique (LMD), Ecole Normale Supérieure under Dr H. Le Treut. This work is reported elsewhere.

Here, we report on sensitivity experiments carried out using versions of the U.K Meteorological Office's Climate model and comparisons with similar work at LMD. The sensitivity experiments, carried out using a low resolution version of the Meteorological Office's Atmospheric General Circulation Model coupled to a static 50m mixed layer ocean are described in the following section. Four different cloud parametrizations were employed. The effect on the earth's radiation budget and on the sensitivity of climate to doubling atmospheric carbon dioxide have been assessed.

In the third section, the Meteorological Office experiments are compared with experiments carried out at LMD and the differences in the responses are explained in terms of differences in the model formulations.

The model's sensitivity to increased carbon dioxide concentrations turns out to be strongly dependent on the particular cloud parametrization used. Hence research has concentrated on validating the cloud schemes used here and explaining their effect on climate sensitivity. In particular, a further control and anomaly experiment were carried out using a revised cloud ice parametrization. The extension of this work has replaced an earlier intention to investigate the sensitivity of climate to changes in effective cloud droplet radius.

In the Fourth section, the impact of a change in horizontal resolution on the climate and climate sensitivity of one version of the UKMO GCM has been assessed. Changes in sensitivity are small compared to those found between models with different cloud parametrizations.

CHAPTER 2

CO₂ AND CLIMATE: THE IMPACT OF CLOUD PARAMETRIZATION

BY

C A SENIOR AND J F B MITCHELL

Abstract

The importance of the representation of cloud in a General Circulation Model (GCM) is investigated by utilising four different parametrization schemes for layer cloud in a low resolution version of the General Circulation Model at the Hadley Centre for Climate Prediction and Research at the United Kingdom Meteorological Office (UKMO). The performance of each version of the model in terms of cloud and radiation is assessed in relation to satellite data from the Earth Radiation Budget Experiment (ERBE). Schemes which include a prognostic cloud water variable show some improvement on those with relative humidity dependent cloud, but all still show marked differences from the ERBE data. The sensitivity of each of the versions of the model to a doubling of atmospheric CO_2 is investigated. Mid and lower level clouds decrease when cloud is dependent on relative humidity and this constitutes a strong positive feedback. However, when interactive cloud water is included this effect is almost entirely compensated for by a negative feedback from the change of phase of cloud water from ice to water. Additional negative feedbacks are found when interactive radiative properties of cloud are included and these lead to an overall negative cloud feedback. The global warming produced with the four models then ranges from 5.4° with a relative humidity scheme to 1.9° with interactive cloud water and radiative properties.

1. Introduction

One of the greatest uncertainties in the study of climate change is the effect of changes in cloud. Clouds regulate the radiative heating of the earth. The presence of cloud increases the planetary albedo and reflects incoming solar radiation, cooling the climate. Clouds also trap outgoing longwave radiation emitted from a relatively warm earth and then re-emit at a colder cloud top temperature reducing the amount of longwave radiation lost to space and warming the climate (the 'greenhouse' effect of cloud). The net effect of cloud has long been uncertain because the two effects are present to a different degree in different types of cloud.

There is a lack of observational data on the extent to which clouds affect the radiation balance of the Earth and this has hindered the development of realistic cloud parametrizations. Early studies with radiative-convective models (eg. Manabe and Wetherald 1967, Schneider 1972) indicate that low cloud cools climate because of its high albedo and relatively warm cloud top temperature. High cloud has a lower albedo and a lower cloud top temperature suggesting that it may warm the earth/atmosphere system. Recent results from satellite data suggest that the net global mean effect from all types of cloud is a cooling of the atmosphere by around $10\text{--}20\text{ Wm}^{-2}$ (Ramanathan et al 1989a). This consists of a cooling due to the reflection of shortwave radiation of $40\text{ to }50\text{ Wm}^{-2}$ and a longwave warming of around 30 Wm^{-2} . The estimated net radiative effect of cloud is thus several times the radiative forcing on doubling CO_2 (about 4 Wm^{-2}) and the longwave and shortwave components are ten times as large. This highlights the potential importance of small changes in cloud for climate change.

Estimates of the sensitivity of climate to doubled CO_2 have ranged from 1.7 K to 5.2 K in different models (see for example Schlesinger and Mitchell 1987, Mitchell et al 1989), much of the difference being related to the simulation of clouds (Cess et al 1990). Early general circulation models used for predicting climate change included fixed cloud amounts estimated from climatology. This allows no scope for changes in cloud that may be forced by a climate perturbation and any feedback these changes may cause on the simulated climate change. The variability of the simulated present day climate and the effect of the diurnal cycle may also be affected. More

recently interactive cloud parametrization schemes have been employed in which cloud is made dependent on relative humidity (eg. Hansen et al 1984, Wilson and Mitchell 1987, Wetherald and Manabe 1986). Although this method includes some of the possible sources of cloud feedback that have been identified, for example changes in cloud amount and height (Wetherald and Manabe 1988), it excludes others such as changes in the radiative properties of cloud (Somerville and Remer 1984, Roeckner et al 1987).

More recent cloud parametrization schemes include a prognostic cloud water variable (e.g. Sundqvist 1978, Smith 1990, Le Treut and LI 1988, Roeckner et al 1987). This allows the radiative properties of cloud to be made dependent on the predicted cloud water path and so includes this further possible source of feedback. Although the later cloud schemes are more detailed, they are not necessarily more accurate and in particular the representation of precipitation and its effect on cloud amount is still uncertain.

In order to study the effect of cloud parametrization schemes on climate sensitivity we have run a version of the United Kingdom Meteorological Office (UKMO) Atmospheric General Circulation Model (AGCM) with four different cloud schemes. In each case a further integration was performed with the same version of the model including doubled CO_2 amounts. The resultant range of warmings on increasing CO_2 indicate the differences in the sign and magnitude of the feedbacks due to cloud. The preliminary results from these experiments have been discussed by Mitchell et al (1989). This paper gives a fuller description of the experiments including a comparison with observational data and a detailed analysis of the cloud feedbacks.

In Section 2 the models, their simulation of present day cloud and radiation fields and the $2 \times \text{CO}_2$ experiments are described. In section 3 the results from the doubled CO_2 experiments are discussed. In section 4 a quantitative evaluation of the climate sensitivity is performed and in section 5 the main conclusions are presented and discussed.

2.1 Model description

The basic model used is a version of the United Kingdom Meteorological Office (UKMO) Atmospheric General Circulation Model (AGCM) coupled to a 50m oceanic mixed layer and a thermodynamic sea-ice model (Wilson and Mitchell

1987). Modifications to the AGCM as described by Mitchell and Warrilow (1987) were included. The AGCM has 11 irregularly spaced levels in the vertical and a horizontal resolution of $5^\circ \times 7.5^\circ$ latitude/longitude. The primitive equations are solved on σ (= pressure/surface pressure) surfaces using a centred finite-difference scheme with a twenty minute time step. The seasonal and diurnal variations of solar radiation are represented and radiative fluxes are calculated every three hours and depend on concentrations of water vapour, CO_2 and ozone, and on temperature and cloud. The longwave fluxes are calculated from an emissivity scheme (Slingo and Wilderspin 1986). A penetrative convection scheme (Gregory and Rowntree 1990) is employed in all the experiments and deep convective cloud amounts are derived from the mass flux calculated in the convection scheme. The reflectivity, transmissivity and longwave emissivity of convective cloud are prescribed as 0.6, 0.3 and 1.0 respectively. The layer cloud schemes used in the four experiments are outlined below. In all the schemes layer cloud is divided into three categories, low, medium and high. Low cloud can occur in the bottom three layers, medium cloud in the next three and high cloud in the next four. Cloud cannot exist in the top layer, the highest cloud occurring at around 60mb. At any one time cloud of a particular category can only exist in one of its layers and this is taken to be the one in which the most cloud is predicted.

(a) Relative Humidity scheme (RH)

The relative humidity scheme (henceforth referred to as RH) used is described in detail by Mitchell and Ingram (1990). The scheme predicts the fractional amount of layer cloud C using a quadratic dependence on the relative humidity (R);

$$\begin{aligned} C &= ((R - R_C)/(100 - R_C))^2 & \text{where } R > R_C \\ &= 0 & \text{where } R < R_C \end{aligned} \quad (1)$$

Cloud amount increases from zero at the threshold level, R_C to full cover at saturation. The threshold is set at 90% except for high cloud (the four layers next to the top) and the layer closest to the surface. For these cloud cover is total at saturation and zero otherwise. The global mean total cloud cover is around 50%. The radiative properties of cloud are fixed and

are given in Table 1. In this scheme the parametrization of non-convective precipitation is separate from the diagnosis of cloud. Supersaturation, which arises from several dynamical and physical processes, is removed to form precipitation.

(b). Cloud Water scheme (CW)

The Cloud Water scheme (henceforth referred to as CW) is that described by Smith (1990). In this scheme a new model variable, the cloud water content q_C , is introduced such that

$$q_T = q + q_C \quad (2)$$

where q_T and q are the total water content and the specific humidity respectively. Strictly q_C has two components q_L , the cloud liquid water content and q_F the cloud ice content. However in this scheme this distinction is made only for the purposes of precipitation. q_T is increased by convergence of water vapour due to large scale advection or convection and by evaporation of precipitation and is reduced by precipitation. Horizontal transport of q_C is ignored. A liquid water temperature T_L is defined as

$$T_L = T - (L_C/C_P)q_L - ((L_C + L_F)/C_P)q_F \quad (3)$$

where T is the temperature, L_C and L_F are the latent heats of condensation and fusion and C_P is the specific heat of air. T_L and q_T are conserved in the presence of condensation or evaporation of cloud. Within any grid box, T_L and q_T are assumed to have a prescribed statistical distribution about their mean value. Within grid box values of q_T in the distribution above saturation are assumed to correspond to saturated air with the excess present as cloud water and ice.

In the parametrization of precipitation, the relative fractions of liquid and ice water content are calculated as functions of temperature between 0°C and -15°C . Above 0°C all cloud water is liquid and below -15°C all cloud water is ice. For cloud liquid water the rate of precipitation is given by;

$$(\dot{q}_L)_P = [C_T \{1 - \exp(-(q_L/C)/C_W)^2\} + C_A P] q_L \quad (4)$$

where C_T , C_W and C_A are constants and C is the cloud amount. In real clouds, water will condense onto virtually any particle that is water soluble and many that are not and almost all such particles are activated at once on reaching saturation. There are large numbers of available cloud condensation nuclei (CCN) and hence condensation is spread over a great number of droplets. Consequently almost all the droplets are too small to achieve an appreciable fall speed. Precipitation, therefore, does not occur until the droplets are large enough to fall and grow through collision and coalescence (eg. Pruppacher and Klett 1978). This process is represented in the cloud scheme by the inclusion of the exponential term in (4), which acts to limit the formation of precipitation when the cloud water content is small. The second term, $C_A P$, allows for the seeding of cloud by precipitation, P , falling through the cloud from the layer above, but this is generally small in the model.

The precipitation of cloud ice from cloud is more efficient than for cloud water. In ice clouds relatively few CCN act as ice condensation nuclei (ICN) (Heymsfield and Sabin 1989, Darlison 1990). Ice particle formation occurs by condensation on particles of suitable crystal structure and usually only begins around saturation with respect to water although, once started, it continues until supersaturation with respect to ice has been removed. Saturation with respect to ice occurs sooner than with respect to water at temperatures below 0°C (the basis of the Bergeron-Findeisen process) and the difference is greatest at -12°C . More importantly, the degree of supersaturation at which ICN become active varies and so the first few droplets to freeze will absorb all the available water preventing others from forming. The activation of so few ICN in ice clouds means that the available water is spread over fewer particles which on average grow to be bigger than water droplets with each one achieving a significant fall speed. As a result ice clouds precipitate more efficiently than water clouds. Sundqvist (1978) represented this process by making C_T , in (4), a function of temperature. In CW a different approach is taken. The rate of precipitation of ice cloud, q_F is given by

$$\dot{q}_F = q_F (V_F / \Delta Z) \quad (5)$$

where V_F is the ice water fall speed, assumed to be a constant 1 ms^{-1} , and

ΔZ is the layer thickness. This implies that ice particles will begin to precipitate as soon as they form with a terminal velocity V_F . For typical values of ice and liquid water contents, q_F and q_L , the simulated dissipation of ice cloud is about an order of magnitude more efficient than that of water cloud. In CW the radiative properties of cloud are still fixed but the values used were derived from a run of the model with interactive radiative properties, as described at (d) below, and are given in Table 2. The radiative effects of both ice and water precipitation below the layers of formation are ignored.

The scheme is representing an ensemble of clouds within a grid box which may be of different phase. It is not attempting to model true mixed-phase clouds. Although the model does not represent the complex mixed phase microphysical processes explicitly, it effectively includes one of the most important aspects, the rapid conversion of water to ice (Mason 1957).

(c). Cloud water scheme including the Heymsfield formula (CWH)

The assumption of a constant fall speed of 1 ms^{-1} for all ice cloud is an over-simplification of the wide range of ice cloud particle shapes and associated fall speeds. This implies that the dissipation of ice cloud is the same at all levels in the atmosphere. Heymsfield (1977) calculates an empirical formula for the precipitation rate of ice cloud as a function of ice water content as;

$$R = 3.6 \times (\text{IWC})^{1.17} \quad (6)$$

where R is the precipitation rate in mm hour^{-1} and IWC is the ice water content in gm^{-2} . This gives a terminal fall speed of ice, V_F , of:

$$V_F = 3.23 \times (\rho \times q_F)^{0.17} \quad (7)$$

where V_F is the terminal fall speed of ice in ms^{-1} , ρ is the air density in gm^{-3} and q_F is the frozen water mass mixing ratio. For typical IWC's this gives fall speeds of 0.2 ms^{-1} for ice clouds near the tropical tropopause and 0.7 ms^{-1} for ice cloud near the freezing level.

This formula has been incorporated into the cloud water scheme described above to give an observationally based parametrization of ice fall speed in

the cloud scheme. This version of the model is henceforth referred to as CWH.

(d). Cloud water scheme with interactive radiative properties (CWRP)

The cloud water scheme (CW) was extended to include a parametrization of the radiative properties of cloud dependent on the cloud water content (The experiment will henceforth be referred to as CWRP). Fits of shortwave albedo, transmissivity and absorptivity as rational functions of the cloud water path and solar zenith angle were made to the scheme of Liou and Wittman (1979) (Figure 1) and are given in Appendix A.

The longwave emissivity ϵ was given by

$$\epsilon = (1 - \exp(-xq)) \quad (8)$$

where q is the condensed water path and $x = 0.13 \text{ m}^2 \text{ g}^{-1}$ for water cloud (Stephens 1978) and $0.065 \text{ m}^2 \text{ g}^{-1}$ for ice cloud.

The scheme including interactive optical properties was run with a 1 ms^{-1} ice fall speed as in CW and not with the Heymsfield formula as in CWH.

2.2 Model simulations of present day climate.

An important requirement for all AGCM's is the adequate simulation of present day climate. This section will briefly describe the simulation of relevant quantities from the control integrations of each version of the model. A comparison of the simulated cloud amount and radiation budget in RH, CW, CWH and CWRP and from satellite data (Ramanathan et al 1989a,b) is presented. For brevity, only July simulations are shown and discussed, although seasonal differences are described where necessary.

(a). Cloud

All the models show broadly similar total cloud amounts. The spatial patterns of total cloud cover are very similar in the cloud water models and so CWH and CWRP are not shown. In July (Figure 2), there are maxima in cloud in the tropics, being mostly high cloud in areas of deep convection, and at

high latitudes. Cloud amounts of greater than 70% occur over the Southern Hemisphere storm track in each model and over the north Atlantic storm track in CW. Cloud cover greater than 50 % persists across both poles in both models. Cross sections of total stratiform cloud for all the models show too little cloud below about 400 mb in the tropics of the cloud water models (Figure 3), when compared to a surface based climatology (Warren et al 1986,1988).

In addition, the simulations with the cloud water schemes have areas of persistent cloud off the coasts of California and the west coasts of South America and southern Africa, these being especially noticeable in July (Figure 2). The north Pacific cloud area is well positioned, those in the Southern Hemisphere are less so. The improvement in the simulation of these areas of cloud over that in RH is due to the improved treatment of boundary layer mixing (Smith 1990). In the cloud water models there is somewhat too much cloud over northern Canada and parts of northern Eurasia (Figure 2(b)).

High latitude winter cloud amounts are greater in RH and CWH than in CW or CWRP (Figure 3). In RH most of the area poleward of 45° S has 70 % or more total cloud coverage (Figure 2(a)), greater than that shown in CW (Figure 2(b)). RH does not distinguish between water and ice cloud. This omission tends to produce persistent cloud in cold regions which would have precipitated faster in the cloud water schemes. In CWH the dissipation of ice cloud increases with IWC. Smith (1990) found, on average, a monotonic relationship between water content and temperature in his model at temperatures below freezing. Typically then, ice cloud at very low temperatures ($<-15^{\circ}$ C), upper levels or high latitudes will have a smaller IWC and therefore dissipate slower than ice cloud in the warmer 'mixed-phase' region. Thus the CWH model simulates larger cloud amounts than CW or CWRP (which both have a fixed 1 ms^{-1} fall speed for ice) in these cold regions.

In the mid-high latitudes of RH cloud cover diminishes from winter to summer. In the cloud water models there is less seasonal variation, especially in the Southern Hemisphere although CW and CWRP show slightly increased cloud amounts from winter to summer in the Northern Hemisphere (Figure 4). Observational evidence indicates that cloud in high latitudes increases in summer (Vowinkel and Orvig 1970). In summer, the boundary layer static stability decreases, allowing mixing throughout a greater vertical depth and the relative humidity decreases. In RH, cloud is directly related

to relative humidity and so also decreases. The simulated zonal mean temperature of the polar boundary layer in summer is between 0 and -15°C , indicating that the cloud in CW, CWH and CWRP is made up of both ice and water cloud. In CW and CWRP pure ice cloud in winter precipitates faster than the mixed phase cloud in summer and thus the winter cloud amounts are slightly smaller. Additionally in CWRP, the cloud albedo is a function of cloud water path and in the polar regions this is lower than the globally averaged values used in CW. Thus less solar radiation is reflected back to space making the summer climate warmer than in CW. This means that a smaller fraction of polar cloud is ice cloud in CWRP and there is a tendency to greater cloud amounts. In CWH a further process occurs at all latitudes which tends to reduce summer cloud amount. Pure ice cloud will be at a slightly higher temperature (but still less than 0°C) in summer than in winter and will have a greater liquid water content (Smith 1990) and so the rate of dissipation of ice cloud will be greater, as discussed above (Section 2.1(c)). This process appears to approximately compensate for the tendency for increased summer cloud amounts in high latitudes as the frequency of the more persistent water cloud increases. Changes in cloud on the inclusion of a cloud water variable are discussed in more detail in Smith (1990).

(b). Radiation and Cloud Radiative Forcing

Cloud cover is not uniquely defined and so comparisons with observations are of limited value. However, the model simulation of the earth's radiation budget is closely tied to the predicted cloud cover and is more easily verified against satellite data (eg. Kyle et al 1985, Barkstrom 1984).

Figure 5 shows the simulated outgoing long wave radiation (OLR) for July from RH, CW and CWRP and satellite data from the Earth Radiation Budget Experiment (ERBE) for July 1985. The simulation of OLR and planetary albedo in CWH is very similar to that in CW and so will not be shown. The excessive cloud amounts in high latitudes found in RH are reduced in CW, CWH and CWRP leading to an improved simulation of OLR especially in the Southern Hemisphere. In the Northern Hemisphere, the OLR is higher and closer to observed over parts of northwest Canada and Alaska, Greenland and northern Eurasia, but over parts of the North Atlantic the OLR is higher than the

satellite data suggests. The relatively low resolution of the models means they do not resolve the ITCZ properly and fail to reproduce the horizontal extent of the reduced OLR ($<225 \text{ Wm}^{-2}$) here. A higher horizontal resolution version of CWH ($2.5^\circ \times 3.75^\circ$), (Senior and Mitchell, in preparation) does a rather better job although still does not capture the low OLR over Africa suggesting that there is too little high cloud there in the model. Annual global mean data from the NIMBUS 7 satellite (Kyle et al 1985) gives an OLR emission of 235.8 Wm^{-2} which compares especially well with 236.4 Wm^{-2} from CWH and reasonably well with 237.7 Wm^{-2} from CWRP. The value of 239.4 Wm^{-2} from CW stems from the combination of small tropical high cloud amounts and a relatively low fixed high cloud emissivity (Table 2). The lower value (233.1 Wm^{-2}) from RH is largely due to excessive high latitude cloud amounts.

The July planetary albedo field for RH, CW and CWRP and from the ERBE data are shown in Figure 6. The albedo is lower in CW and CWRP than in RH and than that derived from satellite data. In general the cloud water models underestimate planetary albedo over parts of the ITCZ (particularly over South America and West Africa) and over the Southern Ocean where there may be too little cloud or too low a value of surface albedo (See Ramanathan et al 1989b). CWRP produces values higher than observed between 40° N and 60° N which may be due to too high a value of cloud albedo. The global mean annual mean albedo estimated from the NIMBUS 7 satellite is 30.2 %. The corresponding values from RH, CW, CWH and CWRP are 30.4 %, 29.0 %, 29.3 % and 29.5 % respectively.

To further illustrate the link between cloud cover and the radiation budget we will use the concept of cloud radiative forcing (CF) (Ramanathan et al 1989a). Cloud forcing is defined as the radiative impact of clouds upon the top of the atmosphere (TOA) radiation budget. Thus;

$$C_F = (Q - Q_C) - (F - F_C) \quad (9)$$

where Q and F represent the incoming solar radiation and the outgoing longwave radiation respectively and the subscript C denotes 'clear-sky' fluxes. These are defined to be the net radiative fluxes in a cloud-free earth in which the atmospheric structure of temperature and water vapour is otherwise the same as in the real atmosphere. Hence cloud forcing is the net cooling or heating of the earth due to instantaneously adding clouds. From

(9), cloud forcing is positive when cloud has a warming effect on the surface/atmosphere system. From the models, cloud forcing can be calculated in two ways, depending on the definition of the 'clear sky' flux. Clear sky fluxes may be obtained from completely clear sky grid boxes adjacent to those from which the total flux is obtained or both fluxes can be calculated for the same grid box using the fractional cloudiness. These two methods are referred to as methods I and II. Method II has been used here. It is often useful to split cloud forcing into its shortwave ($Q - Q_C$) and longwave ($F_C - F$) components. Clouds cool the climate by increasing the amount of shortwave radiation reflected back to space. Shortwave cloud forcing thus arises largely from low level optically thick cloud. Longwave cloud forcing comes mainly from high clouds which absorb longwave radiation from the earth and re-emit at a colder cloud top temperature, reducing the OLR and warming the earth-atmosphere system. The temperature of low cloud is similar to that of the surface and so has a negligible effect on longwave radiation.

The observational cloud forcing data available for comparison is limited (Ramanathan et al 1989a,b, Ardanuy et al 1989). There is considerable variation between so-called observed data, presumably due largely to cloud contamination of 'clear-sky' fluxes. For example, Ardanuy et al (1989) show longwave cloud forcing derived from the NOAA-9 Advanced Very High Resolution Radiometer (AVHRR) and from the ERBE for April 1985 and quote a difference in the globally averaged clear-sky longwave fluxes between the two of nearly 8 Wm^{-2} leading to considerable disparity in the longwave cloud forcing. Ramanathan et al (1989a) quote error margins of 10 Wm^{-2} in general, but note that snow-covered regions may have larger uncertainties because of the difficulty in distinguishing clear from cloudy regions there. In spite of these problems many of the spatial patterns are qualitatively similar in the observed datasets and hence this type of data is still useful for verifying the modelled fluxes. It was felt that the ERBE data (Barkstrom 1984, Ramanathan et al 1989a,b) were the most reliable available. The ERBE is the first multiple-satellite system to provide a diurnal sampling capability which has proved a major area for error in earlier measurements of radiation quantities. The sensors aboard the three satellites involved in the experiment were designed to minimise errors in many areas and much work has gone into the processing of the data to eliminate possible problems such as cloud contamination.

The model simulations of July cloud forcing have been compared with

ERBE data for July 1985 (Figures 7 and 8). Seasonal variations in ERBE cloud forcing data have been shown to be relatively small (Harrison et al 1990), so the discussion below is relevant for all months. The resolution of ERBE data is $2.5^\circ \times 2.5^\circ$ but for comparison with the model output it has been interpolated onto a $5.0^\circ \times 5.0^\circ$ grid. Again, CW and CWH exhibit very similar patterns (although the magnitudes of the forcings are slightly improved in CWH) and so CWH will not be shown.

All the models show strong shortwave cloud forcing associated with the highly reflective clouds along the mid-latitude storm tracks in the Atlantic and Pacific as in the ERBE data (Figure 7). In RH the strongest forcing in the Atlantic is positioned too far north as might be expected from the greater than observed cloud amounts in high latitudes in the summer. In the cloud water models the mid-latitude maxima in shortwave cloud forcing are stronger than in ERBE in both hemispheres but particularly in the Northern Hemisphere (for example over North America), suggesting there is too much cloud there. All models show strong shortwave forcing in the Asian monsoon region (Figure 7) as would be expected from the presence of optically thick convective cloud. However, the simulated monsoon is shifted south-eastwards in each case (not shown) and this leads to a south-eastward extension of the maximum cloud forcing. The magnitude of the forcing is too strong by up to 25 Wm^{-2} in the cloud water models and 50 Wm^{-2} in RH in this region. The area of strong shortwave cloud forcing off the west coast of Central America is rather weak in the cloud water models and although the magnitude is better in RH its position is shifted northwards and eastwards when compared to the satellite data (Figure 7). Errors in the simulation of shortwave cloud forcing may be due to too much cloud or too high a value of cloud albedo or too low a value of surface albedo, or any combination of these. In all the models described here, ocean surface albedo is taken as 6% whereas observations from ERBE suggest that at high latitudes the ocean surface albedo may be as high as 15-20% (Ramanathan et al 1989b).

The largest observed longwave forcing occurs in tropical regions, especially in the Western Pacific where there is a maximum in high cloud (Figure 8(d)). Once again the poor simulation of the monsoon circulation in all the models affects the simulation of the maximum in longwave cloud forcing, pushing it too far east (Figure 8). CWRP shows substantially stronger longwave forcing than CW in this region due to a larger high cloud emissivity in the tropics (Figure 18(b)) than the prescribed value of 0.42.

at all latitudes in CW. RH has a slightly better longwave forcing over Central America than the cloud water models but none of the models simulate well the maximum over Africa where the rainfall is also deficient. All the models show excessive shortwave and longwave forcing over the Southern Ocean. The overestimation of longwave forcing is particularly pronounced in RH, which has a large amount of high cloud between 40° and 70° S in July (Figure 2).

The July global mean net cloud forcing is a cooling of between 25 and 31 Wm^{-2} in each of the models compared to the satellite derived net forcing of around 18 Wm^{-2} (Table 3). This error is exaggerated in the cloud water models by the complementary sign of the errors in each of the individual forcings. Errors of similar magnitude are present in January also.

In summary, there is too much cloud in RH, especially at high latitudes, the amount of high cloud in CWH is more realistic than in CW or CWRP and the distribution of cloud radiative forcing is correspondingly improved.

2.3 Sensitivity Experiments

A further simulation was performed with each version of the model, in which the concentration of CO_2 was doubled to 640 ppm. All these experiments were initiated from earlier $2 \times \text{CO}_2$ experiments. The time taken to reach equilibrium is reduced as the sensitivity of the model to the external forcing is reduced (Hansen et al 1984). For each simulation, the results meaned over June, July and August (JJA) for a ten year period after reaching equilibrium are presented.

3. Model response to doubled CO_2

The global mean annual mean change in surface temperature is reduced from 5.4 K in RH to 2.8 K, 3.3 K and 1.9 K in CW, CWH and CWRP respectively. The largest reductions in the warming coincide with the areas in mid-latitudes where the greatest changes in cloud response occur. Hence, in this section, we consider changes in zonally averaged and geographically varying temperature and relate these to changes in cloud, radiation and cloud forcing.

(a) Temperature changes

All four experiments produce a large warming in the upper tropical troposphere, an amplification of the surface warming in high latitudes in winter and a stratospheric cooling of up to 5° C (Figures 9 and 10). These responses are generally well accepted and have been found in most model simulations with enhanced CO_2 (eg. Willson and Mitchell 1987, Hansen et al 1984 and Wetherald and Manabe 1988, Ingram et al 1989, Meehl and Washington 1989).

The Cloud water models differ from RH in both the magnitude and distribution of the warming. The maximum JJA warming of the upper troposphere is reduced from 8 K in RH to 4 K, 5 K and 3 K in CW, CWH and CWRP respectively (Figure 9). There is also a large reduction in the lower-level mid-latitude warming, from over 6 K in RH to 3-4 K in CW and CWH and around 2 K in CWRP. The pattern is similar in DJF (Figure 10), although the tendency of the maximum in the upper tropospheric tropical warming to penetrate into the summer hemisphere is less clear in CW, CWH and CWRP in this season.

The distribution of the annual mean surface warming in the four models shows some overall similarities (Figure 11). In each case the maximum warming occurs over the sea-ice areas in winter (not shown) and generally the land warms more than the sea, where evaporation occurs in preference to surface warming. There is an overall reduction in the magnitude of the surface warming from over 5° in RH to less than 2° in CWRP. The most noticeable changes in the distribution of the warming occur at high latitudes, in the North Atlantic, North East Pacific and the Southern Ocean, where the warming is reduced by up to 5 K in CWRP. In the Southern Ocean this model actually simulates areas where there is a small cooling (although this is not statistically significant when a two-tailed student's t-test is applied with a 90 % confidence limit). The large temperature differences in middle and high latitudes are associated with the increases in cloud in these regions, as discussed below.

(b). Changes in zonally averaged cloud

The JJA height-latitude cross sections of changes in layer cloud on doubling CO_2 are broadly similar in pattern in all the experiments

(Figure 12). The maximum in high cloud at low latitudes moves upwards as the height of the tropopause increases in all cases, a feature common to many doubled CO_2 experiments (Weatherald and Manabe 1988, Mitchell and Ingram 1990).

In RH, medium-level cloud has generally decreased with the largest reductions in mid-latitudes. In northern high latitudes there is a reduction in cloud in the lowest layer where there was an unrealistically large amount of cloud in the control simulation. The reduction in cloud is smaller in the simulations with cloud water, especially in DJF (not shown), probably because the amount of polar cloud in the controls was considerably less. The cloud response in RH is directly related to the change in relative humidity (not shown). Changes in cloud when using a relative humidity dependent cloud scheme are discussed in more detail by Mitchell and Ingram (1990).

The most notable difference between the response of all the cloud water schemes and that of the relative humidity scheme is the much reduced decreases and some increases in cloud in the temperature band between the 0°C and -15°C isotherms (the dashed lines), especially in the summer hemisphere. These are associated with the parametrization of precipitation of ice and liquid water in the cloud water schemes. In the schemes, the change from water to ice particles occurs between 0°C and -15°C (section 2.1 (b)). As the atmosphere warms, the fraction of water cloud in the mixed phase region increases. Since water cloud is more persistent than ice cloud, the total amount of cloud increases. This can be seen more clearly by considering the changes in zonally averaged liquid and ice cloud water content (Figure 13). In each of the cloud water experiments there are decreases in ice water content but greater increases in liquid water content giving net increases in total water content.

The increases in liquid water content are very similar in CW and CWH but the reduction in ice water content is smaller in CW where there is less ice cloud (see Section 2.2 (a)). The dependence of ice cloud precipitation on ice cloud water content in CWH markedly reduces the efficiency of precipitation, relative to CW, at levels close to the tropical tropopause whilst having less of an impact near the freezing level, where the fall speeds are similar in the two models. The difference in ice precipitation efficiency between CW and CWH at the freezing level is thus quite small and the depletion of ice is large in both cases giving similar cloud changes there. At higher levels the upward shift of cloud due to the raising of the

tropopause is more noticeable in CWH (Figure 12 (b) and (c)) as there is more ice cloud there in the control (Figure 3 (b) and (c)). The similarity between the cloud changes in CW and CWH indicates that the qualitative nature of the changes, of at least lower level cloud, is relatively insensitive to the detailed specification of the dissipation of ice cloud.

In CWRP, the cloud changes are qualitatively similar to those in CW but of smaller magnitude (Figure 12), however when normalised by the zonally averaged changes in temperature (to give the change per degree of warming) they are quantitatively similar as well (not shown). The inclusion of interactive radiative properties allows the albedo and the emissivity of the cloud to rise as the liquid water fraction and total water content increase. So, in CWRP the same cloud feedback processes are occurring as in CW, but are altered by the changes in radiative properties. However, the changes in cloud feedback are not simply scaled by the reduced temperature changes. The greatest impact of interactive radiative properties occurs in the regions of the greatest cloud changes. As discussed below, the largest cloud increases occur below the main region of longwave cooling to space and so changes in emissivity are unimportant here, but the increases in albedo produce a larger shortwave cloud forcing than in CW. The high cloud changes are much smaller, so the increased albedo effect dominates and the relative warming of the surface/troposphere system is reduced (Figure 9). The increases in cloud and cloud water content are consequently also smaller in CWRP than in CW (Figures 12 and 13 (b) and (d)). These rather different cloud changes in CWRP are explained in more detail in the following section together with the changes in radiation.

The seasonal cycle of cloud changes (Figure 14) shows that in RH, CW and CWH the maximum reduction in total cloud occurs at around 30° in both hemispheres in winter and in the Southern Hemisphere summer, but at higher latitudes in northern summer. In CWRP the reductions in cloud are mostly confined to areas equatorward of 40° . In the cloud water experiments the maximum increases in cloud water and cloud occur in the warmer summer hemisphere. This seasonality is especially noticeable in the Northern Hemisphere. The changes in zonal mean cloud in the Southern Hemisphere show less of a seasonal shift and increases occur throughout the year at around 60° S, although the maximum increases still occur in summer. The small seasonal cycle and strong zonality of temperature and cloud changes in the Southern Hemisphere arise from the large percentage of ocean coverage there.

In CW and CWRP increases in cloud spread across Antarctica in DJF whereas in CWH they are confined to lower latitudes. As described in Section 2.2 (a) the relationship between ice cloud precipitation and IWC in CWH means that the depletion of ice cloud by precipitation increases with temperature. Hence over Antarctica where low cloud is ice cloud even in the $2 \times \text{CO}_2$ simulation, the warming due to doubling CO_2 leads to a reduction in cloud amount. In RH, the largest reductions in mid-latitude cloud occur in the summer hemisphere and are related to the changes in relative humidity. The drying of the mid-latitude troposphere by deeper vertical motions has been discussed in detail elsewhere (Mitchell and Ingram 1990, Wetherald and Manabe 1980, 1988).

(c). Changes in the Earth's Radiation Budget

As discussed in section 2.2(b), cloud and radiation are strongly coupled and so changes in cloud are likely to force changes in the Earth's radiation budget. This occurs in several different ways and these are best illustrated by considering the zonal mean changes in low, medium and high cloud individually (Figures 15 and 16) in conjunction with the changes in cloud radiative forcing split into its longwave and shortwave components (Figure 17). In order to avoid overcomplicated diagrams the cloud changes in CWH are shown only in comparison to CW (Figure 16) and the CWH cloud forcing changes are omitted as they are very similar to those in CW. Table 4 shows the global mean changes in the shortwave and longwave cloud forcings and summarises the net effect of the changes in cloud for each experiment.

In RH, the upward shift of the cirrus cloud deck (Figure 12(a)), increases its 'greenhouse' effect. However the overall reduction in high cloud amount, especially in the sub-tropics to mid-latitudes and near 10°N (Figure 15(a)) more than outweighs this and the longwave cloud forcing, the warming effect of cloud, is reduced (Figure 17(b); Table 4, column 1). Lower level clouds, with a smaller 'greenhouse' effect but a high albedo, reduce substantially. This has the effect of lowering the planetary albedo and markedly reducing the size of the shortwave cloud forcing (Figure 17(a); Table 4, column 1). The cooling effect of cloud is then substantially reduced and this dominates over the reduction in longwave warming such that the net impact of cloud is to significantly enhance the warming (Figure 17(c); Table 4, column 1).

In the cloud water models the upward shift of the cirrus deck is less well marked and the changes in high cloud much smaller than in RH, for example near 5° and 40° N (Figures 12 and 15(a)). The overall change in longwave cloud forcing is very small (Figure 17(b); Table 4, columns 2, 3 and 4). In CW and CWH the reductions in low and medium level cloud are much smaller than in RH (for example in medium cloud at 40° N and $20-40^{\circ}$ S) and at higher latitudes there are some increases in cloud. Hence there is only a small reduction in both planetary albedo and reflected solar radiation. The reduction in shortwave cooling is then much less than in RH, though it still dominates over the reduced longwave warming and the net effect is to enhance the warming slightly (Table 4, columns 2 and 3).

The changes in cloud in CWH are qualitatively similar to those in CW (Figure 12(b) and (c), Figure 16). The largest differences occur in high level cloud changes and in medium level cloud changes at higher latitudes. The different treatment of ice cloud precipitation in CWH produces more ice cloud in the control simulation and the changes are correspondingly larger. These lead to a bigger reduction in both longwave warming and shortwave cooling than in CW. The change in shortwave forcing is larger as the changes in medium cloud dominate and the enhancement of the warming by cloud is slightly bigger in CWH than in CW (Table 4, columns 2 and 3).

In CWRP changes in cloud combine with changes in the radiative properties of clouds to substantially alter the strength and sign of the feedbacks due to cloud from those in CW and CWH. As cloud water content increases there are increases in both albedo and emissivity of all types of cloud at most latitudes (Figure 18(c) and (d)). The greater optical depth of medium and low level cloud at mid and high latitudes strengthens the negative feedback from the increases in cloud amount and results in more solar radiation being reflected than in the control or, equivalently, a greater shortwave cooling. (Figure 17 (a); Table 4, column 4). (Contrast this to a slightly reduced shortwave cooling in CW and CWH). Although high cloud albedo also increases the changes in both this and high cloud amount are much smaller than those of lower cloud (Figure 15, Figure 18(c)) and the effects are subsequently small.

As high clouds are far from black in the control runs, changes in their emissivity have a potentially large impact on the OLR. The increases in emissivity and general upward shift of high cloud (Figure 12(d)) imply a larger greenhouse effect, less escaping OLR and a greater longwave cloud

forcing. However at most latitudes this effect is outweighed by the reductions in high cloud amount (Figure 15(a)) producing a net increase in OLR and a reduction in longwave cloud forcing (Figure 17(b)). (In some areas, e.g. around 50° in both hemispheres, there is both an increase in high cloud amount and emissivity but a reduction in longwave cloud forcing. At these latitudes the amount of high cloud in the control is small (Figure 15(a)). The increases on doubling CO_2 are then rather ineffective at moderating the radiation budget. However, the strong downward shift of medium cloud, defined as occurring between $\sigma = 0.85$ and $\sigma = 0.44$, (Figure 12 (d)) is radiatively important. The result is an increase in OLR and a reduction in longwave cloud forcing.) In the tropics there is a 5° southward shift in the maximum in high cloud as well as a general increase in height and this is mirrored in the change in longwave cloud forcing at these low latitudes. Lower level clouds are very nearly black in the control runs and so changes in emissivity are negligible (Figure 18(d)). Overall there is a reduction in the longwave warming (Figure 17(b); Table 4, column 4).

As in all the models the change in shortwave cloud forcing dominates, but here changes in both longwave and shortwave cloud forcing are of the same sign and thus the compound effect is a relatively large cooling (Table 4, column 4).

4. Climate Sensitivity Analysis

To quantify the climate sensitivity of the experiments one can define a climate sensitivity parameter λ (Cess and Potter 1988):

$$\lambda = \Delta T / G \quad (10)$$

where ΔT is the equilibrium change in annual global mean surface temperature on doubling CO_2 and G is the initial radiative perturbation at the TOA, which is taken here to be 4 Wm^{-2} (Lal and Ramanathan 1984). From (9), the change in cloud forcing is

$$\Delta CF = \Delta(Q - Q_C) - \Delta(F - F_C) \quad (11)$$

where Q , Q_C , F and F_C are defined as in 2.2(b) above. Given that G can be defined by

$$G = \Delta F - \Delta Q \quad (12)$$

and assuming that the individual feedbacks on the climate are independent and linear in temperature, the clear-sky climate sensitivity parameter can be defined as

$$\lambda_C = \Delta T / (\Delta F_C - \Delta Q_C) \quad (13)$$

where ΔF_C and ΔQ_C are the changes in the 'clear-sky' fluxes on doubling CO_2 . It follows from (10), (11), (12) and (13) that

$$\lambda / \lambda_C = 1 + \Delta CF / G \quad (14)$$

Following Cess et al (1990) we can define the 'cloud feedback' as the ratio of the sensitivity λ to the sensitivity in the absence of cloud λ_C . This is related to the change in cloud forcing through (14). Table 5 shows these quantities calculated for each of the experiments RH, CW, CWH and CWRP. There is some discrepancy in the λ_C 's found here, in contrast to the good agreement found by Cess et al (1990). This is to be expected since the different cloud schemes produce different simulations of the present day climate and hence alter the contribution of other feedbacks. Note that λ_C is greatest in RH. This is probably because the cloud water schemes lead to a substantial reduction in warming at the sea-ice edge (relative to the global mean). This will reduce the strength of the positive sea-ice feedback. Similarly a reduced global mean warming will reduce the effect of the positive water vapour feedback. Both these effects are manifested in a reduction in λ_C in the cloud water experiments. These effects may be more important in the models presented here as they all include an annual cycle whereas those described by Cess et al (1990) were all perpetual July experiments and were forced with ± 2 K sea surface temperature (SST) anomalies. At best the assumptions of linearity and independence of the feedback processes in this analysis are only approximately true. The advantage of using λ / λ_C to define cloud feedback is that it provides a simple and objective method of comparison of results from different models.

In RH, clouds increase the sensitivity substantially ($\lambda > \lambda_C$, Table 5) consistent with several other experiments using relative humidity based

cloud (e.g. Hansen et al 1984, Wetherald and Manabe 1988). In CW and CWH the net effect is small and in CWRP the effect of cloud is to reduce the model's sensitivity (Table 5). Somerville and Remer (1984) and Somerville and Jacobellis (1988), using radiative-convective models with interactive cloud radiative properties, have suggested that clouds would produce a negative feedback, whereas Roeckner et al (1987) using a low resolution general circulation model coupled to a mixed layer ocean and including interactive cloud radiative properties simulated a positive cloud feedback (see also Roeckner 1988, Schlesinger 1988).

Clearly there are many inter-related processes occurring within these experiments and the use of an interactive ocean and a seasonal cycle introduce further degrees of freedom. One way of circumventing this problem is to use fixed ± 2 K SST perturbations with a perpetual July simulation (as, for example, in Cess et al 1990). This type of experiment has been performed with 3 of the versions of the model described here, RH, CW and CWRP. The result of applying a similar analysis to that used above (although, of course, prescribing ΔT and calculating G) is a total change in the order of the climate sensitivity, from $RH > CW > CWRP$ in the experiments described here (Table 5) to $CWRP > RH > CW$ in the ± 2 K SST experiments. A detailed analysis of these experiments is to be described elsewhere (Mitchell, in preparation), however it is worth considering the impact of the major differences in the two approaches. The use of a latitudinally invariant SST perturbation ($\Delta T = 4$ K) is likely to result in a rather different cloud response than if there is a geographically varying temperature change. For example, as described in section 3(b), the low and medium cloud changes in CWRP, together with increased cloud albedos inhibit the surface temperature warming and therefore prevent further cloud changes. Thus, cloud changes and temperature changes are strongly coupled and realistic cloud feedbacks on doubling CO_2 can only be simulated by using realistic changes in surface temperature (± 2 K integrations are only relevant to ± 2 K SST perturbations). The inhibition of a seasonal cycle is manifested in the constraint of λ_c (as described above and see also Cess et al 1990) because sea-ice extents are fixed and there is no feedback from changes in snow and ice coverage. This also may mislead estimates of the relative magnitude or even the sign of the cloud feedback. Therefore, it is difficult to draw any conclusions concerning a model's sensitivity to increased atmospheric CO_2 concentrations from such idealized experiments.

5. Summary and discussion

1. The simulation of present day cloud amount depends substantially on the cloud schemes used. The simulation of the earth's radiation budget is marginally improved in the cloud water scheme simulations but there are still significant differences from satellite data and it should be emphasised that, although more detailed, the scheme still only represents cloud in a crude manner.

2. Two additional inter-related cloud feedback processes are evident in the experiments with the cloud water scheme:

(i) The increasing fraction of liquid water cloud relative to ice cloud produces a strong negative feedback and reduces the warming of the surface/troposphere system.

(ii) The incorporation of a parametrization of cloud radiative properties dependent on the cloud water path produces a further negative feedback.

The first of these is probably qualitatively realistic although exaggerated in these models. The Heymsfield formula used in CWH is intended to represent the fall speed averaged over the particles of ice in a homogeneous cloud and not the grid-box average fall speed required in a GCM. The threshold of -15°C for ice cloud is relatively warm. Water clouds may exist at temperatures as low as -40°C , below which they freeze spontaneously (eg. Mason 1957). Whilst the correct value for the threshold limit is uncertain, and indeed the use of a threshold is a simplification of the real processes occurring, the type of cloud that is causing the 'phase-change' feedback is not high cold cloud with a low water content but warmer sheets of cloud with high water contents in synoptic-scale disturbances. These type of clouds are then just what are simulated in the cloud water scheme with a -15°C threshold. Other factors such as the evaporation of ice crystals to leave smaller radiatively important ice particles (Heymsfield and Sabin 1989) are less likely to be important for

this particular feedback process as the air is generally saturated throughout low levels in frontal systems. Nevertheless, a change of the threshold to a colder temperature than -15°C might have some impact on the feedback process and this is certainly an area for future study. Much work is required to understand the microphysical processes of ice and mixed phase cloud better. It should be noted that the simulated increases in cloud in the cloud water models are dependent on the relative dissipation rates of ice and water cloud and are correspondingly uncertain, although inclusion of an observationally based parametrization of the dissipation of cloud ice does not substantially alter the simulated cloud increases.

The second feedback process depends on the relationships between cloud water and radiative properties which are also uncertain, particularly for the ice phase. An improved parametrization of cloud radiative properties in terms of cloud water content and a prescribed effective radius (Slingo 1989) is being incorporated into the next generation of the UKMO models. However it is not yet known how to best represent the radiative effects of non spherical ice particles. Consideration is also being given to the problem of defining the cloud water content of convective clouds.

3. Not only is the global mean warming reduced but the distribution is also altered. The largest proportional reduction in the warming occurs in mid-high latitudes. The low resolution of the models used in the present experiments means that they do not produce a realistic regional simulation and hence the regional changes have not been analysed in detail. Nevertheless, a high resolution version of the CWH model with a much improved regional simulation of the control climate produces very similar zonal and global mean feedbacks.

The results presented have profound implications. The range of climate sensitivities found with the four cloud schemes emphasises the uncertainty in the role of clouds in climate change and highlights the need for a more detailed representation of cloud.

In the longer term, there is a need to learn more about the microphysics of clouds and to improve the parametrizations of the most important cloud processes in large-scale models. This can best be done by comparing model parametrization schemes with results from field studies.

Until recently the simplicity of cloud parametrizations in large scale models has meant that the microphysical data available have been too detailed for comparison. Recently a variety of field studies have been organised to look at the effect of clouds on climate. Of particular relevance in this area are the FIRE program (First International Satellite Cloud Climatology Project (ISCCP) Regional Experiment) and ICE (International Cirrus Experiment). FIRE consists of two phases, the stratocumulus phase (Albrecht et al 1988) and the cirrus phase (Starr 1987). One of the aims of these projects is to examine the influence of these particular types of clouds on climate. Studies of this kind will provide the modelling community with much needed data on wider aspects of cloud physics and, in the long term will hopefully provide more reliable physically based cloud parametrization schemes that will help to reduce the uncertainties in the simulation of climate change.

Acknowledgements

We would like to thank William Ingram who derived the expressions for the cloud radiative properties given in Appendix A, and for many helpful comments and much useful discussion during the preparation of this paper. We should also like to thank Julia Slingo for comments that helped to clarify much of the paper. We acknowledge Dr. Bruce R. Barkstrom and the National Space Science Data Center through the World Data Center-A for Rockets and Satellites for making ERBE data available. This project was supported by CEC contact no. EVHC 0040 UK(H).

Appendix A

Fits of shortwave albedo (Re), transmissivity (Tr) and absorptivity (Ab) as rational functions of cloud water path (LWP) and solar zenith angle (μ_0) were made to the scheme of Liou and Wittman (1979). For water cloud, the stratus cloud approximations of Liou and Wittman were used. These gave;

$$Re_W = \frac{(k_6 - k_7 \mu_0) LWP + k_8 (1 - \mu_0)}{1 + k_9 LWP}$$

$$Tr_W = \frac{k_1 (\mu_0 - 1) + 1}{1 + k_2 LWP}$$

$$Ab_W = 1 - Re_W - Tr_W$$

and for ice cloud the cirrus cloud approximations of Liou and Wittman were used to give;

$$Re_I = k_{12} \left\{ \frac{(1 + k_{10} LWP)}{(1 + k_{13} LWP)} - \mu_0 \frac{(1 + k_{11} LWP)}{(1 + k_{14} LWP)} \right\}$$

$$Tr_I = \begin{cases} \frac{k_3 \mu_0 LWP}{1 + k_4 LWP} + \frac{1}{1 + k_5 LWP} & \text{where } Tr_I + Re_I < 1.0 \\ 1 - Re_I & \text{where } Tr_I + Re_I > 1.0 \end{cases}$$

$$Ab_I = 1 - Re_I - Tr_I$$

Where the values of the constants are;

$$\begin{aligned} k_1 &= 0.5390 \\ k_2 &= 0.01202 \text{ m}^2 \text{ g}^{-1} \\ k_3 &= 0.05160 \text{ m}^2 \text{ g}^{-1} \\ k_4 &= 0.1045 \text{ m}^2 \text{ g}^{-1} \\ k_5 &= 0.02302 \text{ m}^2 \text{ g}^{-1} \\ k_6 &= 0.009260 \text{ m}^2 \text{ g}^{-1} \\ k_7 &= 0.0007512 \text{ m}^2 \text{ g}^{-1} \\ k_8 &= 0.4914 \\ k_9 &= 0.01020 \text{ m}^2 \text{ g}^{-1} \\ k_{10} &= 0.08452 \text{ m}^2 \text{ g}^{-1} \\ k_{11} &= 0.1015 \text{ m}^2 \text{ g}^{-1} \\ k_{12} &= 0.1812 \\ k_{13} &= 0.02045 \\ k_{14} &= 0.03839 \text{ m}^2 \text{ g}^{-1} \end{aligned}$$

Graphs of the functions for the case $\mu_0 = 0.8$ are shown in Figure 1.

Table 1 Cloud Radiative Properties from RH

CLOUD	ALBEDO	TRANSMISSIVITY	EMISSION
LOW	0.6	0.3	1.0
MEDIUM	0.6	0.3	1.0
HIGH	0.2	0.75	0.75

Table 2 Cloud radiative Properties from CW and CWH

CLOUD	ALBEDO	TRANSMISSIVITY	EMISSION
LOW	0.56	0.3	0.91
MEDIUM	0.52	0.3	0.94
HIGH	0.18	0.75	0.42

Table 3 Global mean cloud forcing for July

FORCING	ERBE	RH	CW	CWH	CWRP
LW	29.8	31.7	27.8	30.6	30.1
SW	-48.4	-57.2	-56.3	-57.2	-61.1
NET	-17.7	-25.5	-28.5	-26.6	-31.1

Table 4 Changes in global mean annual mean cloud forcing

FORCING	RH	CW	CWH	CWRP
ΔLW	-4.08	-1.19	-1.54	-0.56
ΔSW	6.13	1.39	2.27	-0.48
ΔNET	2.04	0.2	0.73	-1.04

Table 5 Climate Sensitivity Analysis

MODEL	ΔT	λ	ΔCF	λ_C	λ/λ_C
RH	5.4	1.35	2.05	0.89	1.52
CW	2.8	0.7	0.21	0.67	1.04
CWH	3.3	0.83	0.73	0.70	1.19
CWRP	1.9	0.47	-1.0	0.63	0.75

References

- Albrecht, B.A., D.A. Randall, S. Nicholls, 1988. Observations of marine stratocumulus during FIRE. *Bull. Am. Met. Soc.*, 69, 618-626.
- Ardanuy, P.E, L.L. Stowe, A. Gruber, M. Weiss, C.S. Long, 1989. Longwave cloud radiative forcing as determined from Nimbus-7 observations. *Journal of Climate*, 2, 766-799.
- Barkstrom, B.R, 1984. The earth radiation budget experiment (ERBE). *Bull. Am. Met. Soc.*, 65, 1170-1185.
- Cess, R.D. and G.L. Potter, 1988. A methodology for understanding and intercomparing atmospheric climate feedback processes in general circulation models. *J. Geophys. Res.*, 93, 8305-8314.
- Cess, R.D., G.L. Potter, J.P. Blanchet, G.J. Boer, A.D. Del Genio, M. Deque, V. Dymnikov, V. Galin, W.L. Gates, S.J. Ghan, J.T. Kiehl, A.A. Lacis, H. Le Treut, Z.-X. Li, X.-Z. Liang, B.J. McAvaney, V.P. Meleshko, J.F.B. Mitchell, J.J. Morcrette, D.A. Randall, L. Rikus, E. Roeckner, J.F. Royer, U. Schlese, D.A. Sheinin, A. Slingo, A.P. Sokolov, K.E. Taylor, W.M. Washington, R.T. Wetherald, I. Yagai and M.-H. Zhang, 1990. Intercomparison and interpretation of climate feedback processes in 19 atmospheric general circulation models. *J. Geophys. Res.*, 95, 16601-16615.
- Darilison A.G., 1988. The role of ice nucleus distributions in cirrus cloud formation: a numerical simulation of the microphysics. *Met.O.15 internal report no.77*.
- Gregory, D. and P.R. Rowntree, 1990. A mass flux convection scheme with representation of cloud ensemble characteristics and stability dependent closure. *Monthly Weather Review*, 118, 1483-1506.

- Hansen, J.E., A. Lacis, D. Rind, G. Russell, P. Stone, I. Fung, R. Ruedy and J. Lerner, 1984. Climate Sensitivity: Analysis of Feedback Mechanisms. In *Climate Processes and Climate Sensitivity* (ed. J. Hansen and T. Takahashi) Geophysical Monograph, 29 130-163. American Geophysical Union, Washington DC.
- Harrison, E.P., P. Minnis, B.R. Barkstrom, V. Ramanathan, R.D. Cess and G.G. Gibson, 1990. Seasonal variation of cloud radiative forcing derived from the Earth Radiation Budget Experiment. *J. Geophys. Res.*, 95, 18687-18703.
- Heymsfield, A.J., 1977. Precipitation development in stratiform ice clouds: A microphysical and dynamical study. *J. Atmos. Sci.*, 34, 367-381.
- Heymsfield, A.J. and R.M. Sabin, 1989. Cirrus crystal nucleation by homogeneous freezing of solution droplets. *J. Atmos. Sci.*, 46, 2252-2264.
- Ingram, W.J, C.A. Wilson and J.F.B. Mitchell, 1989. Modeling climate change: an assessment of sea ice and surface albedo feedbacks. *J. Geophys. Res.*, 94 8609-8622.
- Kyle, H.L, Ardanuy, P.E and Hurley E.J, 1985. The status of the Nimbus-7 earth radiation budget data set. *Bull. Amer. Met. Soc.*, 66, 1378-1388.
- Lal, M and V. Ramanathan, 1984. Effects of moist convection and water vapour radiative processes on climate sensitivity. *J. Atmos. Sci.*, 41, 2238-2249.
- Le Treut, H. and Z.-X. Li, 1988. Using Meteosat data to validate a prognostic cloud generation scheme. *Atmospheric Research*, 21, 273-292.
- Liou, K-N. and G.D. Wittman, 1979. Parameterization of the radiative properties of clouds. *J. Atmos. Sci.*, 36, 1261-1273.
- Manabe, S. and R.T. Wetherald, 1967. Thermal equilibrium of atmosphere with a given distribution of relative humidity. *J. Atmos. Sci.*, 24, 241-259,
- Mason, B.J, 1957. *The physics of clouds*. Clarendon, Oxford.

- Meehl, G.A. and W.M. Washington, 1989. CO₂ climate sensitivity and snow-sea-ice albedo parametrization in an atmospheric GCM coupled to a mixed-layer ocean model. *Climatic change*, 16, 283-306.
- Mitchell, J.F.B. and W.J. Ingram, 1990. On CO₂ and Climate: Mechanisms of changes in cloud. Submitted to *Journal of Climate*.
- Mitchell, J.F.B., C.A. Senior and W.J. Ingram, 1989. CO₂ and Climate: A missing feedback?. *Nature*, 341, 132-134.
- Mitchell, J.F.B. and D.A. Warrillow, 1987. Summer dryness in Northern mid-latitudes. *Nature*, 330, 238-240.
- Pruppacher, H.R. and J.D. Klett, 1978. *Microphysics of clouds and precipitation*. Reidel, 714.
- Ramanathan, V., R.D. Cess, E.F. Harrison, P. Minnis, B.R. Barkstrom, E. Ahmad, D. Hartmann, 1989a. Cloud-radiative forcing and Climate: Results from the Earth Radiation Budget Experiment. *Science*, 243, 57-63.
- Ramanathan, V., B.R. Barkstrom and E.F. Harrison, 1989b. Climate and the Earth's radiation budget. *Physics Today*, May, 22-32.
- Roeckner, E., U. Schlese, J. Biercamp, and P. Loewe, 1987. Cloud optical depth feedbacks and climate modelling. *Nature*, 329, 138-140.
- Roeckner, E., 1988. Reply to comment on 'Cloud optical depth feedbacks and climate modelling'. *Nature*, 335, 304.
- Schlesinger, M.E., 1988. Comment on 'Cloud optical depth feedbacks and climate modelling'. *Nature*, 335, 303-304.
- Schlesinger, M.E. and J.F.B. Mitchell, 1987. Climate model simulations of the equilibrium climatic response to increased carbon dioxide. *Rev. of Geophys.*, 25, 760-798.

Schneider, S.H., 1972. Cloudiness as a global model feedback mechanism: The effects on the radiation balance and surface temperature of variations in cloudiness. *J. Atmos. Sci.*, 29, 1413-1422.

Slingo, A., 1989. A GCM Parametrization for the shortwave radiative properties of water cloud. *J. Atmos. Sci.*, 46, 1419-1427.

Slingo, A, and R.C. Wilderspin, 1986. Development of a revised longwave radiation scheme for an atmospheric general circulation model. *Q. J. R. Meteorol. Soc.*, 112, 371-386.

Smith, R.N.B., 1990. A scheme for predicting layer cloud and their water content in a general circulation model. *Q. J. R. Meteorol. Soc.*, 116, 435-460.

Somerville, R.C.J. and L.A. Remer, 1984. Cloud optical thickness feedbacks in the CO₂ climate problem. *J. Geophys. Res.*, 89, 9668-9672.

Somerville, R.C.J. and S. Iacobellis, 1988. Air-Sea Interactions and cirrus cloud feedbacks on climate. Am. Met. Soc. 7th Conf. *Ocean-Atmos. Interaction*, 53-55.

Starr, D.O'C., 1987. A cirrus cloud experiment: Intensive field observations planned for FIRE. *Bull. Amer. Met. Soc.*, 68, 119-124.

Stephens, G.L., 1978. Radiation profiles in extended water clouds. 2. parameterization Schemes. *J. Geophys. Res.*, 35, 2123-2132.

Sundqvist, H., 1978. A parametrization scheme for non-convective condensation including prediction of cloud water content. *Q. J. Royal. Meteorol. Soc.*, 104, 677-690.

Vowinckel, E. and S. Orvig, 1970. The climate of the North Polar Basin. In Orvig, s. (ed), *World survey of climatology 14, Climate of the Polar Regions*, New York, pp. 129-252.

Warren, S.G, C.J. Hahn, J. London, R.M. Chervin and R.L Jenne, 1988. Global distribution of total cloud cover and cloud type amounts over land, *NCAR Tech.Note NCAR/TN-273+STR*, Nat. Cent. for Atmos. Res., Boulder, Colo.

Warren, S.G, C.J. Hahn, J. London, R.M. Chervin and R.L Jenne, 1988. Global distribution of total cloud cover and cloud type amounts over the ocean, *NCAR Tech. Note NCAR/TN-273+STR*, Nat. Cent. for Atmos. Res., Boulder, Colo.

Wetherald, R.T. and S. Manabe, 1980. Cloud cover and climate sensitivity. *J. Atmos. Sci.*, 37, 1485-1510.

Wetherald, R.T. and S. Manabe, 1986. An investigation of cloud cover change in response to thermal forcing. *Climate change*, 8, 5-23.

Wetherald, R.T. and S. Manabe, 1988. Cloud feedback processes in a general circulation model. *J. Atmos. Sci.*, 45, 1397-1415.

Wilson, C.A. and J.F.B. Mitchell, 1987. A doubled CO2 climate sensitivity experiment with a global climate model including a simple ocean. *J. Geophys. Res.*, 92, 131315-13343.

Figure Captions

1. Cloud radiative properties as a function of Liquid Water Path (LWP) at $\mu_0 = 0.8$. From the parametrization by Liou and Wittman: Solid line, Water cloud (Stratus) and crossed solid line, Ice cloud (Cirrus). Polynomial fits to the parametrization of Liou and Wittman: Dashed line, Water cloud and Crossed dashed line, Ice cloud.

- (a) Reflectivity
- (b) Transmissivity
- (c) Absorptivity

2. Total fractional cloud amounts from ten year July means. Contours at 10% and every following 20% and areas with values greater than 50% are stippled.

- (a) RH
- (b) CW

3. Height-latitude cross section of zonally averaged cloud cover from ten year July means. The height co-ordinate is sigma (=pressure/surface pressure). Contours every 5%, stippled above 15%.

- (a) RH
- (b) CW
- (c) CWH
- (d) CWRP

4. Latitude-time cross section of zonally averaged cloud cover from ten year July means. Contours every 1%, stippled above 6%.

- (a) RH
- (b) CW
- (c) CWH
- (d) CWRP

5. Outgoing Longwave radiation at the top of the atmosphere in Wm^{-2} from ten year July means. Contours every 25 Wm^{-2} , stippled below 225 Wm^{-2} .

- (a) RH
- (b) CW
- (c) CWRP
- (d) ERBE data for July 1985

6. Planetary albedo from ten year July means. Contours every 10%, stippled above 30%.

- (a) RH
- (b) CW
- (c) CWRP
- (d) ERBE data for July 1985

7. Shortwave Cloud forcing from ten year July means. Contours every 25 Wm^{-2} , stippled below -75 Wm^{-2} .

- (a) RH
- (b) CW
- (c) CWRP
- (d) ERBE data for July 1985

8. Longwave Cloud forcing from ten year July means. Contours every 20 Wm^{-2} , stippled above 40 Wm^{-2} .

- (a) RH
- (b) CW
- (c) CWRP
- (d) ERBE data for July 1985

9. Height-latitude cross section of equilibrium changes in ten year JJA means of temperature on doubling CO_2 . The height co-ordinate is σ (=pressure/surface pressure). Contours every 1 K, reductions stippled.

- (a) RH
- (b) CW
- (c) CWH
- (d) CWRP

10. As Figure 9 but for ten year DJF means.

11. Ten year annual mean change in surface temperature on doubling CO_2 . Contours every 1 K up to +4K then at every 2K, reductions stippled.

- (a) RH
- (b) CW
- (c) CWH
- (d) CWRP

12. Height-latitude cross section of equilibrium changes in total cloud amount for ten year JJA means on doubling CO_2 . The height co-ordinate is σ (=pressure/surface pressure). Areas of reduction are stippled and the contours are every 1%. The dashed lines are the 0 and -15° C contours from the control simulation.

- (a) RH
- (b) CW
- (c) CWH
- (d) CWRP

13. Height-latitude cross section of equilibrium changes in cloud water for ten year JJA means on doubling CO_2 . The height co-ordinate is sigma. Areas of reduction are stippled. The dashed lines are the 0 and -15°C contours from the control simulation.

- (a) Liquid water content only from CW. Contours every $4 \times 10^{-6} \text{ kg kg}^{-1}$
- (b) Ice water content only from CW. Contours every $4 \times 10^{-7} \text{ kg kg}^{-1}$
- (c) and (d) as (a) and (b) but for CWH
- (e) and (f) as (a) and (b) but for CWRP.

14. Time-Latitude diagrams of the change in total fractional cloud cover on doubling CO_2 throughout the year. Values are ten year means from each month. Contours every 0.02, stippled where positive.

- (a) RH
- (b) CW
- (c) CWH
- (d) CWRP

15. Zonally averaged changes in fractional cloud cover for ten year JJA means on doubling CO_2 . Solid line, CW. Dashed line, RH. Solid and crossed line CWRP.

- (a) High cloud
- (b) Medium cloud
- (c) Low cloud

16. Zonally averaged changes in fractional cloud cover for ten year JJA means on doubling CO_2 . Solid line, CW. Crossed dashed line, CWH.

- (a) High cloud
- (b) Medium cloud
- (c) Low cloud

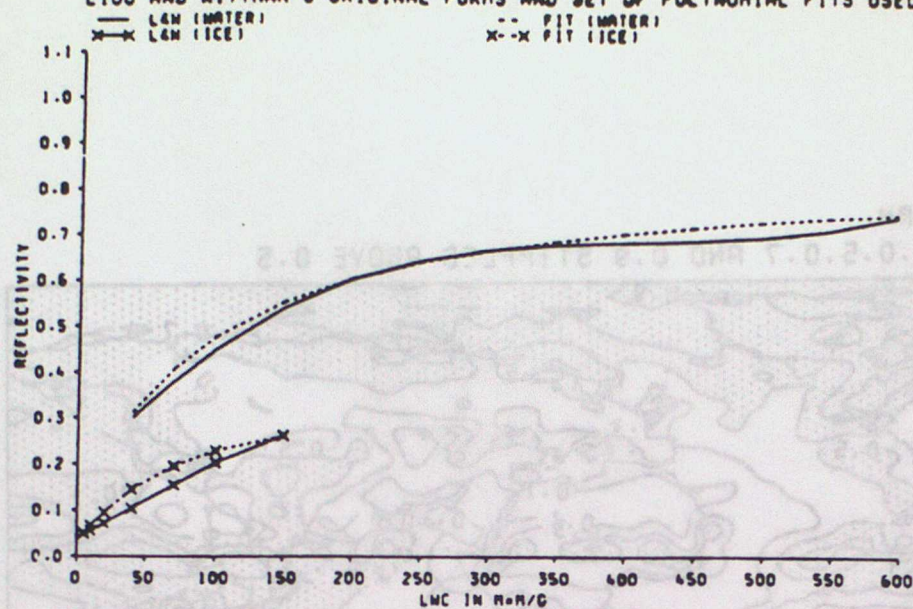
17. Zonally averaged change in cloud forcing at the TOA for ten year JJA means on doubling CO_2 in Wm^{-2} . Solid line, CW. Dashed line, RH. Crossed solid line, CWRP.

- (a) Cloud shortwave forcing
- (b) Cloud longwave forcing
- (c) Net cloud forcing

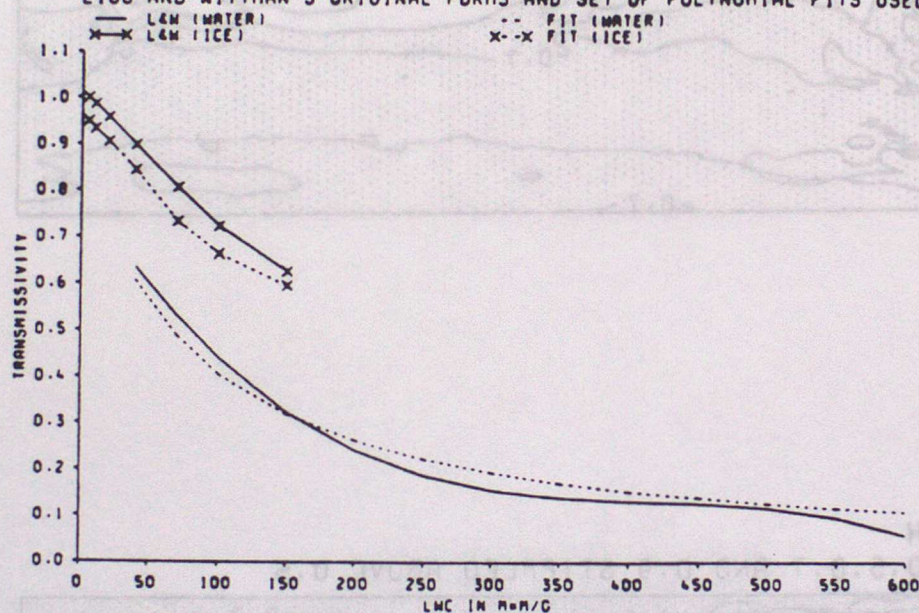
18. Zonally averaged cloud albedo and emissivity for ten year JJA means and the changes on doubling CO_2 . Solid line, high cloud. Dashed line, medium cloud. Dashed crossed line, low cloud.

- (a) Cloud albedo from the control.
- (b) Cloud emissivity from the control.
- (c) Changes in cloud albedo on doubling CO_2
- (d) Changes in cloud emissivity on doubling CO_2

(a) CLOUD REFLECTIVITY AS A FUNCTION OF LWP AT $\mu_{0.0} = 0.8$
 LIOU AND WITTMAN'S ORIGINAL FORMS AND SET OF POLYNOMIAL FITS USED



(b) CLOUD TRANSMISSIVITY AS A FUNCTION OF LWP AT $\mu_{0.0} = 0.8$
 LIOU AND WITTMAN'S ORIGINAL FORMS AND SET OF POLYNOMIAL FITS USED



(c) CLOUD ABSORPTIVITY AS A FUNCTION OF LWP AT $\mu_{0.0} = 0.8$
 LIOU AND WITTMAN'S ORIGINAL FORMS AND SET OF POLYNOMIAL FITS USED

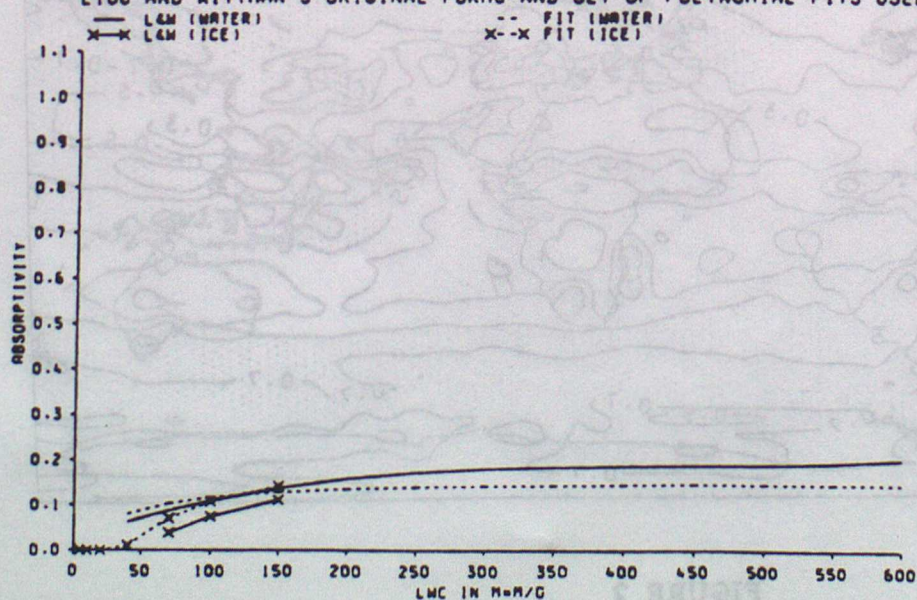


FIGURE 1

- (a) TOTAL CLOUD AMOUNT
TEN YEAR JULY MEAN RH
CONTOURS AT 0.1.0.3.0.5.0.7 AND 0.9 STIPPLED ABOVE 0.5



- (b) TOTAL CLOUD AMOUNT
TEN YEAR JULY MEAN CW
CONTOURS AT 0.1.0.3.0.5.0.7 AND 0.9 STIPPLED ABOVE 0.5

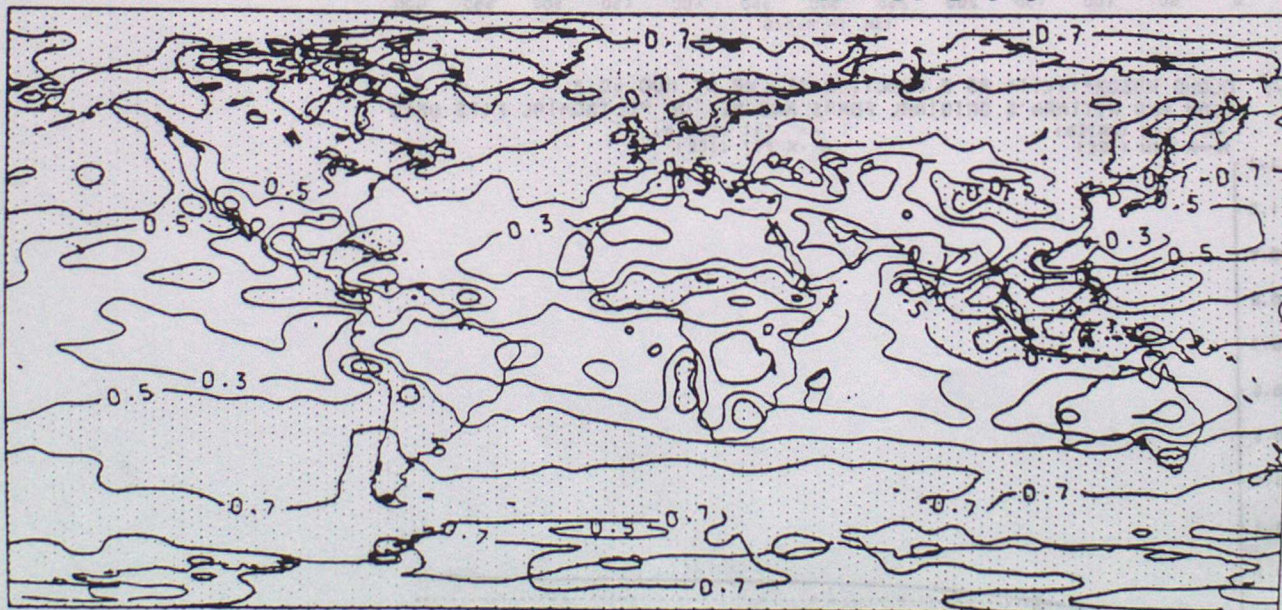
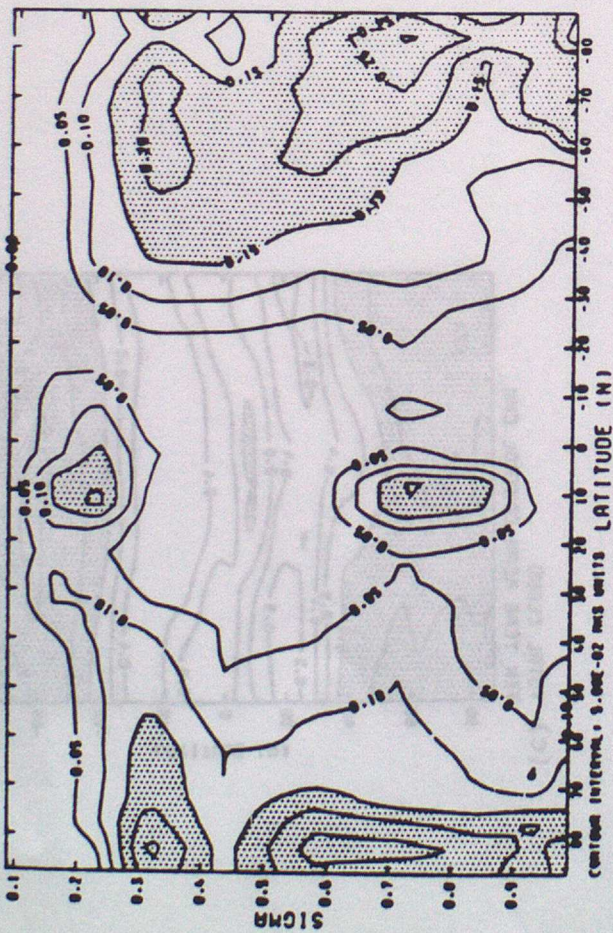
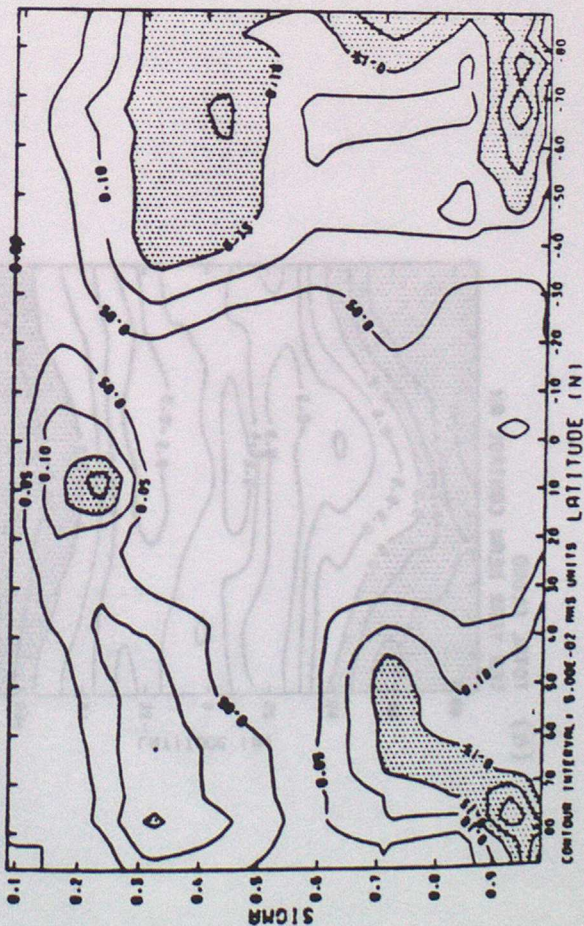


FIGURE 2

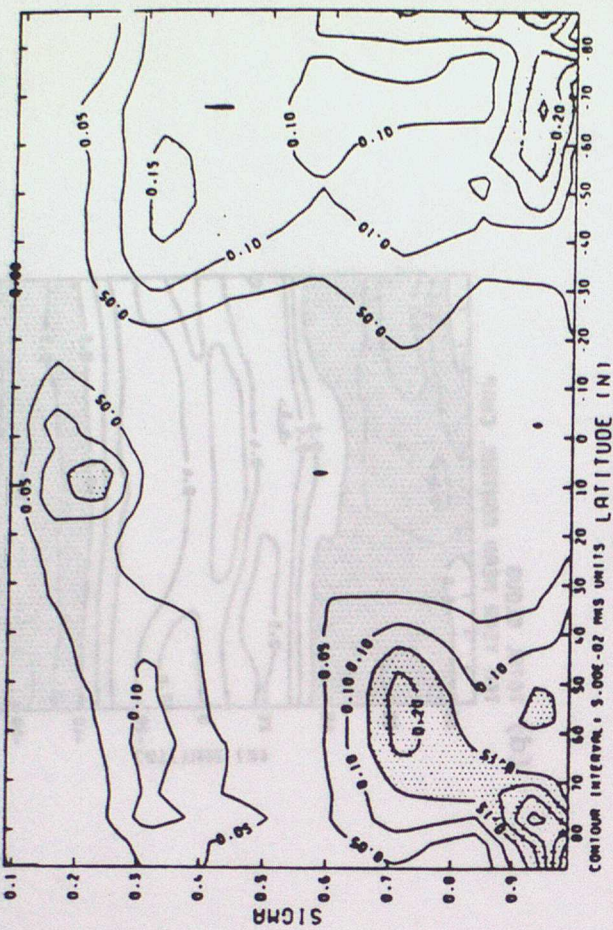
(a) SIGMA-LATITUDE CROSS-SECTION OF ZONAL MEAN LAYER CLOUD COVER
 CONTOURS EVERY 5%. VALUES OVER 15% STIPPLED
 TEN YEAR JULY MEAN RH



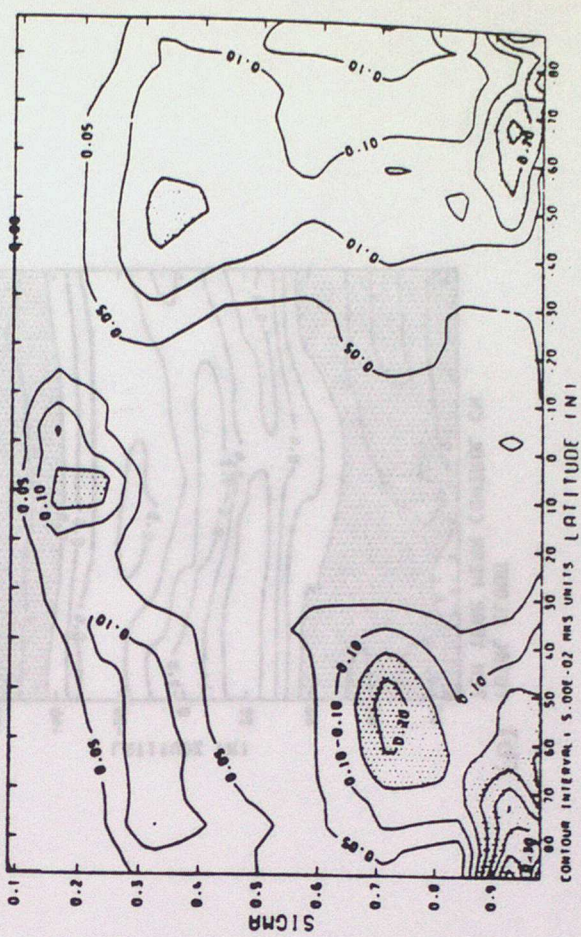
(c) SIGMA-LATITUDE CROSS-SECTION OF ZONAL MEAN LAYER CLOUD COVER
 CONTOURS EVERY 5%. VALUES OVER 15% STIPPLED
 TEN YEAR JULY MEAN CHH



(b) SIGMA-LATITUDE CROSS-SECTION OF ZONAL MEAN LAYER CLOUD COVER
 CONTOURS EVERY 5%. VALUES OVER 15% STIPPLED
 TEN YEAR JULY MEAN CH



(d) SIGMA-LATITUDE CROSS-SECTION OF ZONAL MEAN LAYER CLOUD COVER
 CONTOURS EVERY 5%. VALUES OVER 15% STIPPLED
 TEN YEAR JULY MEAN CHRP



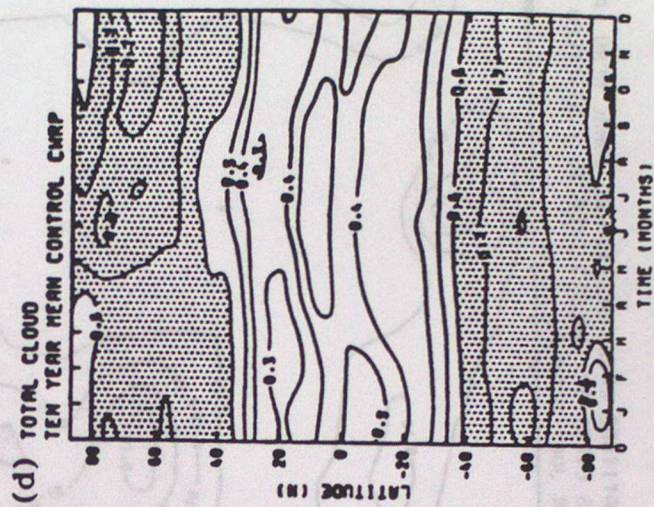
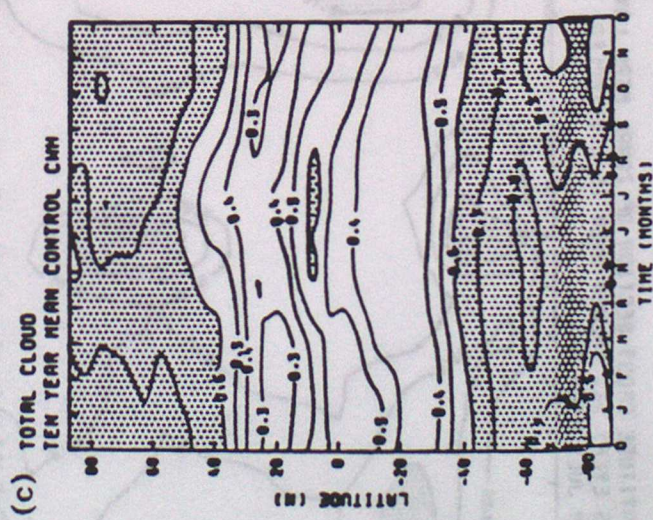
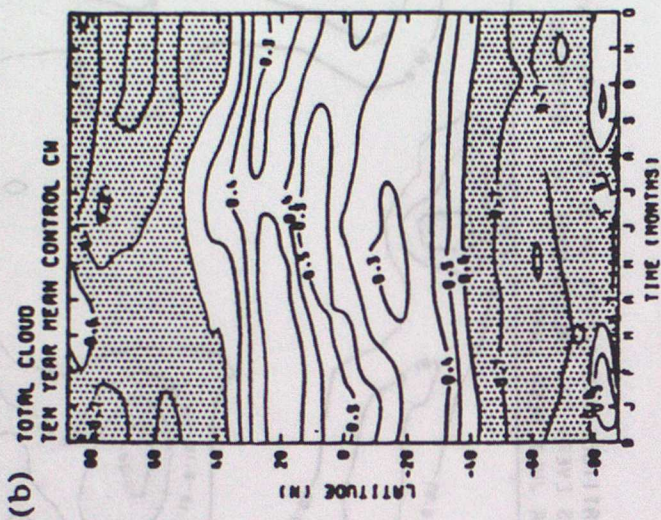
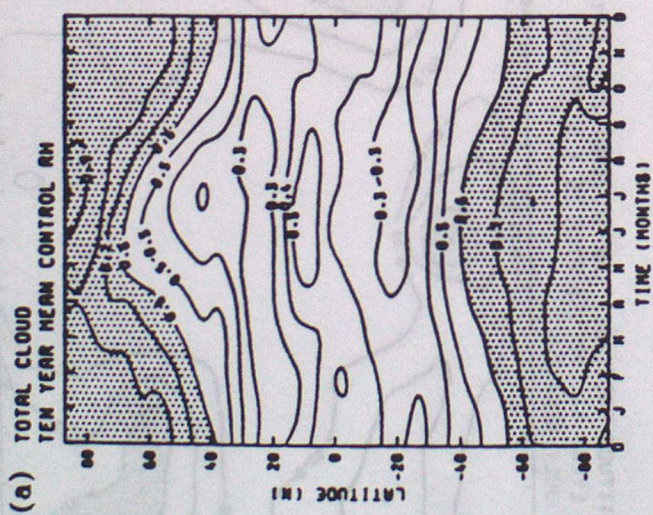


FIGURE 4

(a) OUTGOING LONGWAVE RADIATION

TEN YEAR JULY MEAN RH

CONTOURS EVERY 25 MM-2. STIPPLED BELOW 225 MM-2



(b) OUTGOING LONGWAVE RADIATION

TEN YEAR JULY MEAN CM

CONTOURS EVERY 25 MM-2. STIPPLED BELOW 225 MM-2



(c) OUTGOING LONGWAVE RADIATION

TEN YEAR JULY MEAN CWP

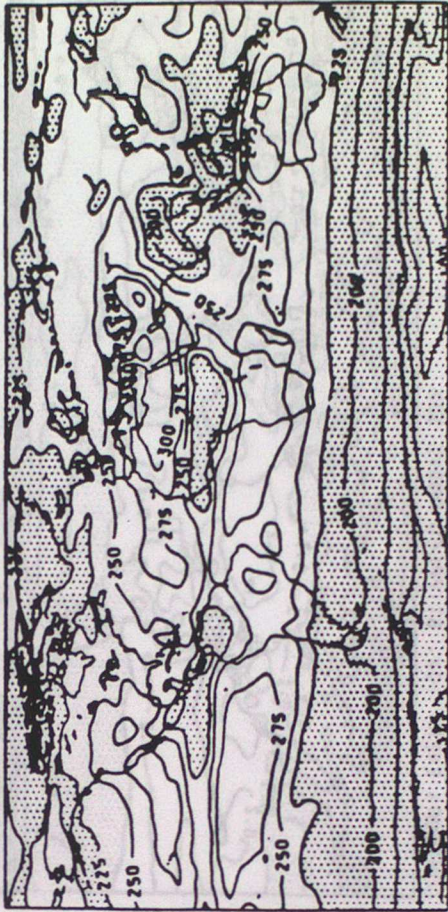
CONTOURS EVERY 25 MM-2. STIPPLED BELOW 225 MM-2



(d) OUTGOING LONGWAVE RADIATION

ERBE DATA FOR JULY 1985

CONTOURS EVERY 25 MM-2. STIPPLED BELOW 225 MM-2



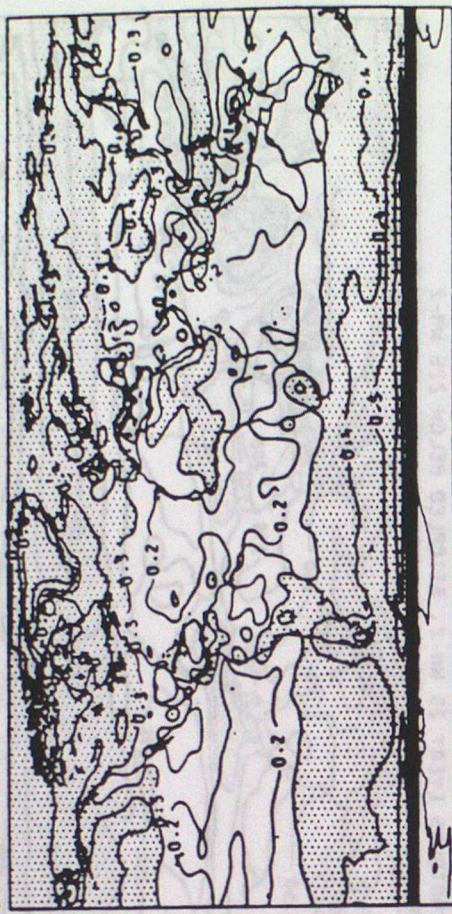
(a)

PLANETARY ALBEDO
TEN YEAR JULY MEAN AM
CONTOURS EVERY 10%. STIPPLED ABOVE 30%



(b)

PLANETARY ALBEDO
TEN YEAR JULY MEAN CM
CONTOURS EVERY 10%. STIPPLED ABOVE 30%



(c)

PLANETARY ALBEDO
TEN YEAR JULY MEAN CMRP
CONTOURS EVERY 10%. STIPPLED ABOVE 30%



(d)

PLANETARY ALBEDO
ERRA DATA FOR JULY 1985
CONTOURS EVERY 10%. SHADED ABOVE 30%

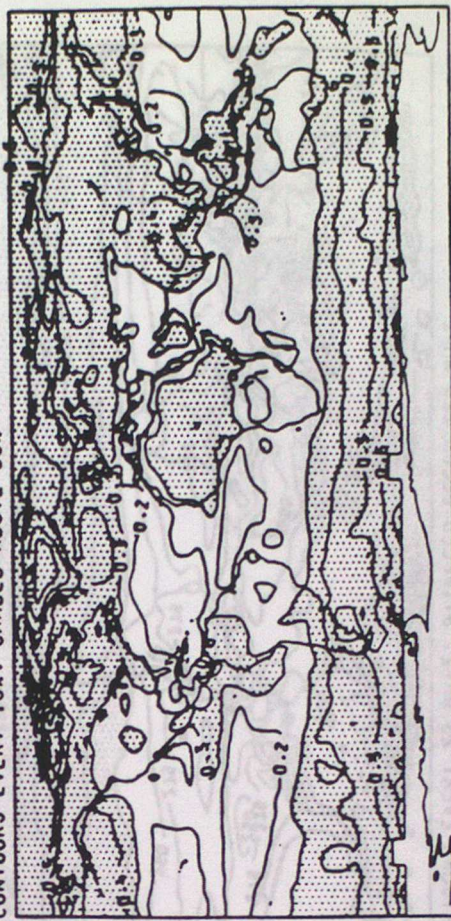


FIGURE 6

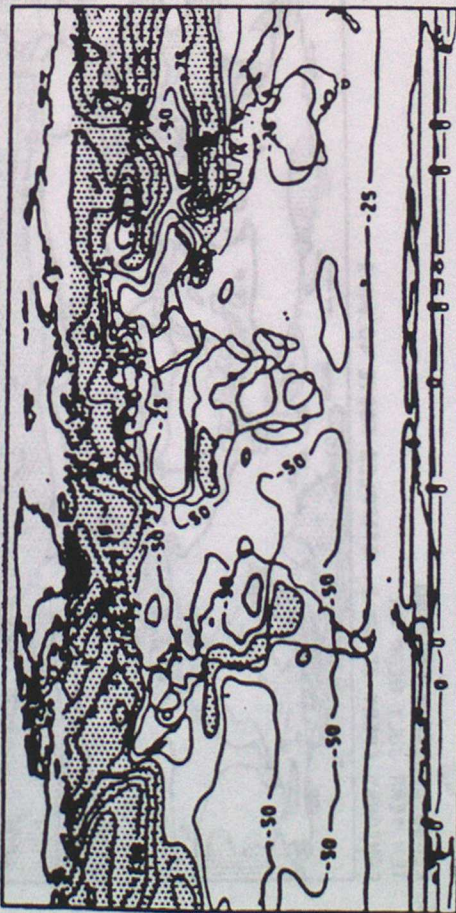
(a) CLOUD SHORTWAVE FORCING
TEN YEAR JULY MEAN RM
CONTOURS EVERY 25 MW-2. STIPPLED BELOW -75 MW-2



(b) CLOUD SHORTWAVE FORCING
TEN YEAR JULY MEAN CM
CONTOURS EVERY 25 MW-2. STIPPLED BELOW -75 MW-2



(c) CLOUD SHORTWAVE FORCING
TEN YEAR JULY MEAN CNRP
CONTOURS EVERY 25 MW-2. STIPPLED BELOW -75 MW-2

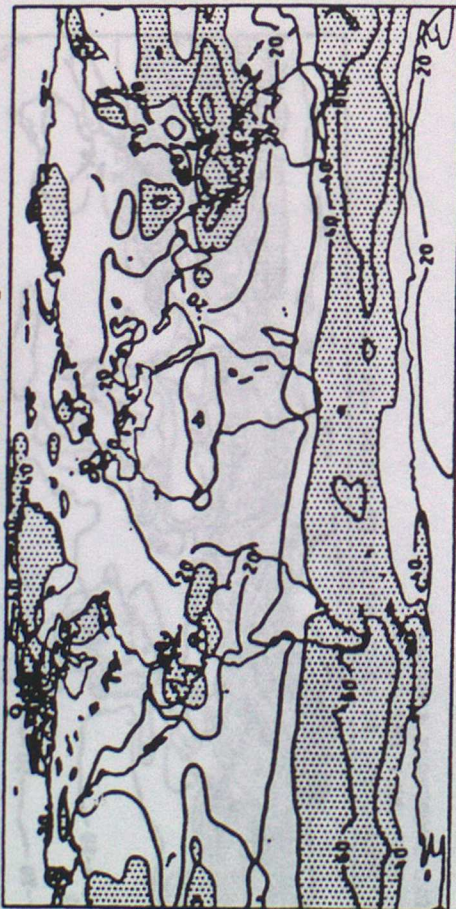


(d) CLOUD SHORTWAVE FORCING
ERBE DATA FOR JULY 1985
CONTOURS EVERY 25 MW-2. STIPPLED BELOW -75 MW-2



(a) CLOUD LONGWAVE FORCING
TEN YEAR JULY MEAN RH

CONTOURS EVERY 20 MM-2. STIPPLED ABOVE 40 MM-2



(b) CLOUD LONGWAVE FORCING
TEN YEAR JULY MEAN CM

CONTOURS EVERY 20 MM-2. STIPPLED ABOVE 40 MM-2



(c) CLOUD LONGWAVE FORCING
TEN YEAR JULY MEAN CHRP

CONTOURS EVERY 20 MM-2. STIPPLED ABOVE 40 MM-2

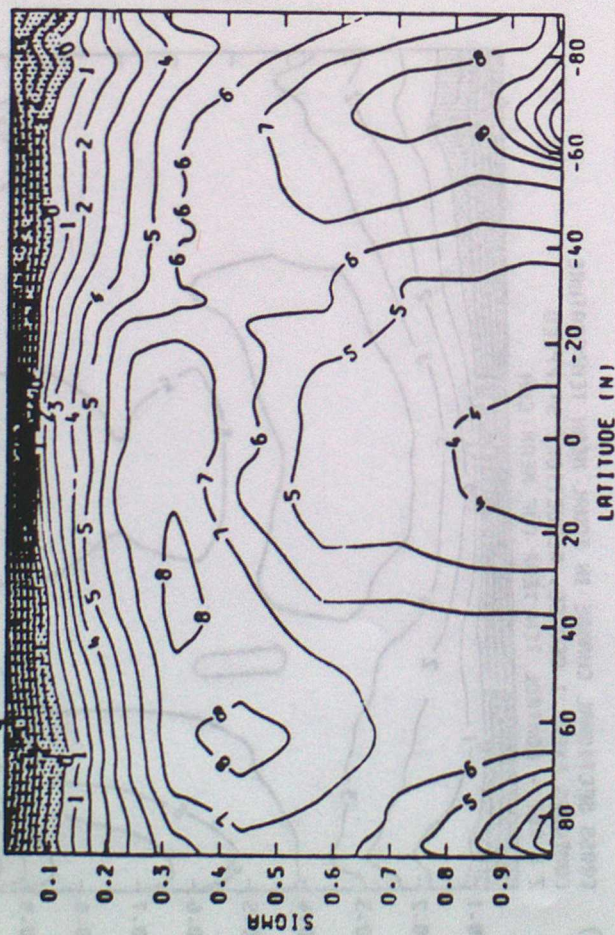


(d) CLOUD LONGWAVE FORCING
ERBE DATA FOR JULY 1985

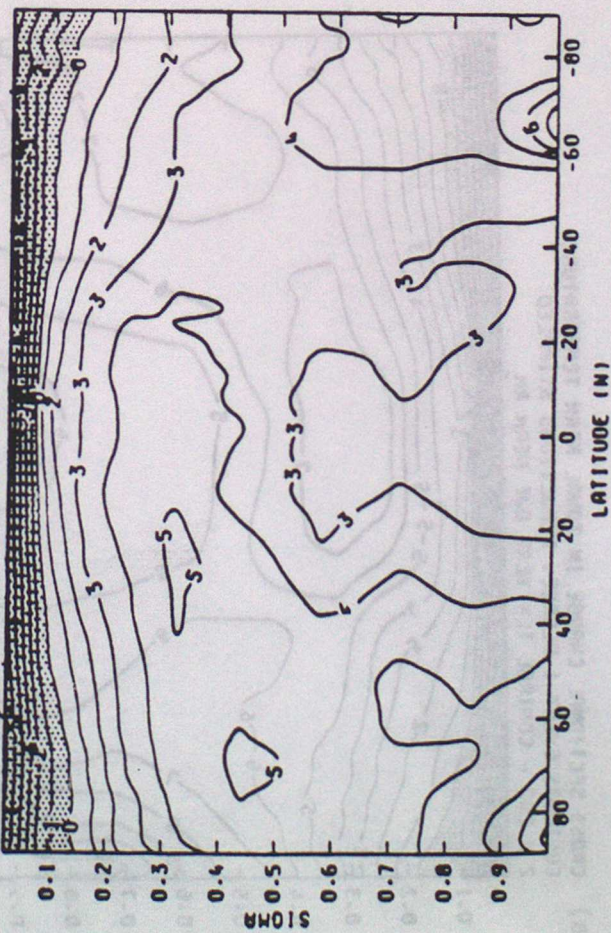
CONTOURS EVERY 20 MM-2. STIPPLED ABOVE 40 MM-2



(a) CROSS SECTIONAL CHANGE IN ZONAL MEAN TEMPERATURE
 CONTOURS EVERY 1 DEGREE. REDUCTIONS STIPPLED
 2 X CO₂ - CONTROL TEN YEAR JJA MEAN RH



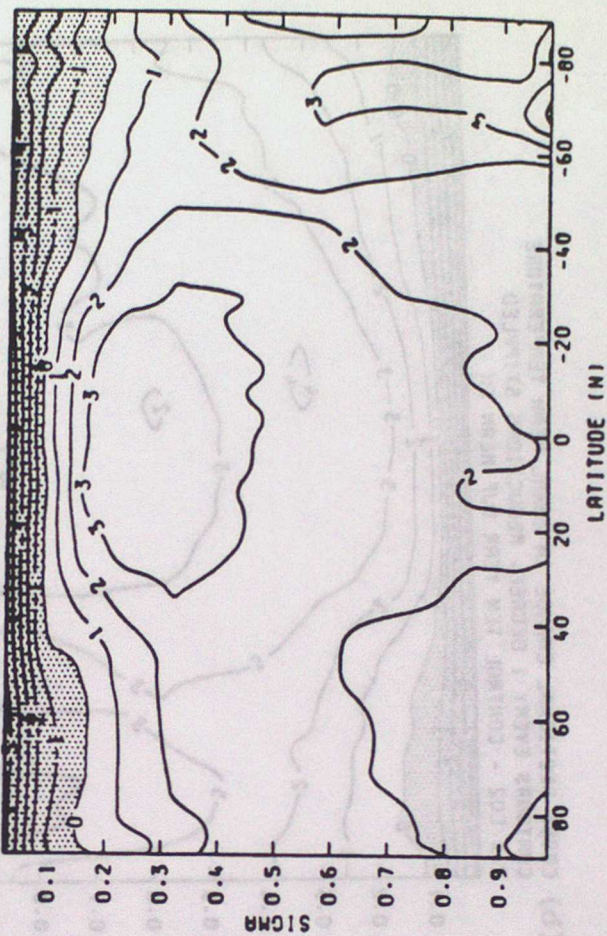
(c) CROSS SECTIONAL CHANGE IN ZONAL MEAN TEMPERATURE
 CONTOURS EVERY 1 DEGREE. REDUCTIONS STIPPLED
 2 X CO₂ - CONTROL TEN YEAR JJA MEAN CMH



(b) CROSS SECTIONAL CHANGE IN ZONAL MEAN TEMPERATURE
 CONTOURS EVERY 1 DEGREE. REDUCTIONS STIPPLED
 2 X CO₂ - CONTROL TEN YEAR JJA MEAN CM



(d) CROSS SECTIONAL CHANGE IN ZONAL MEAN TEMPERATURE
 CONTOURS EVERY 1 DEGREE. REDUCTIONS STIPPLED
 2 X CO₂ - CONTROL TEN YEAR JJA MEAN CNRP



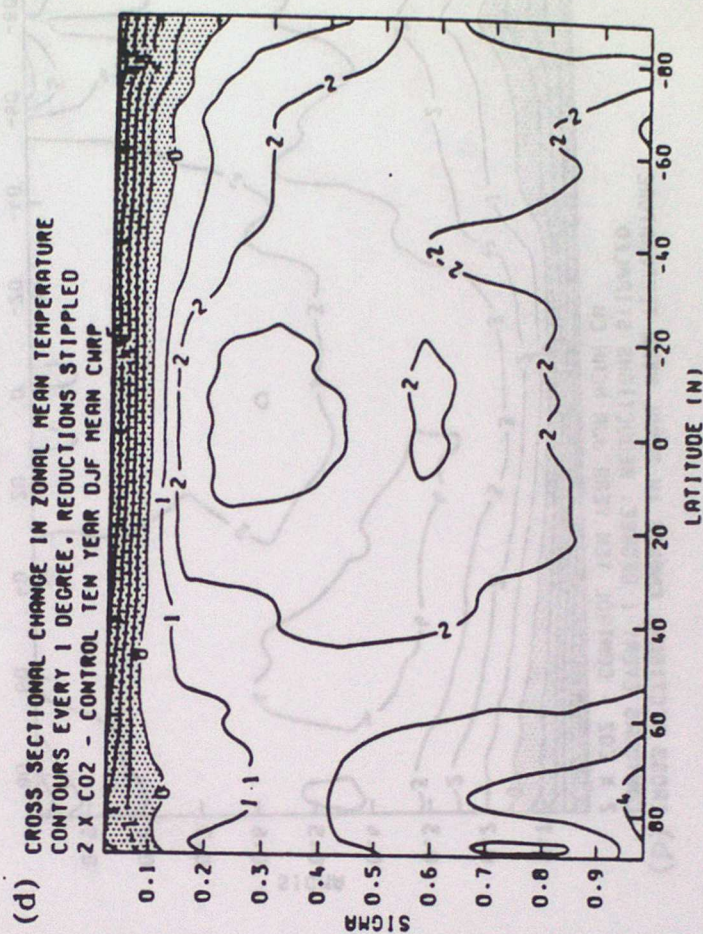
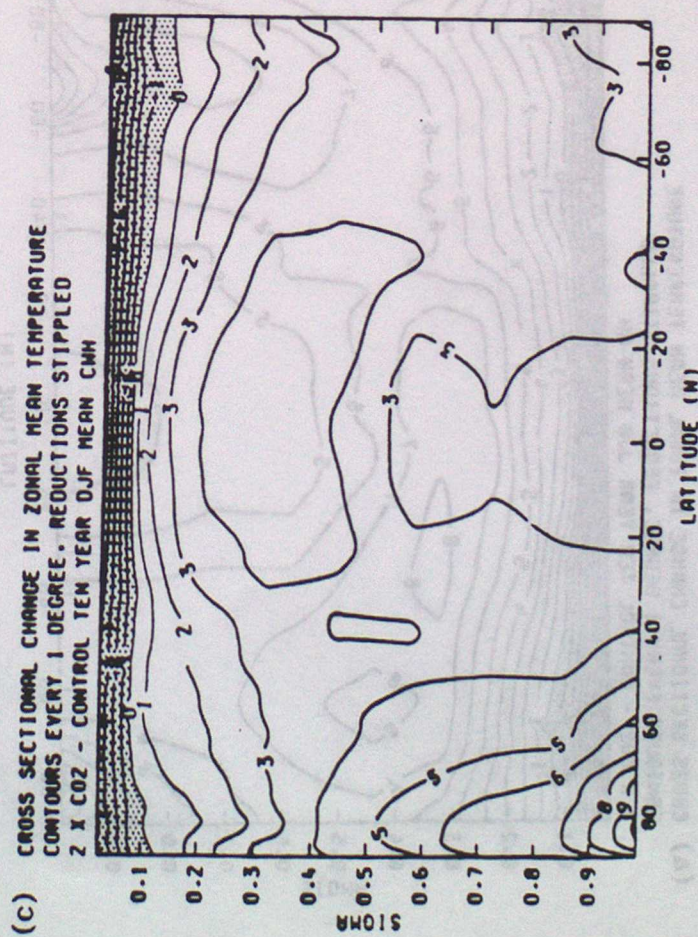
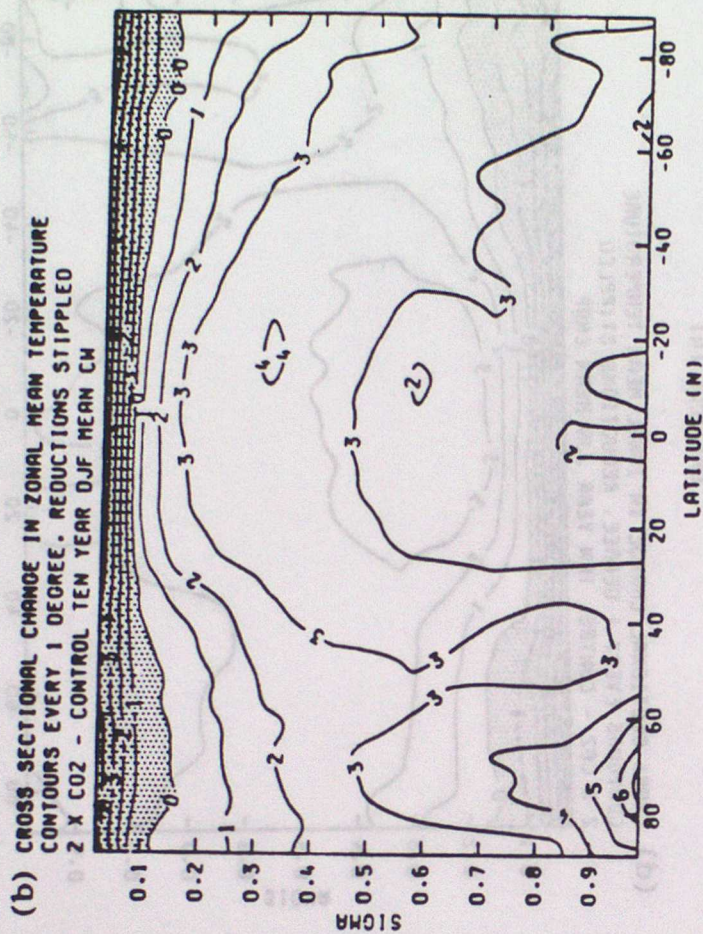
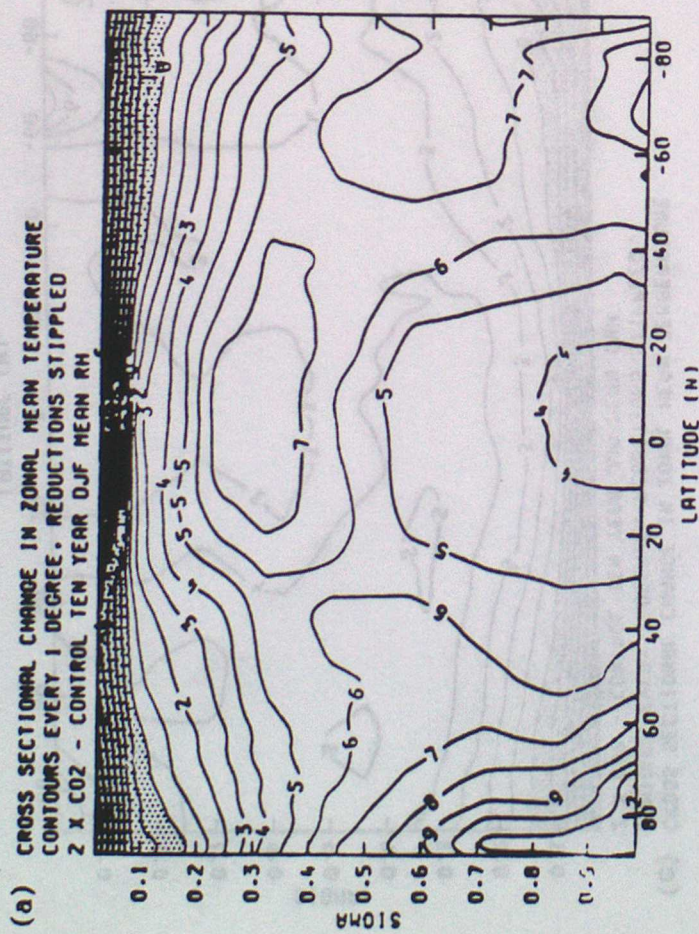
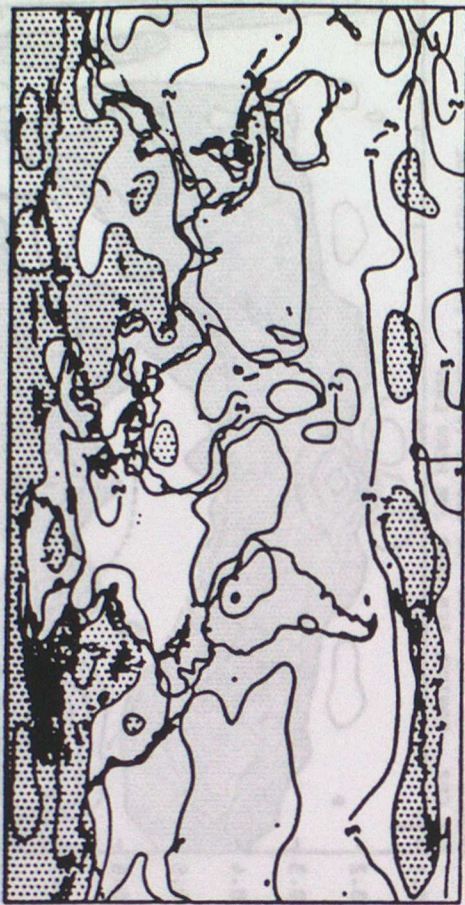


FIGURE 10

(a) SIMULATED ANNUAL MEAN EQUILIBRIUM CHANGE IN SURFACE TEMPERATURE DUE TO A DOUBLING OF CO₂ RH



(b) SIMULATED ANNUAL MEAN EQUILIBRIUM CHANGE IN SURFACE TEMPERATURE DUE TO A DOUBLING OF CO₂ CM



(c) SIMULATED ANNUAL MEAN EQUILIBRIUM CHANGE IN SURFACE TEMPERATURE DUE TO A DOUBLING OF CO₂ CMH



(d) SIMULATED ANNUAL MEAN EQUILIBRIUM CHANGE IN SURFACE TEMPERATURE DUE TO A DOUBLING OF CO₂ CMRP



FIGURE 11

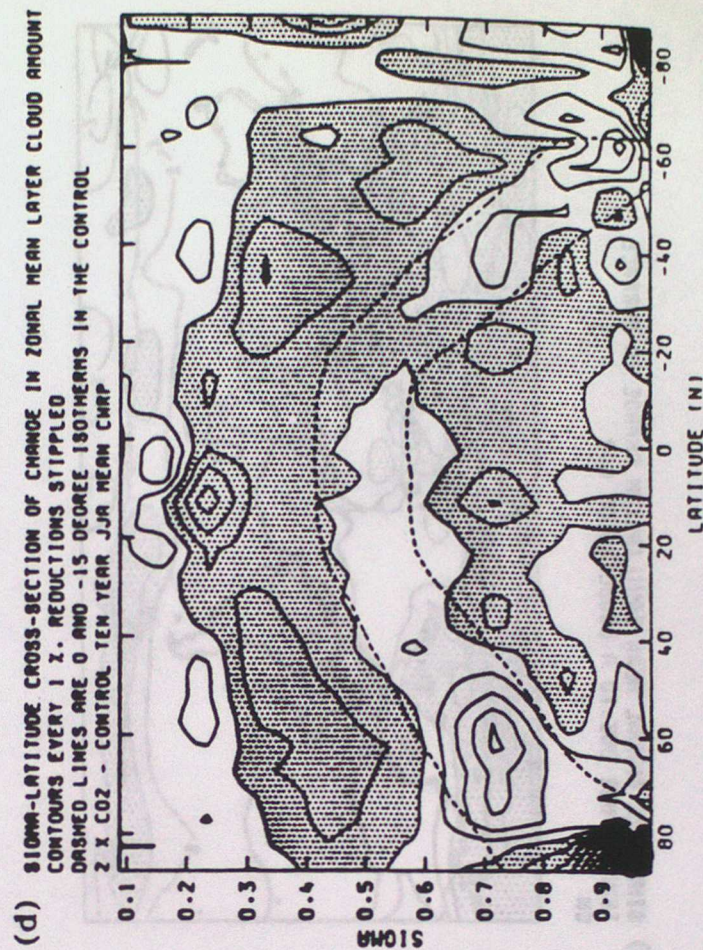
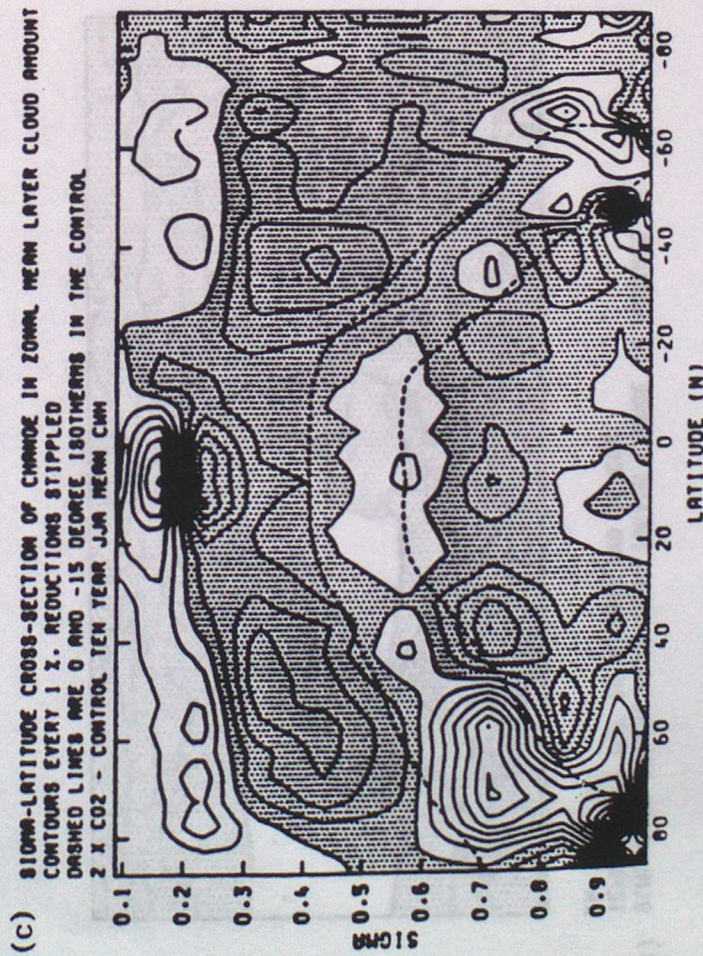
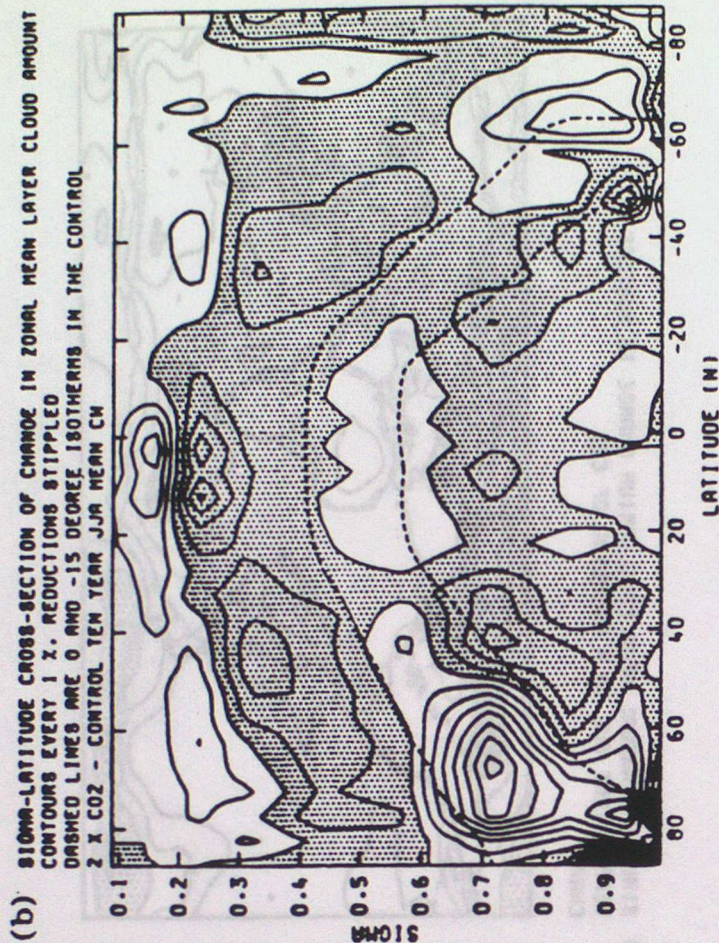
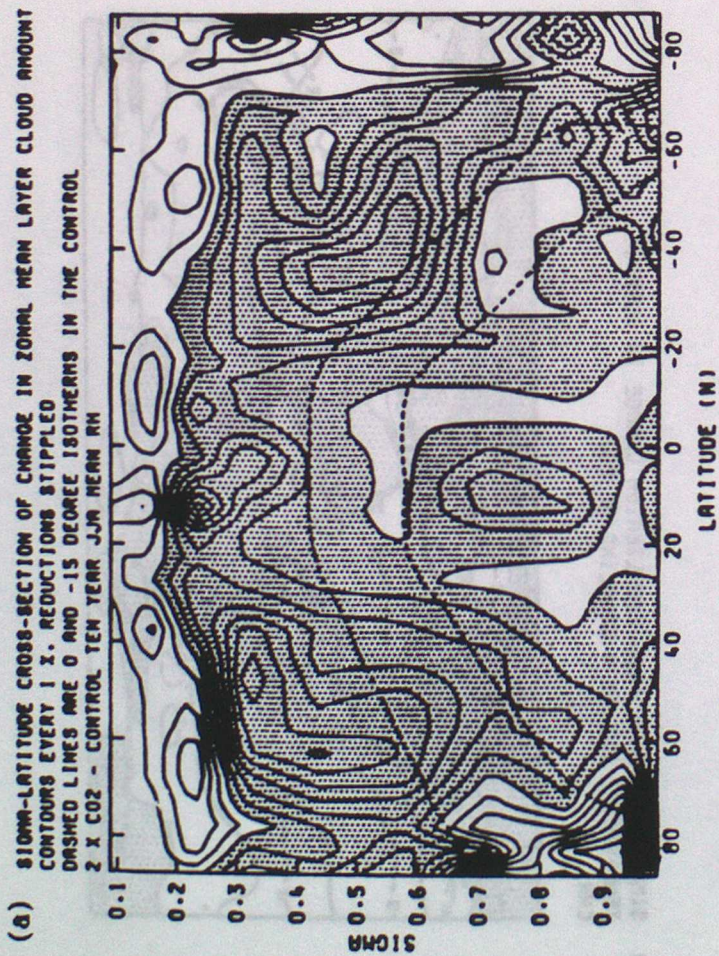


FIGURE 12

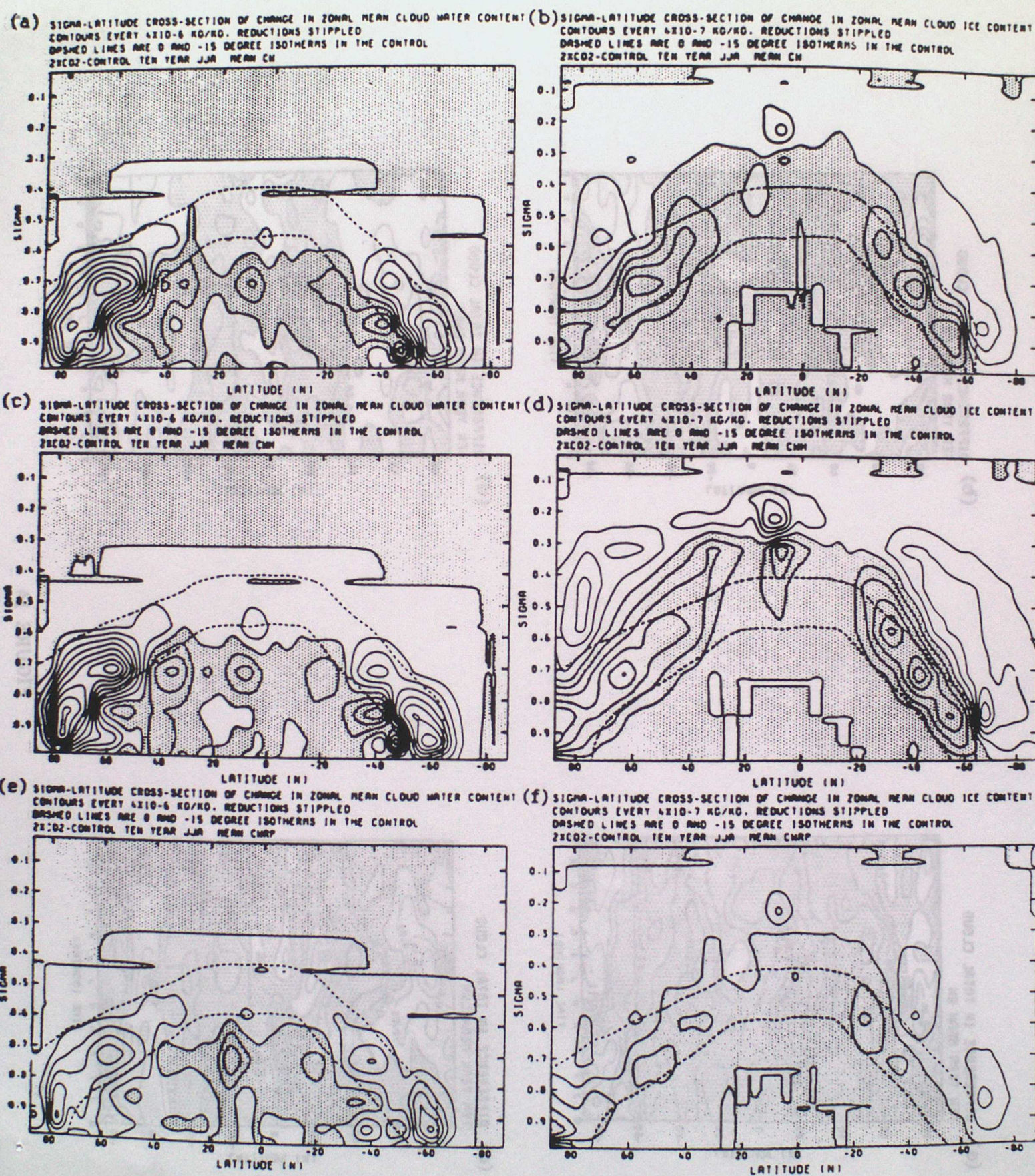


FIGURE 13

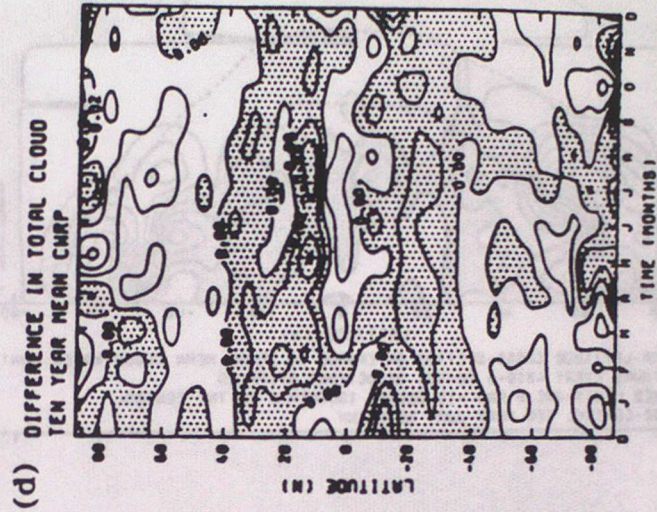
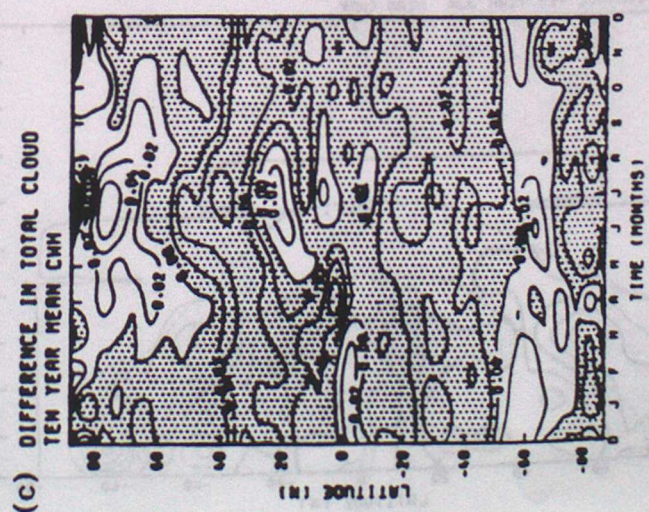
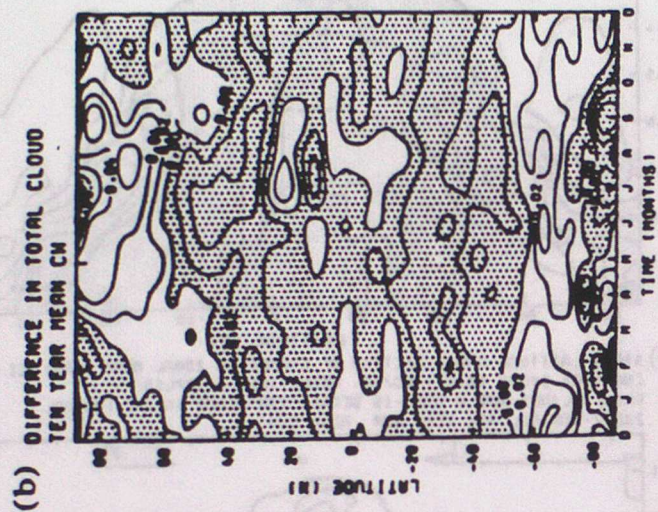
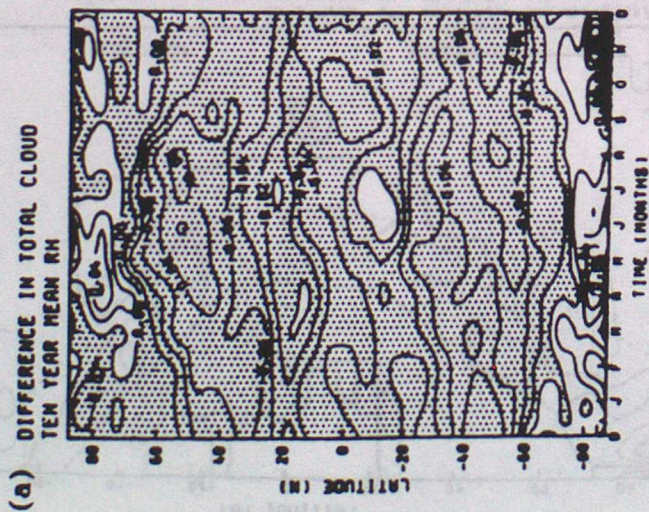


FIGURE 14

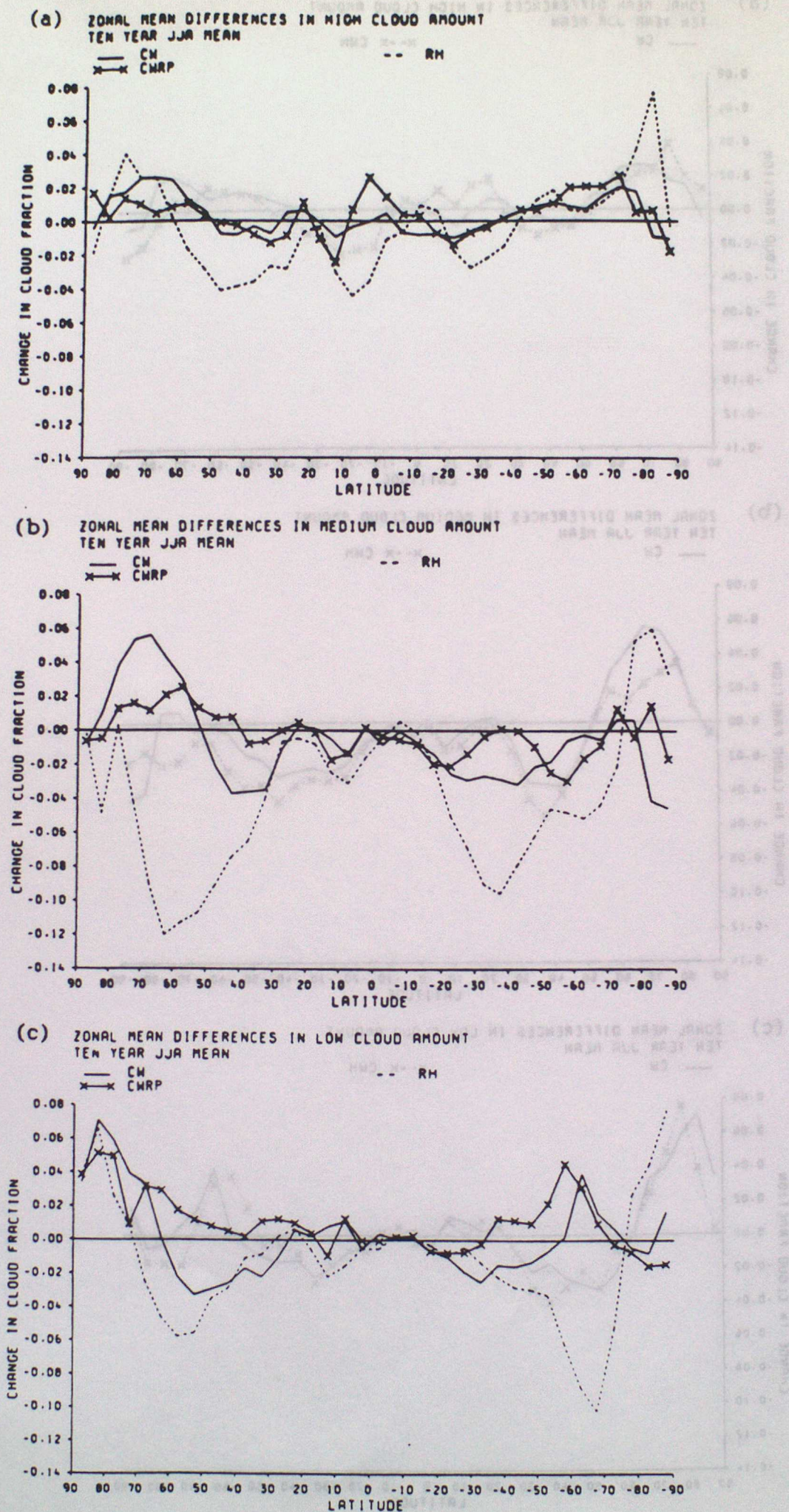
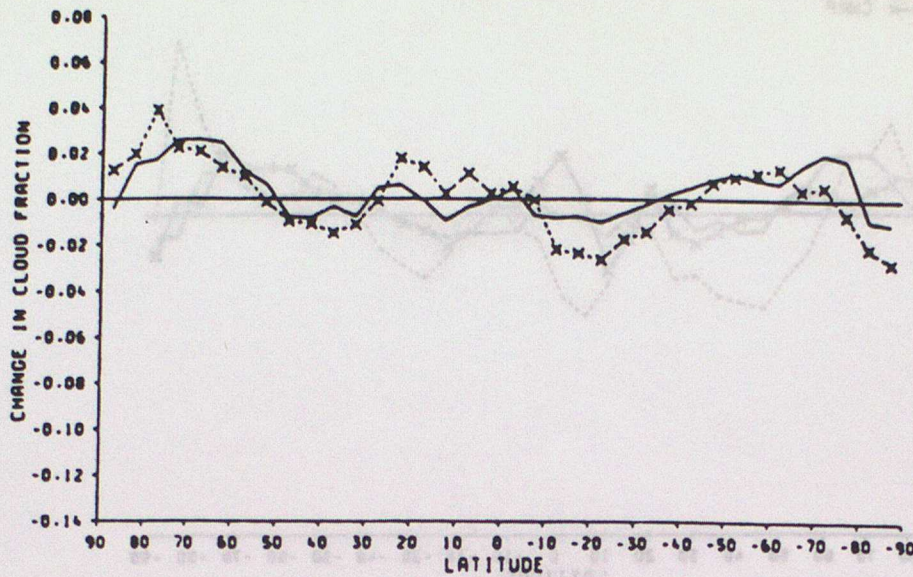
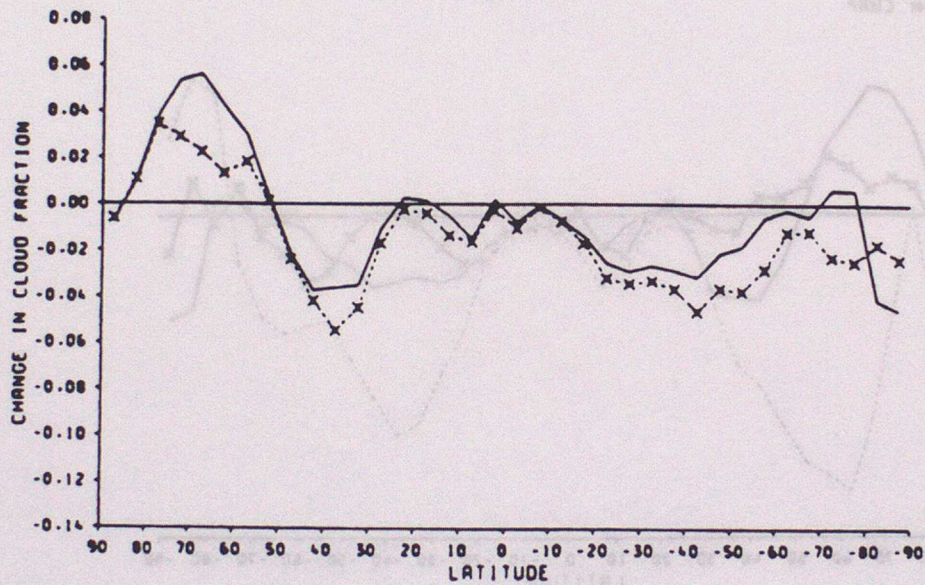


FIGURE 15

(a) ZONAL MEAN DIFFERENCES IN HIGH CLOUD AMOUNT
TEN YEAR JJA MEAN
— CM
x--x CWH



(b) ZONAL MEAN DIFFERENCES IN MEDIUM CLOUD AMOUNT
TEN YEAR JJA MEAN
— CM
x--x CWH



(c) ZONAL MEAN DIFFERENCES IN LOW CLOUD AMOUNT
TEN YEAR JJA MEAN
— CM
x--x CWH

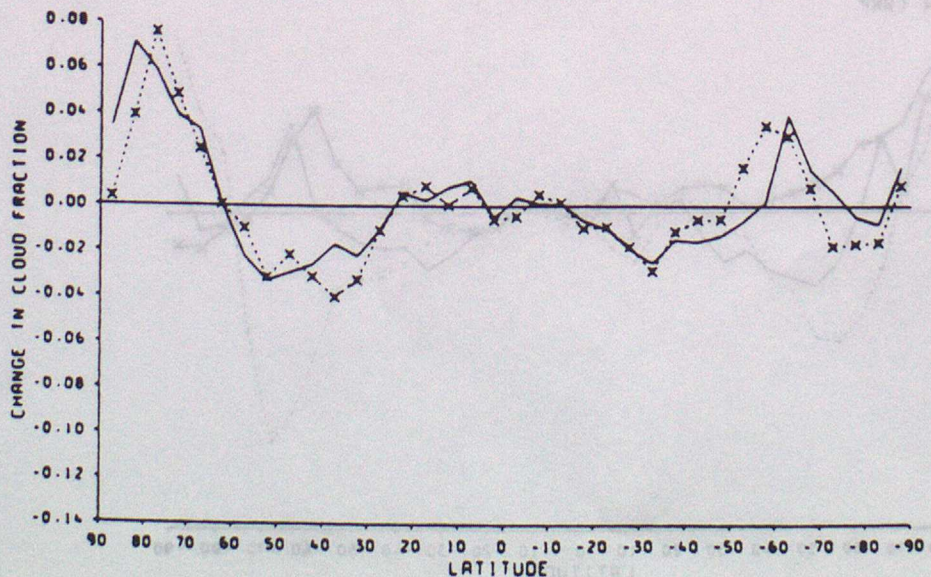
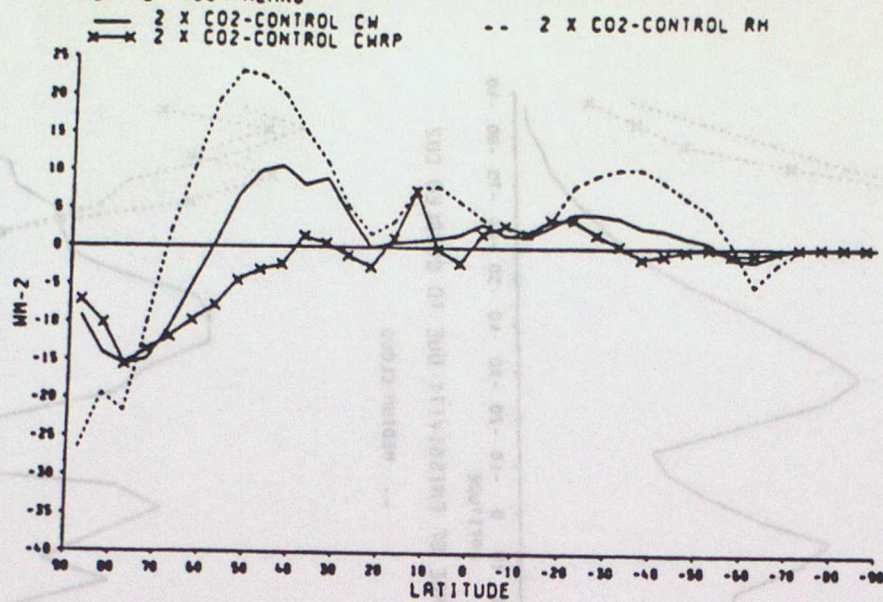
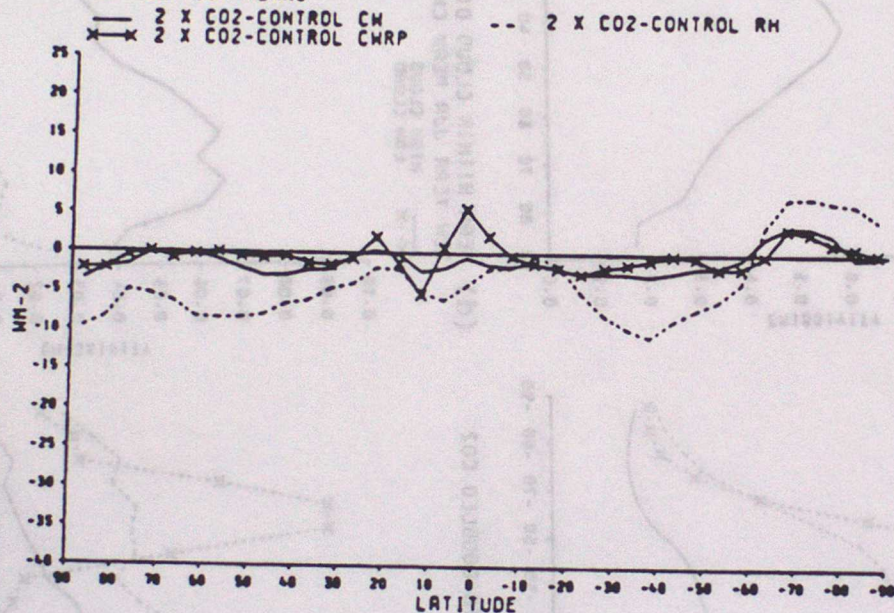


FIGURE 16

(a) ZONAL MEAN DIFFERENCES IN CLOUD SHORTWAVE FORCING
TEN YEAR JJA MEANS



(b) ZONAL MEAN DIFFERENCES IN CLOUD LONGWAVE FORCING
TEN YEAR JJA MEANS



(c) ZONAL MEAN DIFFERENCES IN CLOUD NET FORCING
TEN YEAR JJA MEANS

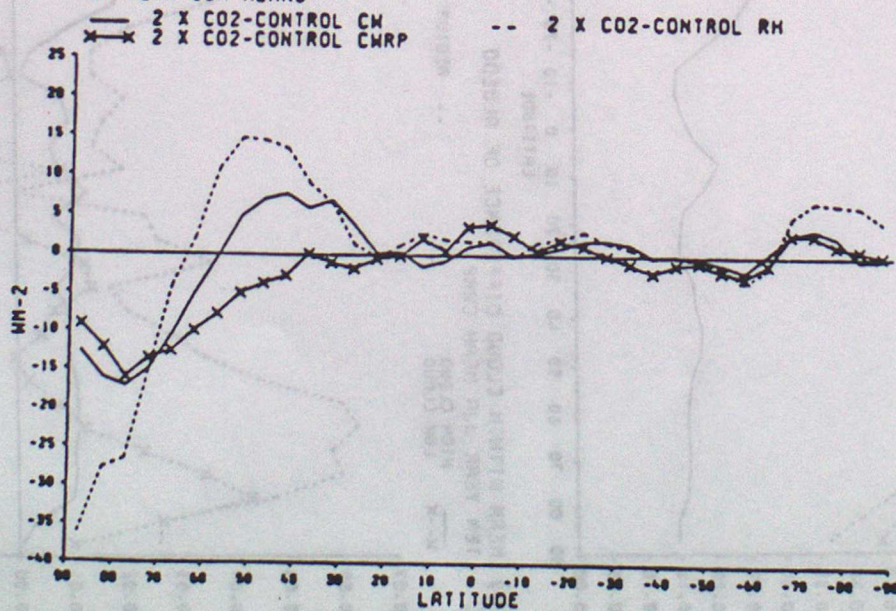
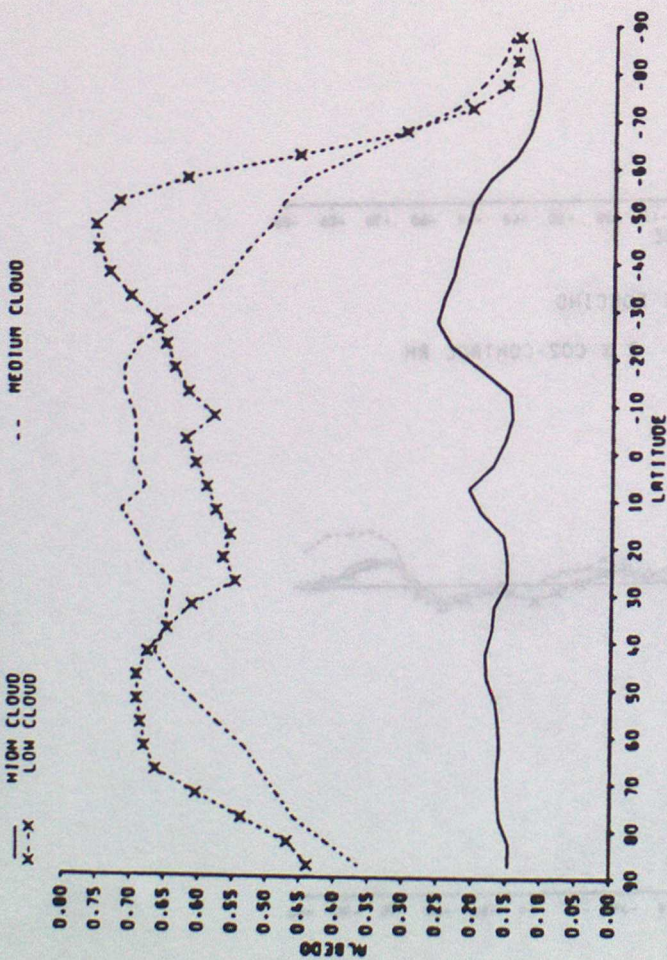
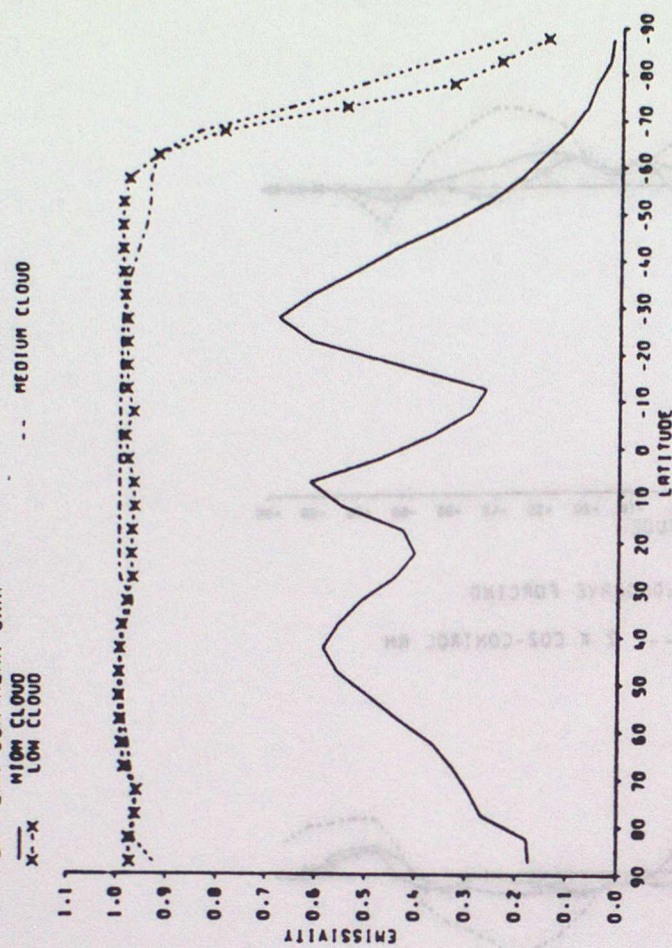


FIGURE 17

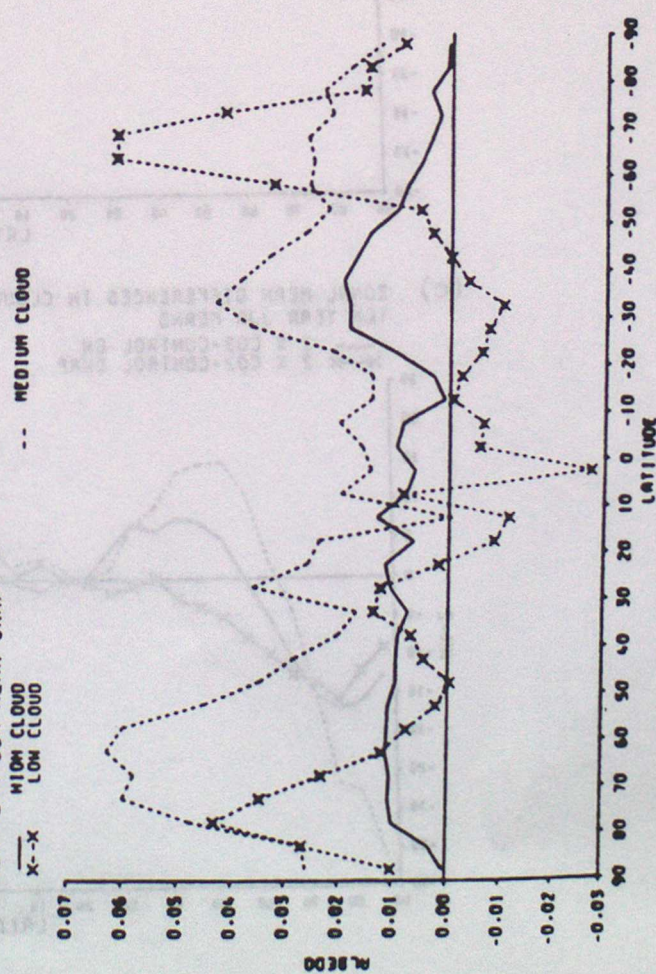
(a) MEAN WITHIN CLOUD ALBEDO
TEN YEAR JJA MEAN CHRP



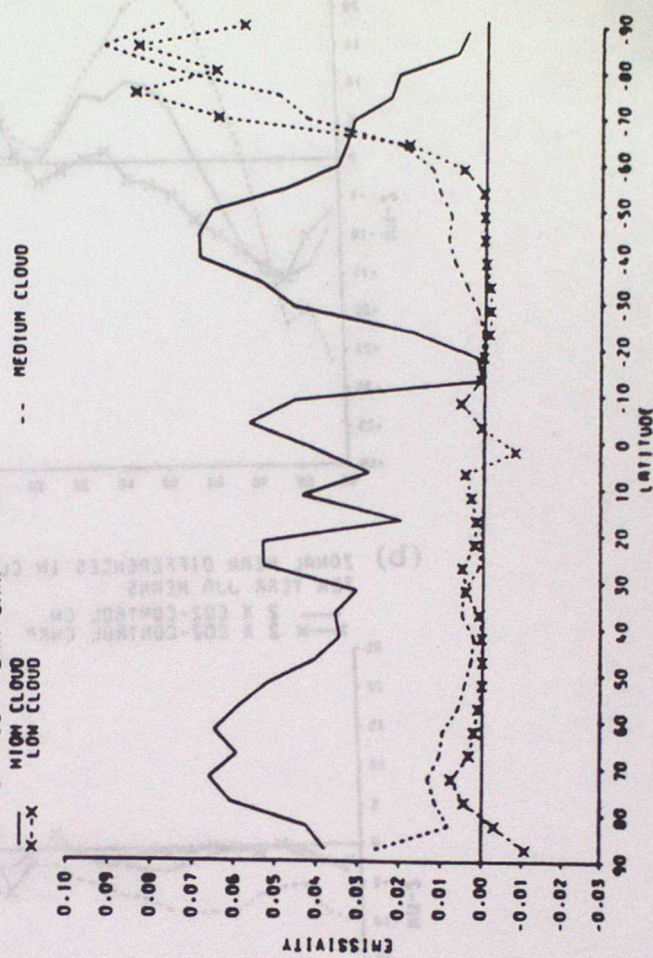
(b) MEAN WITHIN CLOUD EMISSIVITY
TEN YEAR JJA MEAN CHRP



(c) MEAN WITHIN CLOUD DIFFERENCE OF ALBEDO
TEN YEAR JJA MEAN CHRP



(d) MEAN WITHIN CLOUD DIFFERENCE OF EMISSIVITY DUE TO DOUBLED CO2
TEN YEAR JJA MEAN CHRP



CHAPTER 3

A COMPARISON OF THE SIMULATION OF CLOUD AND RADIATION IN FOUR VERSIONS OF
THE UKMO MODEL AND THE LMD MODEL

BY

C A SENIOR, H LE TREUT AND Z-X LI

Introduction

The importance of cloud feedback on the sensitivity of General Circulation Models (GCM's) has been the subject of much recent work (eg. Cess et al 1990, Mitchell et al 1989). A comparison of the cloud feedback from 19 GCM's showed that even in models with similar cloud parametrizations the sensitivity varied greatly (Cess et al 1990). Mitchell et al (1989) showed that the introduction of interactive cloud radiative properties into their model with a prognostic cloud water scheme reduced its sensitivity by 30%. It is constructive to try and understand the differences in the cloud parametrizations which force the models to behave differently and to compare the simulations of cloud and radiation from the models with satellite data. In the longer term, this type of comparison should help to determine whether the most important cloud processes are being correctly modelled.

In this paper we aim to discuss the different sensitivities of two GCM's from The Hadley Centre for Climate Prediction and Research at the Meteorological Office, U.K (UKMO) and the Laboratoire de Meteorologie Dynamique (LMD), France and to relate these differences to the detailed parametrizations and responses of clouds in each model. Four versions of the UKMO model with different cloud schemes were used and one version of the LMD model.

1. The Models

(a) UKMO

The four versions of the UKMO model are described by Senior and Mitchell (this volume), with particular reference to the cloud parametrization schemes used. All have a horizontal resolution of $5^\circ \times 7.5^\circ$ Latitude/Longitude and 11 vertical sigma (=pressure/surface pressure) levels. The timestep is 20 minutes in each case. All the models consist of an atmospheric model coupled to a simple 50m thermodynamic mixed layer (or 'slab') ocean which has a fixed oceanic heat convergence intended to represent the transfer of heat by dynamical oceanic currents (see for example Wilson and Mitchell 1987).

Three of the models (referred to as CW, CWH and CWRP, see Senior and Mitchell (this volume) for a full explanation of these) use a prognostic

cloud water parametrization which is based on that of Smith (1990). The other version (RH) uses a relative humidity based cloud scheme (See Mitchell and Ingram (1991))

(b) LMD

The LMD model used is that described by Li (1990) based on the standard version of the LMD model (Sadourny and Laval 1984) with a cloud parametrization scheme based on that of Le Treut and Li (1988,1991). The model has a horizontal resolution of $5.0^\circ \times 7.5^\circ$ latitude/longitude and 11 vertical levels and is integrated with a timestep of 30 minutes. This model consists of an atmospheric component only with prescribed climatological Sea Surface Temperatures (SST'S)

2. The cloud schemes

Below is a brief description of the cloud parametrization scheme of Le Treut and Li (1988, 1991) (described in more detail by Le Treut and Li (1991)) and the way in which it differs from that of Smith (1990) (discussed in more detail by Senior and Mitchell, this volume). For the specific values of the tunable parameters used in the runs shown below see Li (1990).

In the scheme of Le Treut and Li (1988, 1991) the cloud water content, q_1 , is included as a prognostic variable of the model and is predicted according to the equation

$$\frac{\delta q_1}{\delta t} + V \cdot \nabla q = C - E - P$$

where C,E and P are condensation, evaporation and precipitation respectively and q_1 is the cloud water content in Kg Kg^{-1} .

Condensation occurs due to supersaturation and convection and evaporation occurs when cloud water is predicted in areas of non-saturation until the model reaches saturation. Importantly, the production of condensed water by convection is calculated by the convection schemes and input directly into equation (1). In Smith's scheme the production of condensed water by convection is ignored and there is no direct effect of convection on the cloud water. The two conserved variables in the scheme are the total

water content q_t and the ice/liquid water temperature T_i which are defined by,

$$q_t = q + q_i$$

$$T = T - \frac{L_i}{\bar{C}_p}$$

Smith (1990) obtains a fractional cloudiness by utilising the statistical approach of Sommeria and Deardorf (1977) for the distribution of the conserved variables. Le Treut and Li (1988) take a more simplified approach by assuming that the predicted model temperature, T , does not vary within a grid box and that the total water content, q_t , has a uniform distribution between $q_t + \Delta q$ and $q_t - \Delta q$.

Then, taking q_s to be the saturation water vapour mixing ratio at temperature T , the cloud cover, or fraction of the grid box in which condensation occurs is denoted by f , where

$$f = \frac{q_t + \Delta q - q_s}{2\Delta q}$$

and $0 \leq f \leq 1$. Δq is taken to be;

$$\Delta q = a q_t$$

where a is tunable parameter.

For the purposes of precipitation both schemes aim to take into account cloud microphysics in some simplified way, and in particular the well known Bergeron process (eg. Mason 1957) that implies that cloud ice precipitation is more efficient than cloud water precipitation. For the precipitation of cloud liquid water both schemes use the ideas of Sundqvist (1978) although the tunable constants are set to different values. The version of the LMD model described here also uses the Sundqvist formula for cloud ice precipitation. In this model the cloud top is defined as the level where the downward accumulated liquid (or ice) water content is greater than a critical value. The ice-cloud regime is then separated from the water-cloud one when the cloud top temperature is colder than -10°C . Smith uses a different formulation for cloud ice precipitation that implies an order of

magnitude greater rate of precipitation for ice than water. The transition zone from water-cloud to ice-cloud is set from 0°C to -15°C by the atmospheric local temperature not the cloud top temperature as in the LMD model. In the UKMO CWH model, Smith's scheme is enhanced by the use of the empirical relationship between cloud ice fallspeed and cloud ice content documented by Heymsfield (1977).

In the LMD model, the shortwave cloud radiative property is characterized by the cloud optical thickness (τ) which is deduced from the liquid (or ice) water content by the following formula

$$\tau = \frac{3}{2} \frac{W}{r_e}$$

where r_e , the effective radius of cloud droplets is empirically related to the liquid water content. In the CWRP model, the shortwave albedo, transmissivity and absorptivity are obtained as functions of the cloud water path and solar zenith angle (see Senior and Mitchell, this volume).

In both the LMD and CWRP models, the longwave emissivity ϵ is given by

$$\epsilon = 1 - e^{(-xW)}$$

where x is the absorption coefficient. In the CWRP model, x is taken as $0.13 \text{ m}^2 \text{g}^{-1}$ for water cloud and $0.065 \text{ m}^2 \text{g}^{-1}$ for ice cloud. In the LMD model, x is kept constant as $0.13 \text{ m}^2 \text{g}^{-1}$ for both ice and water cloud. In the other three UKMO models the cloud radiative properties are kept fixed.

Thus, to summarise, the main differences between the two cloud parametrization schemes are;

- (a) the direct relationship between the convection schemes and the cloud water content in the LMD model,
- (b) the difference in precipitation of cloud water and cloud ice.
- (c) the manner in which the cloud radiative properties are specified.

3. A comparison of the present day climates of the UKMO and LMD models.

The emphasis of the comparison will be on cloud, radiation and related variables although some low level and surface variables will also be considered. A more detailed discussion of the climatology of the UKMO models in terms of cloud and radiation is given by Senior and Mitchell (this

volume). All the results from the UKMO models are means over the last 10 years from 15 year integrations and the LMD results are from a 15 month integration (Li (1990), from which many of the charts are reproduced).

3.1 Temperature

Figures 1 and 2 show zonally averaged height-latitude cross-sections of temperature from the five models and a 1958-1973 climatology from Oort (1983). The troposphere is, on average, too cold in all cases, a deficiency common to many models of this resolution. This is particularly evident over the winter pole, again true in many comparable models. Stratospheric polar temperatures are also too cold in all the models especially in winter which is probably partly due to the low vertical resolution. Li (1990) suggests that some of the errors in the LMD model may be explained by the lack of parametrization of gravity waves. A version of the LMD model which includes a parametrization of gravity wave drag shows a reduction in the winter stratospheric cooling. However, a higher resolution version of the UKMO CWH model which also incorporates a parametrization of gravity wave drag (Palmer et al 1986) shows similar systematic errors in polar and tropospheric temperatures to those at lower resolution (Senior and Mitchell, in preparation). Otherwise all the models show a reasonable simulation of zonally averaged temperature.

3.2 Mean Sea Level Pressure (PMSL)

All the models show qualitatively similar patterns of the zonally averaged time evolution of PMSL (Figure 3). In DJF, there is low pressure at mid-high northern latitudes ($60-90^{\circ}$ N) which arises from the dominant Aleutian and Icelandic low pressure systems in winter. All the models simulate the sub-tropical high pressure systems at $20-40^{\circ}$ N reasonably well, but in the tropics the UKMO models have lower pressures than the LMD model. The DJF Southern Hemisphere circumpolar trough is not at all well represented in any of the models, with very weak gradients at around 60° S. The UKMO models have higher pressure over the poles than the LMD model.

In JJA the UKMO models show pressures greater than 1010 mb polewards of 40° N which are likely to be higher than observed and are certainly greater than those in the LMD model. At lower latitudes there is generally low pressure which arises from the continental heat lows dominating the weakened sub-tropical highs over the oceans. There is still low pressure at low

latitudes. The Southern Hemisphere sub-tropical highs are well simulated in all models and the Southern Hemisphere circumpolar trough is better represented although still too weak in all the models. Once again the pressure over the poles is greater in the UKMO models.

3.3 Top of the Atmosphere Radiation (TOA)

All of the models show a good simulation of the net TOA radiation with sources of energy at low latitudes and sinks at high latitudes and a net storage of heat in the summer hemisphere and a net loss of heat in the winter hemisphere (Figure 4). In RH and LMD there are quantitative differences from climatology in the Northern Hemisphere summer by around 20 Wm^{-2} representing too large a storage of heat. This is better simulated by the UKMO cloud water models. All the models show too little heat storage at low latitudes in spring and autumn by up to 10 Wm^{-2} . In both hemispheres in summer, the UKMO models show a heating over the entire hemisphere including the pole of up to 60 Wm^{-2} , whereas both the LMD model and data from the NIMBUS 6 satellite (Stephens et al 1981) indicate a cooling of both poles throughout the year.

3.4 Cloud

Figures 5 and 6 show graphs of zonally averaged total cloud amount from the four UKMO models (Part (a)), and the LMD model and the observational retrievals for 1979 from Hughes and Henderson-Sellers (1985) (Part (b)). Both RH and LMD show excessive cloud at high latitudes in both seasons, when compared to the observations with cover exceeding 80% polewards of 60° in the winter hemisphere. The UKMO cloud water models show less high latitude cloud cover although there is probably still too much cloud in Northern winter, especially over the continents. The vertical distributions of layer cloud (Figures 7 and 8) are similar in LMD and RH with greater than 15% cover over both poles at all levels in both seasons. In the LMD model in southern summer there are large areas of greater than 35% cover below 500mb. The UKMO cloud water models show much less overall cloud cover at high latitudes, especially at mid and upper levels with cloud increasing in summer over the poles as is observed (Vowinckel and Orvig 1970). At sub-tropical latitudes all the models show too little low cloud which is likely to be due to the problem of simulating marine stratus and RH, CW and CWRP all show perhaps

too little tropical high cloud.

The different amounts of predicted cloud cover arise from the different way that ice and water cloud are treated in the models (For the UKMO models this is discussed in detail by Senior and Mitchell (this volume)). Although ice cloud is allowed to precipitate earlier than water cloud in the LMD model, the rate of precipitation is not changed. This, then, allows more cloud to exist at colder temperatures than in the UKMO cloud water models (CW, CWH and CWRP), where ice cloud precipitates at an order of magnitude greater rate than water cloud. In RH there is no distinction between ice and water clouds and so cold cloud does not dissipate as fast as in the other UKMO models. Thus the differences in cloud cover in the various models do not arise through tuning but because of different assumptions about ice/water partitioning and precipitation. This reflects particularly the crucial importance of cirrus cloud physics

3.5 Cloud Water Content

All the UKMO models have very similar values of zonally averaged vertically integrated cloud water content, q_1 (Figure 9(a)) but the cloud water content in the LMD model is substantially lower than that in any of the three UKMO cloud water models in both seasons with the maximum values of q_1 being about half those in the UKMO models. (Figure 9(b), here CW only shown for comparison). Figure 9(b) also shows observed Scanning Multichannel Microwave Radiometer (SMMR) data (redrawn from Njoku and Swansen 1983). The UKMO models compare reasonably well at most latitudes (see also Smith 1990) but the LMD values are very much lower. Li (1990) concludes that the LMD values of cloud water content are only half that of the SMMR data. It should be noted that the amount of cloud water is crucially dependent on the assumptions used for precipitation and that it is possible to produce realistic cloud water contents in the LMD model by adjusting these assumptions. This type of 'tuning' also affects the cloud amount although to a lesser degree. There are no observations to compare the vertical structure of the models, which are all qualitatively similar in both seasons (Figures 10 and 11), with the largest cloud water contents occurring at mid-high latitudes, where cloud amount is also a maximum in the UKMO models. However, although the LMD model has insufficient cloud water at all levels it is perhaps particularly small at upper levels.

3.6 Cloud Forcing

Table 1 shows the cloud radiative forcing for each of the four UKMO experiments and the LMD experiment in comparison with observed data from the Earth Radiation Budget Experiment (ERBE) (Barkstrom 1984). Cloud radiative forcing is defined as the instantaneous impact of cloud on the radiative budget at the top of the atmosphere (Ramanathan et al 1989), and can be split into its solar and longwave components (see, for example, Senior and Mitchell (this volume) for an extended definition of this),

(a) Solar Cloud Forcing (SCF)

Figure 12 shows the time-latitude evolution of the zonally averaged solar cloud forcing from the five models and from ERBE data (Barkstrom 1984). All the models show the strong negative SCF occurring at mid-latitudes ($50-60^\circ$) in the summer hemisphere in both DJF and JJA, as in the ERBE data. This represents a strong cooling of the atmosphere by the reflection of solar radiation mostly by low and medium level clouds in the mid-latitude storm track regions. The UKMO models all show too great a shortwave forcing, especially in the Northern Hemisphere ($120-140 \text{ Wm}^{-2}$ compared to the ERBE value of $100-110 \text{ Wm}^{-2}$) whilst the LMD model shows too small a forcing in both hemispheres (80 Wm^{-2} compared to $100-110 \text{ Wm}^{-2}$ in ERBE in the Northern Hemisphere and 100 Wm^{-2} to 150 Wm^{-2} in the Southern Hemisphere). However the zonally averaged pattern of very strong solar forcing in summer and weak forcing in winter is well produced by all of the models. In the tropics, all the models show the seasonal shift of the ITCZ, indicated by an area of strong solar cloud forcing, north to around $10-15^\circ \text{ N}$ in JJA and south to $10-15^\circ \text{ S}$ in DJF. The area weighted global mean value of SCF (Table 1) is dominated by tropical and subtropical regions. Here the UKMO models overestimate the forcing by up to 13 Wm^{-2} when compared to ERBE data but do rather better at higher latitudes. The LMD model also slightly overestimates the tropical forcing but has compensatory underestimates at higher latitudes, as discussed above, and therefore produces a global mean value very close to that from the ERBE data.

(b) Longwave Cloud Forcing (LCF)

The largest areas of observed longwave cloud forcing occur over the ITCZ, and over the Northern and Southern Hemisphere storm tracks, in areas of greatest high cloud amount (Figure 13(e)). This pattern can be seen in

the time evolution of the zonally averaged longwave cloud forcing in all the models (Figure 13(a),(b),(c) and (d)). As discussed above, in the LMD model the values of q_1 are very small, especially at upper levels, which leads to very small values of longwave cloud forcing at all latitudes and in all months. The distribution of LCF is also poor with very little evidence of a poleward decrease in summer as in the ERBE data. The global mean annual mean longwave cloud forcing (Table 1) is about half that in the ERBE data. The version of the LMD model shown here is untuned and as mentioned in section 3.5 with some adjustment to the ice precipitation threshold, much more realistic values of q_1 and therefore LCF can be achieved. However the distribution of LCF remains poor, so realistic tropical values of LCF are accompanied by unrealistically strong LCF at higher latitudes. This feature of the LMD GCM is associated with the poor representation of cirrus cloud physics and is, perhaps, its major deficiency. The simulations by the UKMO cloud water models are much better than the LMD model. In general the maximum longwave forcing in the tropics is rather too small although that in CWRP is closer to the ERBE data than CW or CWH. The Northern Hemisphere storm track is too weak in CW and CWH but again slightly stronger and more realistic in CWRP, however all the UKMO models show too strong a Southern Hemisphere storm track in JJA and too weak a one in DJF. Nonetheless the global mean value in all the UKMO models is within 5 Wm^{-2} of that from the ERBE data, although all three underestimate it slightly.

(c) Net Cloud Forcing (NCF)

The pattern of Net cloud forcing is dominated by the solar cloud forcing and so all the models show errors similar to those discussed above (compare Figure 14 to Figure 12). In LMD the LCF is so weak that it has very little impact on the net cloud forcing and the resultant global mean (Table 1) is a very strong overall cooling dominated by the SCF. Although the UKMO models had much more realistic values of LCF the excessive strength of the SCF dominates and all the models have a global mean NCF of -28 to -33 Wm^{-2} compared to the ERBE value of -17.2 Wm^{-2} (Table 1).

4. Changes on doubling atmospheric CO₂ concentration

Experiments

A further integration of each of the models was performed in which atmospheric CO₂ concentration was doubled.

In the UKMO models, the temperature of the slab ocean is allowed to change as the atmospheric forcing changes although the heat convergence remains unchanged from that used in the control simulation. For each version of the model the results presented are meaned over the last ten years of the experiment.

For the perturbation experiment with the LMD model, the results of a 2 x CO₂ experiment which predicted SST changes (the slab experiment of Wilson and Mitchell 1987) are used to give the seasonally varying SST anomaly and the experiment was run for 15 months.

4.1 Changes in Temperature

(a) Zonally Averaged

All the models show quantitatively similar results with a warming of the troposphere and a cooling of the stratosphere, the largest warming occurring at high latitudes in the winter hemisphere below about 500mb and the tropical warming increasing with height (Figure 15 and 16). The RH model and the LMD model show the largest warmings especially over the sea-ice areas. In the UKMO cloud water models, the global mean temperature change is much reduced but also the distribution of the warming is different with particular areas of greatly reduced warming over the Southern Ocean (eq 40-50° S) in both seasons and at mid-high latitudes in the Northern Hemisphere as well. Also, the high-latitude amplification of the warming is confined to lower altitudes than in RH and LMD. These areas are where the largest cloud feedbacks occur, as will be discussed below (See also Senior and Mitchell, this volume).

(b) Surface temperature

A similar picture can be seen in the pattern of annual mean surface temperature response with the greatest warmings occurring in the LMD model and in RH (Figure 17), especially at high latitudes and over sea-ice. It must be stressed that the sea surface temperature change in LMD is fixed to

be that from Wilson and Mitchell (1987), which is very similar to that simulated by RH. All of the models show a greater warming over land than sea and in the UKMO cloud water models the greatest reduction in the warming occurs over the oceans and in particular over the Southern Ocean and the North Atlantic.

4.2 Changes in PMSL

All the models show the largest changes at high latitudes with very small changes equatorwards of 30° in either hemisphere or season (Figure 18). The LMD model has reductions in PMSL in areas where sea-ice is reducing, especially in winter, agreeing with the results found in reduced sea-ice experiments (eg Mitchell and Senior 1989, Mitchell and Hills 1986). This is also true in the UKMO models in the Northern Hemisphere although the changes in the Southern Hemisphere are less consistent.

4.3 Changes in Cloud cover

All the models show increased high cloud cover as the height of the tropopause moves upwards in response to the warming of the troposphere (Wetherald and Manabe 1988). The changes in low and medium level cloud are, however, substantially different in different models (Figures 19 and 20). The LMD and RH models show marked reductions in low and mid-level cloud especially at mid-high latitudes in both seasons. These reductions are likely to be related to changes in relative humidity (Mitchell and Ingram 1991). In contrast to this all the UKMO models show substantial increases in cloud between the 0 and -15° C isotherms, especially in the summer hemisphere, where cloud water content changes from frozen to liquid. Qualitatively similar changes in cloud water content are seen in the LMD model (discussed below) but these are of much smaller magnitude and the relative humidity changes appear to dominate.

4.4 Changes in Cloud Water Content

In the UKMO cloud water models (CW,CWH,CWRP) the changes in cloud water content (Figures 21 and 22 (a),(b) and (c)) show a very similar pattern to the changes in cloud. In the region between the 0° and -15° C isotherms, where cloud water changes from frozen to liquid as the atmosphere begins to warm, there are increases in cloud water content because the liquid water does not convert to precipitation as quickly as frozen water (the basis of

the Bergeron-Findeison process). In the LMD model there is a threshold for frozen to liquid conversion of -10°C below which all cloud water is frozen. As with the UKMO models there is a marked increase in cloud water content on the cold side of the threshold as the atmosphere warms and more cloud water is diagnosed as liquid, although this increase is enhanced in winter in the LMD model and in Summer in the UKMO models. In the LMD model the rate of precipitation of cloud water does not depend on state, but the threshold above which precipitation may occur is an order of magnitude higher for liquid water than for frozen water. Therefore precipitation does not occur so readily and more cloud water remains in the atmosphere.

The cloud water changes in the UKMO models are large (Figure 21 and 22 (a),(b) and (C)). In the LMD model the changes in q_1 are an order of magnitude smaller than those in the UKMO models (Figures 21 and 22) as the total amount of q_1 in this model is very small. Thus the impact of changes in cloud water content, q_1 , on the cloud amount changes in the LMD scheme will be very small compared to the changes in RH.

4.5 Change in Net cloud forcing

Table 2 shows the change in longwave, shortwave and net cloud forcing from the 5 experiments and Figure 23 the time-latitude evolution of the net cloud forcing. In all the models there is a reduction in the longwave warming of the atmosphere which is associated with overall reductions in high cloud amount, which outweigh the general upward shift of the high cloud maximum, which would otherwise tend to trap more OLR and therefore increase the longwave cloud forcing. This reduction in LCF then implies a reduced warming of the climate system. Conversely the changes in SCF act, with the exception of CWRP (for further explanation see Senior and Mitchell, this volume), to enhance the warming of the climate system, but as can be seen, to vastly different degrees. The changes in SCF are affected by changes in lower cloud. In the UKMO models there are some reductions in medium and low level cloud but these are largely ameliorated by increases in medium and low cloud between 0 and -15°C . Whilst the change in SCF in the LMD model is not particularly large, when coupled with the very small change in LCF (which results from the very low values of cloud water content at upper levels) it gives a global mean net cloud feedback that is very large and positive (Table 2) and the net cloud feedback is, in fact, positive at most latitudes (Figure 23). Note that the global mean change in

solar cloud forcing in RH is nearly twice the size of that in the LMD model, but is mostly compensated by a relatively large change in longwave cloud forcing (Table 2).

5. Summary and conclusions

A comparison of the radiation budget and cloud distribution of GCM's from two different institutions and from satellite data has been performed. The models show some similarities but also many differences and all the models have errors when compared to satellite data. One explanation is the comparatively low resolution of the models. The differences in the various model climatologies is likely to be mainly due to the different assumptions in the cloud parametrization schemes used. The cloud water schemes of Le Treut and Li (1988, 1991) and Smith (1990) appear initially to be quite similar but actually differ in detail, especially in the formulation of precipitation. The climatology of the LMD model is in fact more similar to that of the RH model with a relative humidity based cloud scheme than those of the UKMO cloud water models.

The change in cloud forcing on doubling CO_2 has been related to the cloud feedback (Ramanathan et al 1989). Using this definition, the cloud feedback from the models ranges from large and positive to small and negative, with the LMD model simulating a large positive feedback close to that found in RH. The change of phase feedback found in the models using the prognostic cloud water scheme of Smith (1990) is not found in the LMD model. The changes in cloud water content from LMD are similar to those found in CW, CWH and CWRP but the magnitude of the changes is much smaller and the relative increase in q_g compared to q dominates the change in cloud fraction.

The differences in the response of the UKMO and LMD models are then at least partly due to the differences in the parametrization schemes used and only a greater knowledge of the actual microphysical processes occurring will prove which method, if either, is closer to reality.

Table 1 Global mean annual mean cloud forcing

FORCING	ERBE	RH	CW	CWH	CWRP	LMD
LW	30.5	32.5	26.7	29.6	28.8	16.8
SW	-47.7	-60.9	-56.2	-57.8	-58.4	-49.8
NET	-17.2	-28.4	-29.5	-28.2	-29.6	-33.0

Table 4 Changes in global mean annual mean cloud forcing

FORCING	RH	CW	CWH	CWRP	LMD
Δ LW	-4.08	-1.19	-1.54	-0.56	-0.3
Δ SW	6.13	1.39	2.27	-0.48	3.8
Δ NET	2.04	0.2	0.73	-1.04	3.5

References

- Barkstrom, B.R., 1984. The earth radiation budget experiment (ERBE). *Bull. Am. Met. Soc.*, 65, 1170-1185.
- Cess, R.D., G.L. Potter, J.P. Blanchet, G.J. Boer, A.D. Del Genio, M. Deque, V. Dymnikov, V. Galin, W.L. Gates, S.J. Ghan, J.T. Kiehl, A.A. Lacis, H. Le Treut, Z.-X. Li, X.-Z. Liang, B.J. McAvaney, V.P. Meleshko, J.F.B. Mitchell, J.J. Morcrette, D.A. Randall, L. Rikus, E. Roeckner, J.F. Royer, U. Schlese, D.A. Sheinin, A. Slingo, A.P. Sokolov, K.E. Taylor, W.M. Washington, R.T. Wetherald, I. Yagai and M.-H. Zhang, 1990. Intercomparison and interpretation of climate feedback processes in 19 atmospheric general circulation models. *J. Geophys. Res.*, 95, 16601-16615.
- Heymsfield, A.J., 1977. Precipitation development in stratiform ice clouds: A microphysical and dynamical study. *J. Atmos. Sci.*, 34, 367-381.
- Hughes, N.A. and A. Henderson-Sellers, 1985. Global 3-D reanalysis of total cloud amount: Climatology for 1979. *J. of Clim. and Appl. Meteorol.*, 24, 669-686.
- Le Treut, H. and Z.-X. Li, 1988. Using Meteosat data to validate a prognostic cloud generation scheme. *Atmospheric Research*, 21, 273-292.
- Le Treut, H. and Z.-X. Li, 1991. Sensitivity of an atmospheric general circulation model to prescribed SST changes: feedback effects associated with the simulation of cloud optical properties. *Climate Dynamics*, 5, 175-187.
- Li, Z.-X., 1990. Etude de l'interaction nuage-rayonnement dans la contexte du changement climatique du a l'augmentation des gaz a effet de serre dans l'atmosphere. *Phd. Thesis*, University of Paris.
- Mason, B.J., 1957. *The physics of clouds*. Clarendon, Oxford.

- Mitchell, J.F.B and C.A. Senior, 1989, The antarctic winter; Simulations with climatological and reduced sea-ice extents. *Q. J. R. Meteorol. Soc.*, 115, 225-246.
- Mitchell, J.F.B and T.S. Hills, 1986, Sea-ice and the antarctic winter circulation, a numerical experiment. *Q. J. R. Meteorol. Soc.*, 112, 953-969.
- Mitchell, J.F.B, C.A. Senior and W.J. Ingram, 1989. CO₂ and Climate: A missing feedback?. *Nature*, 341, 132-134.
- Mitchell, J.F.B and W.J. Ingram, 1991. On CO₂ and Climate: Mechanisms of changes in cloud. Submitted to *Journal of Climate*.
- Njoku, P.L. and Y.K. Swansen, 1983. Global measurements of sea surface temperature wind speed and atmospheric water vapour content from satellite microwave radiometry. *Mon. Weather. Rev.*, 111, 1977-1987.
- Oort, A.H., 1983. Global atmospheric circulation statistics 1958-1973, NOAA professional paper no. 14. U.S Government printing office, Washington D.C.
- Palmer, T.N., G.J. Schutts and R. Swinbank, 1986. Alleviation of the systematic westerly bias in general circulation and numerical weather prediction models through an orographic gravity wave drag parametrization. *Q. J. R. Meteorol. Soc.*, 112, 1001-1039.
- Ramanathan, V, R.D. Cess, E.F. Harrison, P. Minnis, B.R. Barkstrom, E. Ahmad, D. Hartmann, 1989. Cloud-radiative forcing and Climate: Results from the Earth Radiation Budget Experiment. *Science*, 243, 57-63.
- Sadourny, R. and K. Laval, 1984. January and July performance of the LMD general circulation model. *New perspectives in climate modelling*. Eds. A. Berger and C. Nicolis. Elsevier, Amsterdam.
- Senior, C.A. and J.F.B. Mitchell, 1991. CO₂ and Climate: The impact of cloud parametrization. This Volume

Senior, C.A. and J.F.B. Mitchell, 1991. The impact of resolution on simulations of present day and 2 x CO₂ climates. In preparation.

Smith, R.N.B., 1990. A scheme for predicting layer cloud and their water content in a general circulation model. *Q. J. R. Meteorol. Soc.*, 116, 435-460.

Sommeria, G. and J.W. Deardorff, 1977. Subgrid-scale condensation in models of non-precipitating clouds. *J. Atmos. Sci.*, 34, 344-355.

Stephens, G.L., G.G. Campbell and T.H. Vonder Haar 1981. Earth Radiation Budgets. *J. Geophys. Res.*, 86, 9739-9760.

Sundqvist, H., 1978. A parametrization scheme for non-convective condensation including prediction of cloud water content. *Q. J. Royal. Meteorol. Soc.*, 104, 677-690.

Vowinckel, E. and S. Orvig, 1970. The climate of the North Polar Basin. In Orvig, s. (ed), *World survey of climatology 14, Climate of the Polar Regions*, New York, pp. 129-252.

Wetherald, R.T. and S. Manabe, 1988. Cloud feedback processes in a general circulation model. *J. Atmos. Sci.*, 45, 1397-1415.

Wilson, C.A. and J.F.B. Mitchell, 1987. A doubled CO₂ climate sensitivity experiment with a global climate model including a simple ocean. *J. Geophys. Res.*, 92, 13315-13343.

Figure Captions

Unless otherwise stated all UKMO models are Ten year means and the LMD model is one year.

1. Height latitude cross-sections of zonally averaged DJF temperature from the control experiments. Contours every 5 K.

(a) RH	(d) CWRP
(b) CW	(e) LMD
(c) CWH	(f) 1958-1973 climatology from Oort (1983)

2. As Figure 1 but for JJA

3. Time-latitude cross-sections of zonally averaged PMSL. Contours every 2 mb.

(a) RH	(d) CWRP
(b) CW	(e) LMD
(c) CWH	

4. Time-latitude cross-sections of zonally averaged net radiative flux at the TOA. Contours every 20 Wm^{-2} , shaded where negative.

(a) RH	(d) CWRP
(b) CW	(e) LMD
(c) CWH	(f) 1979 Nimbus-6 data from Stephens et al (1981)

5. Zonal mean total cloud amount for DJF.

(a) Solid line, CW. Dashed line, RH. Dashed and crossed, CWH. Solid and crossed, CWRP. Expressed as a fraction.

(b) Solid line, 3-d Nephanalysis for 1979 (from Hughes and Henderson-Sellers (1983)) Chain dotted line, LMD. Expressed as a %.

6. As Figure 5 but for JJA.
7. Height-latitude cross section of zonally averaged DJF cloud cover. Contours every 5%, stippled above 15% (a-d only).

(a) RH	(d) CWRP
(b) CW	(e) LMD
(c) CWH	
8. As Figure 7 but for JJA.
9. Zonally averaged vertical integral of total cloud water content in gm^{-2} .

(a) Solid line, CW. Dashed and crossed, CWH. Solid and crossed, CWRP.
(b) Solid line, CW. Dashed line, LMD. Crosses, SMMR data for July 11-Aug 10 1978. (from Njoku and Swansen (1978))
10. Height-latitude cross sections of zonally averaged cloud water content.

(a) CW. Contours at 0.01, 0.02, 0.05, and every 0.1 $\text{g mb}^{-1} \text{m}^{-2}$, stippled above 0.2.
(b) CWH. Contoured as (a)
(c) CWRP. Contoured as (a)
(d) LMD. Contours at 0.01, 0.02, 0.04 and every 0.04 $\text{g mb}^{-1} \text{m}^{-2}$
11. As Figure 10 but for JJA.
12. Time-latitude cross-sections of zonally averaged solar cloud forcing. Contours every 10 Wm^{-2} . Stippled below -60 Wm^{-2} (a-c and e only).

(a) CW	(d) LMD
(b) CWH	(e) ERBE data for Apr 1985- Apr 1986
(c) CWRP	

13. As figure 12 but for longwave cloud forcing. Contours every 10 Wm^{-2} , stippled above 30 Wm^{-2} (a-c and e only).
14. As Figure 12 but for net cloud forcing. Contours every 10 Wm^{-2} , stippled where negative (a-c and e only).
15. Height-latitude cross section of equilibrium changes in ten year DJF means of temperature on doubling CO_2 . Contours every 1 K, reductions stippled.
- (a) RH (d) CWRP
(b) CW (e) LMD
(c) CWH
16. As Figure 9 but for ten year JJA means.
17. Ten year annual mean change in surface temperature on doubling CO_2 . Contours every 1 K up to +4K then at every 2K, reductions stippled.
- (a) RH (d) CWRP
(b) CW (e) LMD
(c) CWH
18. Time-latitude cross-sections of change in zonally averaged PMSL on doubling CO_2 . Contours every 1 mb, reductions stippled.
- (a) RH (d) CWRP
(b) CW (e) LMD
(c) CWH
19. Height-latitude cross section of changes in DJF layer cloud amount on doubling CO_2 . Areas of reduction are stippled and the contours are every 1%. The dashed lines are the 0 and -15°C contours from the control simulation.

- (a) RH (d) CWRP
(b) CW (e) LMD
(c) CWH

20. As Figure 19 but for JJA.

21. Height-latitude cross section of changes in DJF cloud water on doubling CO_2 . Contours every $4 \times 10^{-2} \text{ g mb}^{-1} \text{ m}^{-2}$ (except where stated). Areas of reduction are stippled. The dashed lines are the 0 and -15°C contours from the control simulation.

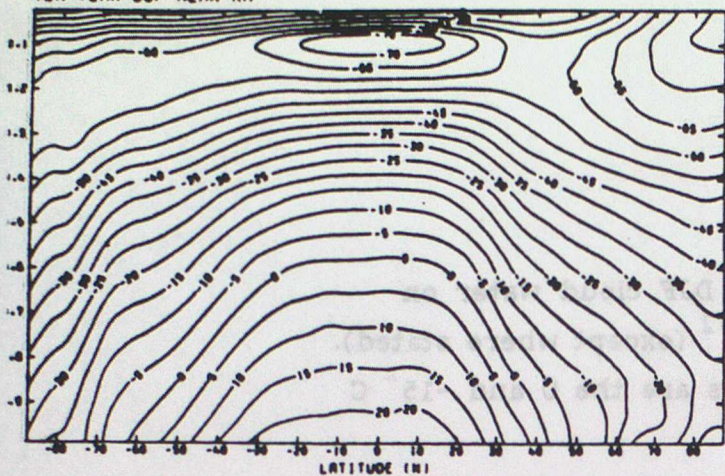
- (a) RH (d) CWRP
(b) CW (e) LMD. Contours every $0.01 \text{ g mb}^{-1} \text{ m}^{-2}$.
(c) CWH

22. As Figure 21 but for JJA.

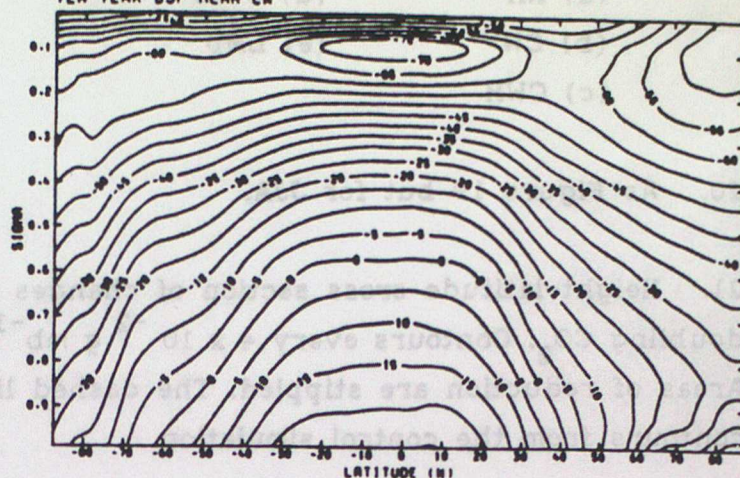
23. Time-Latitude cross sections of the change in net cloud forcing on doubling CO_2 . Contours every 2 Wm^{-2} , stippled where negative.

- (a) CW (c) CWRP
(b) CWH (e) LMD

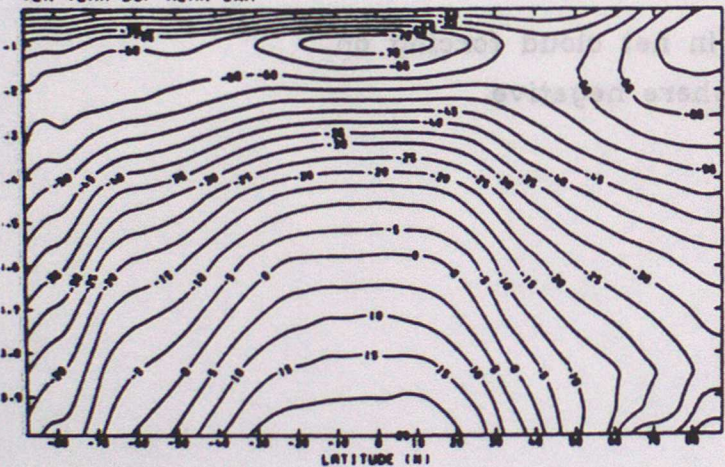
a) TEMPERATURE
CONTOURS EVERY 5 DEGREES
TEN YEAR DJF MEAN RH



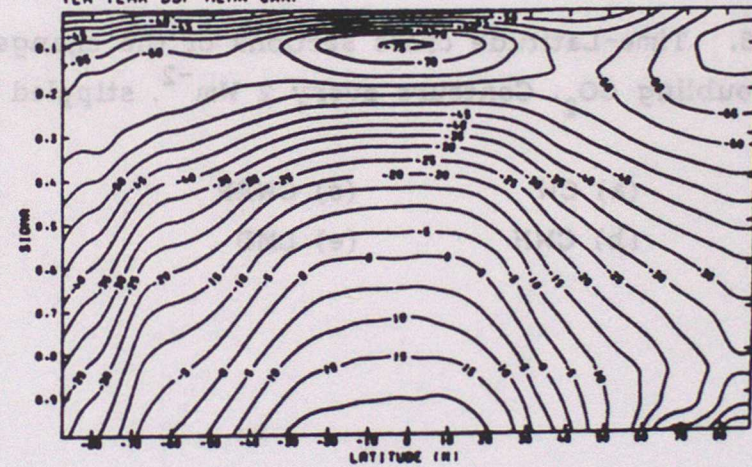
b) TEMPERATURE
CONTOURS EVERY 5 DEGREES
TEN YEAR DJF MEAN CM



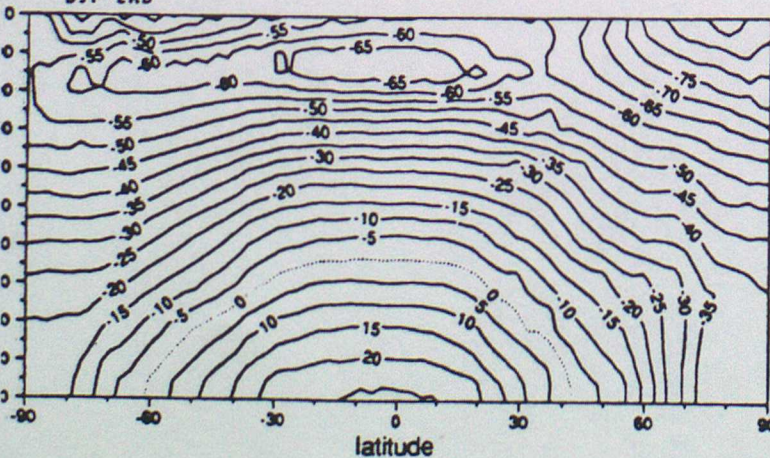
c) TEMPERATURE
CONTOURS EVERY 5 DEGREES
TEN YEAR DJF MEAN CHH



d) TEMPERATURE
CONTOURS EVERY 5 DEGREES
TEN YEAR DJF MEAN CHRP



e) TEMPERATURE
CONTOURS EVERY 5 DEGREES
DJF LMD



f) TEMPERATURE
CONTOURS EVERY 5 DEGREES
DJF OBSERVATION

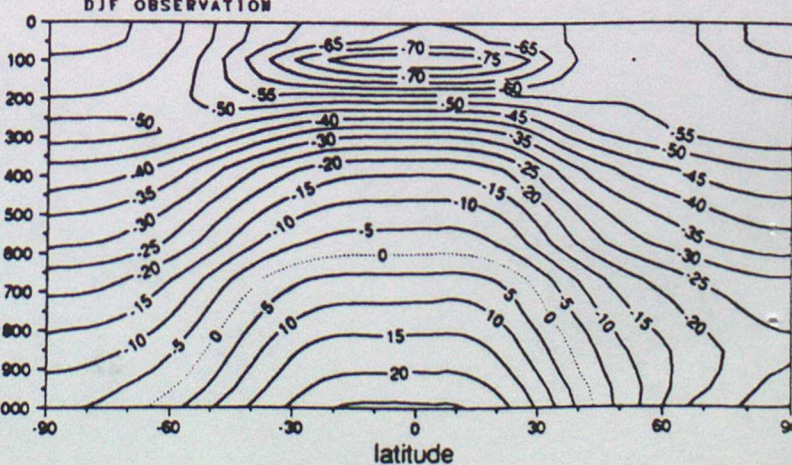
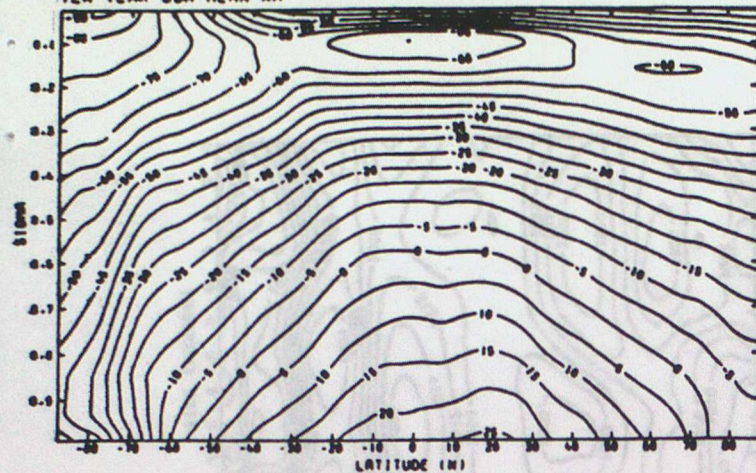
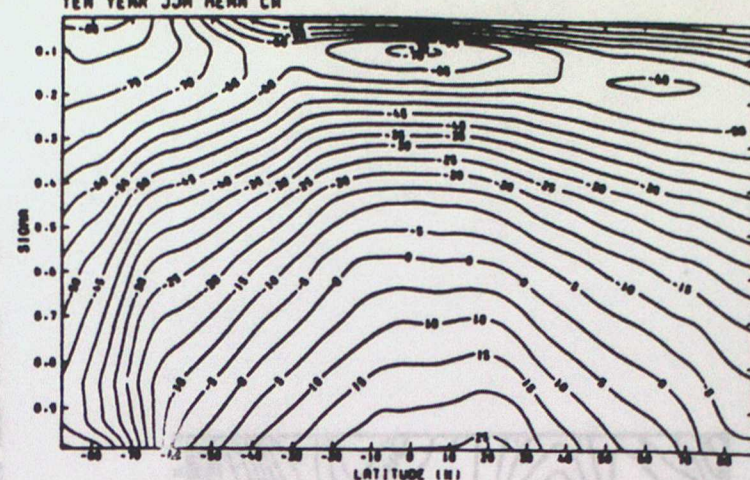


FIGURE 1

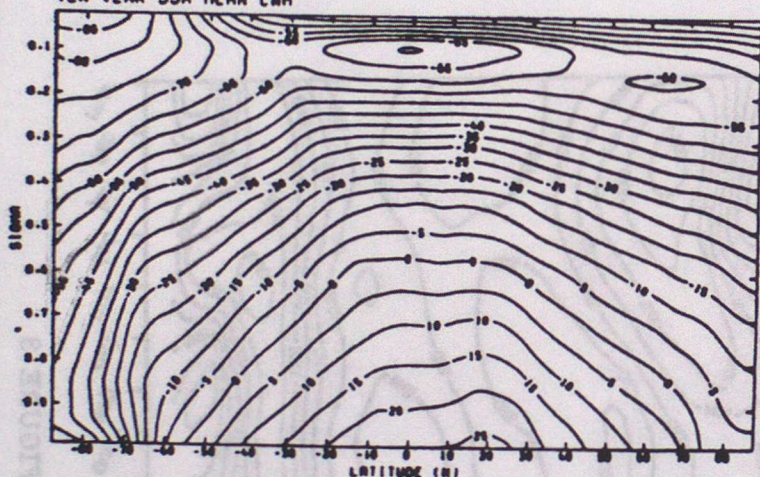
(a) TEMPERATURE
CONTOURS EVERY 5 DEGREES
TEN YEAR JJA MEAN RH



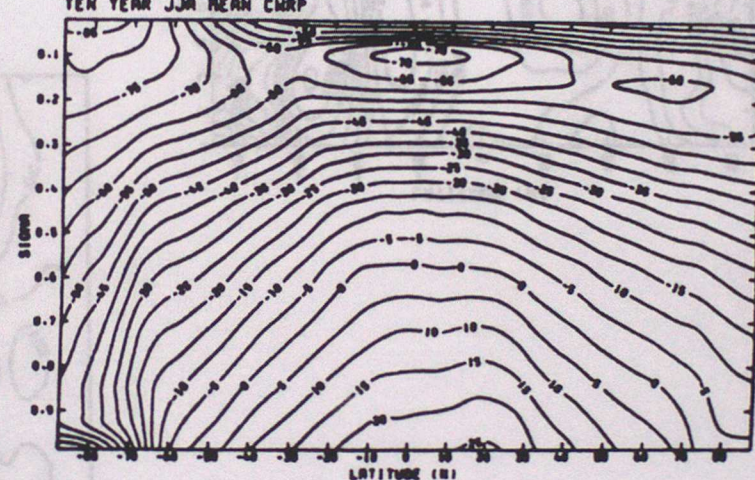
(b) TEMPERATURE
CONTOURS EVERY 5 DEGREES
TEN YEAR JJA MEAN CH



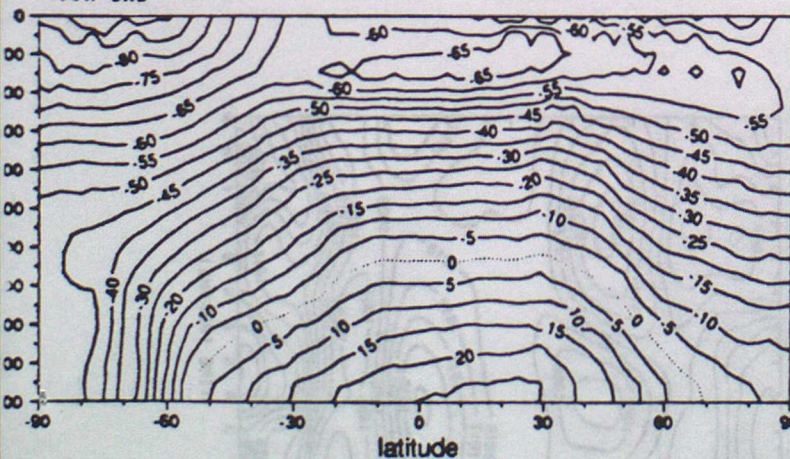
(c) TEMPERATURE
CONTOURS EVERY 5 DEGREES
TEN YEAR JJA MEAN CWH



(d) TEMPERATURE
CONTOURS EVERY 5 DEGREES
TEN YEAR JJA MEAN CWP



(e) TEMPERATURE
CONTOURS EVERY 5 DEGREES
JJA LND



(f) TEMPERATURE
CONTOURS EVERY 5 DEGREES
JJA OBSERVATION

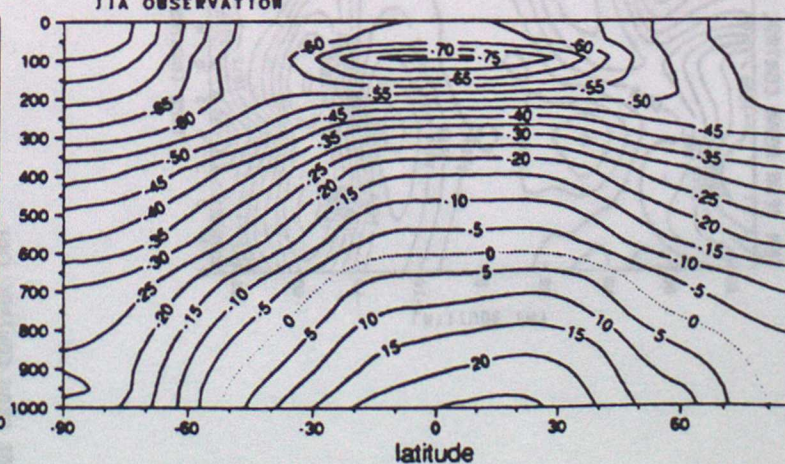


FIGURE 2

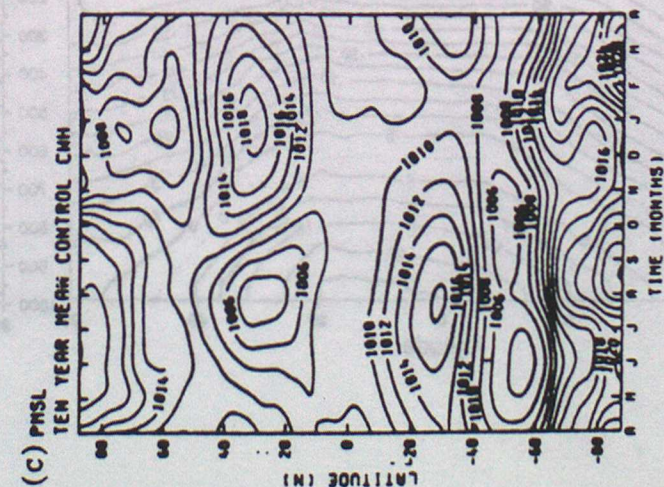
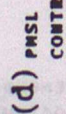
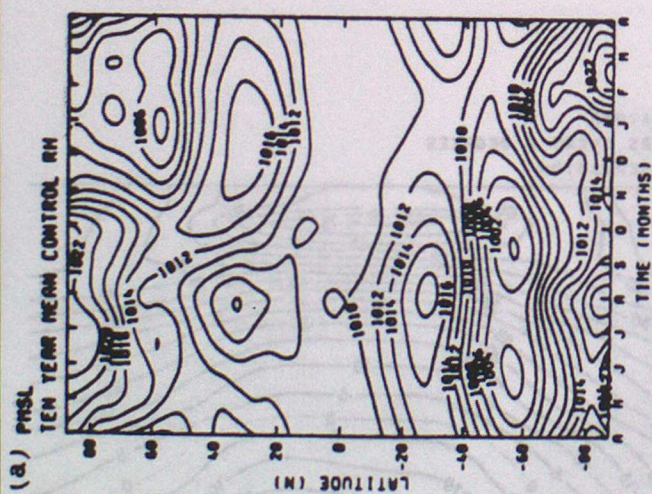
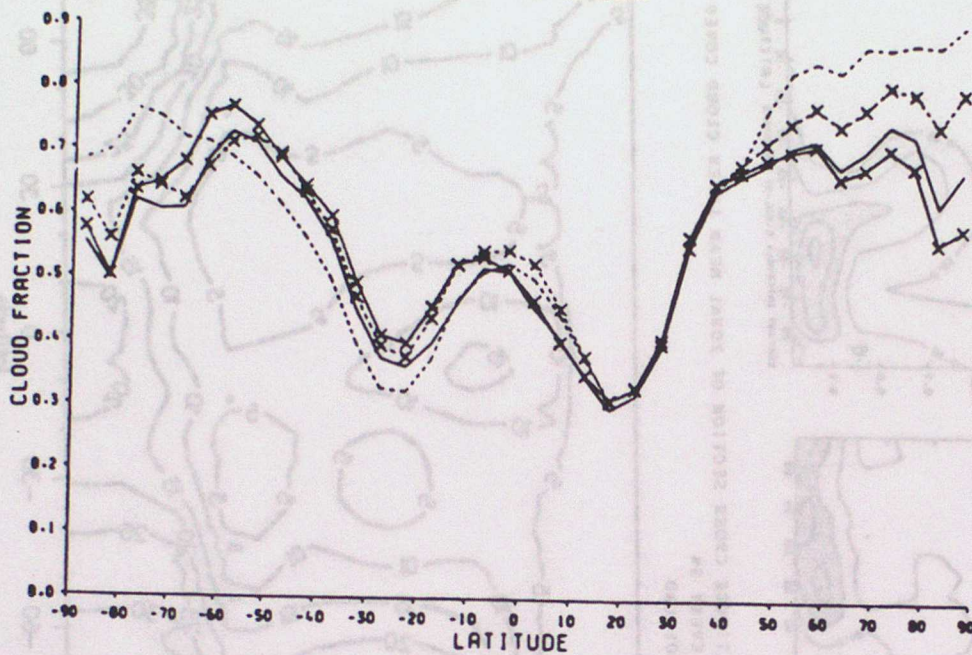


FIGURE 3

(a) ZONAL MEAN TOTAL CLOUD AMOUNT
TEN YEAR DJF MEAN



(b) ZONAL MEAN TOTAL CLOUD AMOUNT
DJF

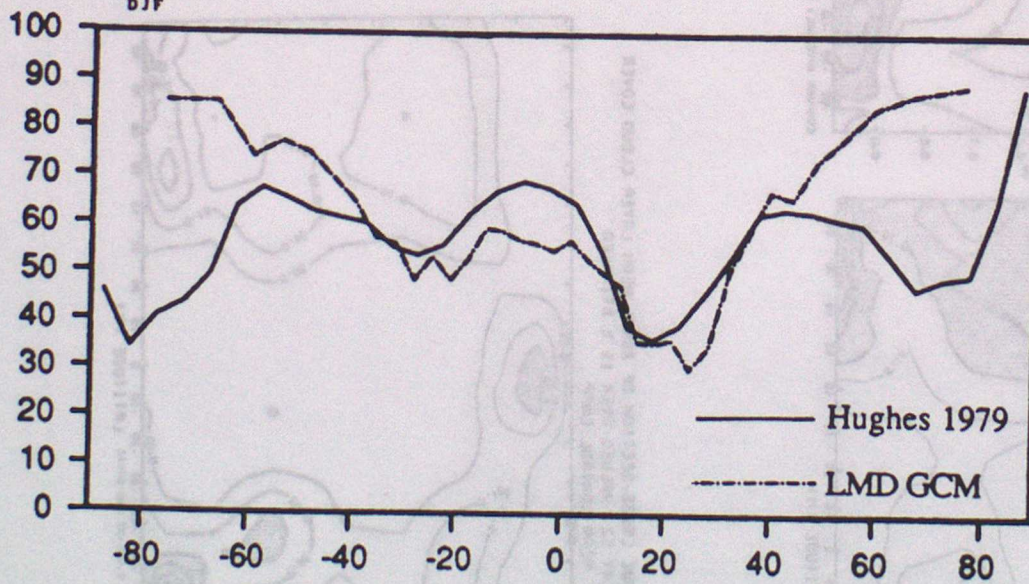
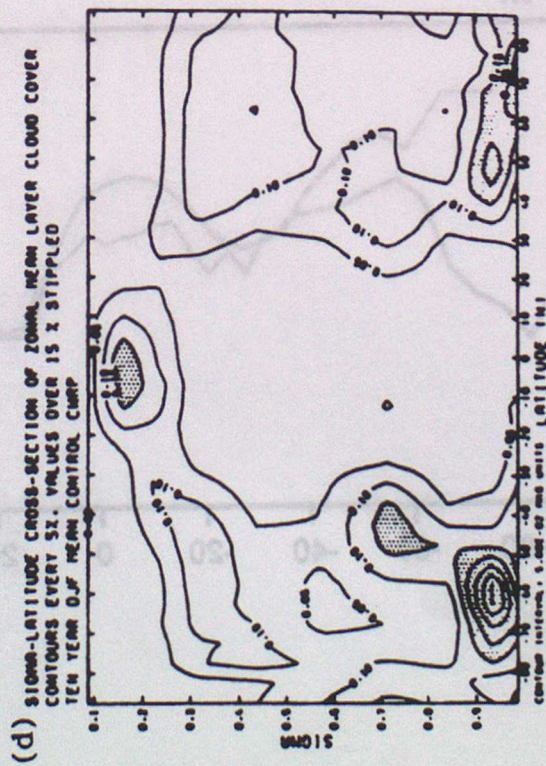
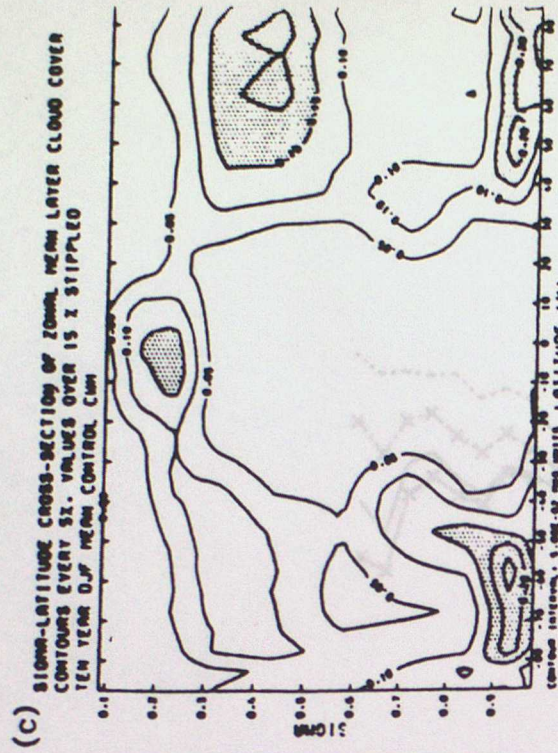
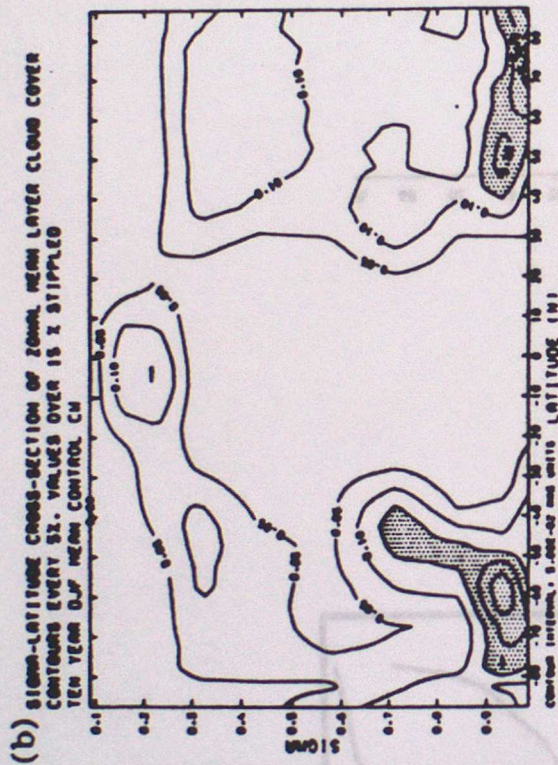
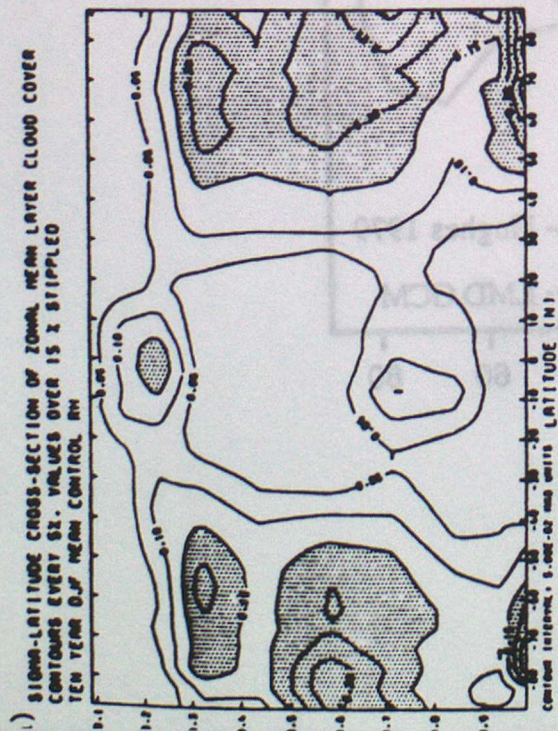


FIGURE 5



(e) HEIGHT-LATITUDE CROSS SECTION OF ZONAL MEAN LAYER CLOUD COVER
 CONTOURS EVERY 5%
 DJF CONTROL LMD

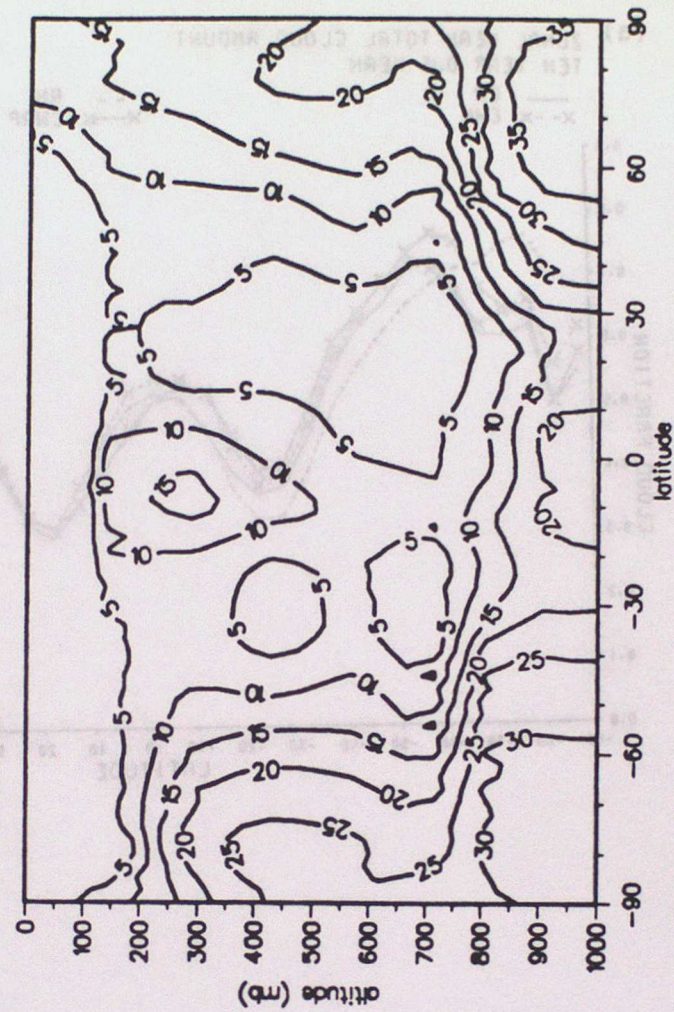
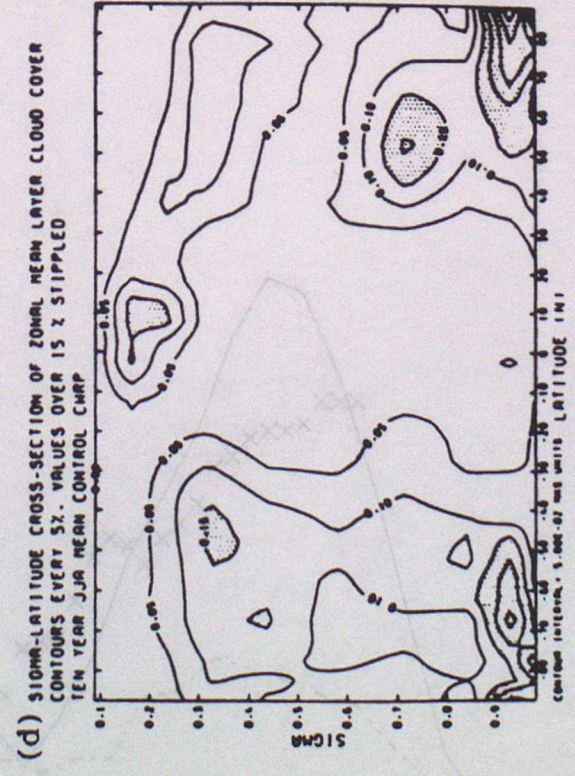
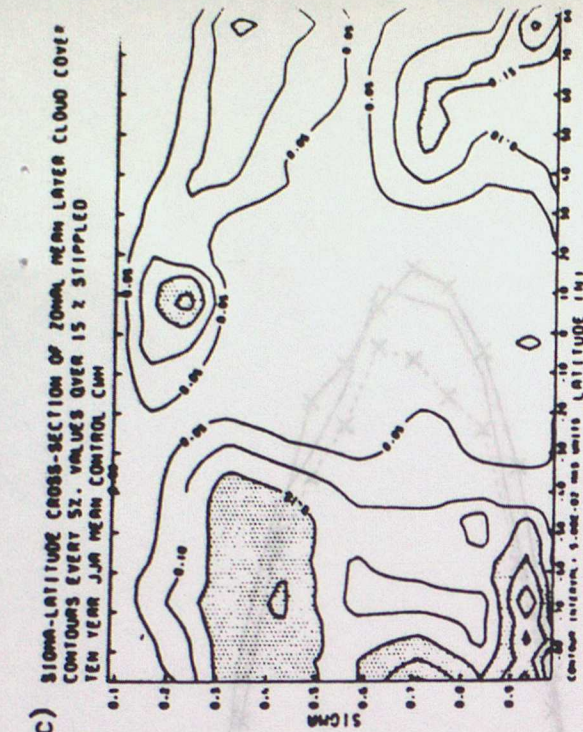
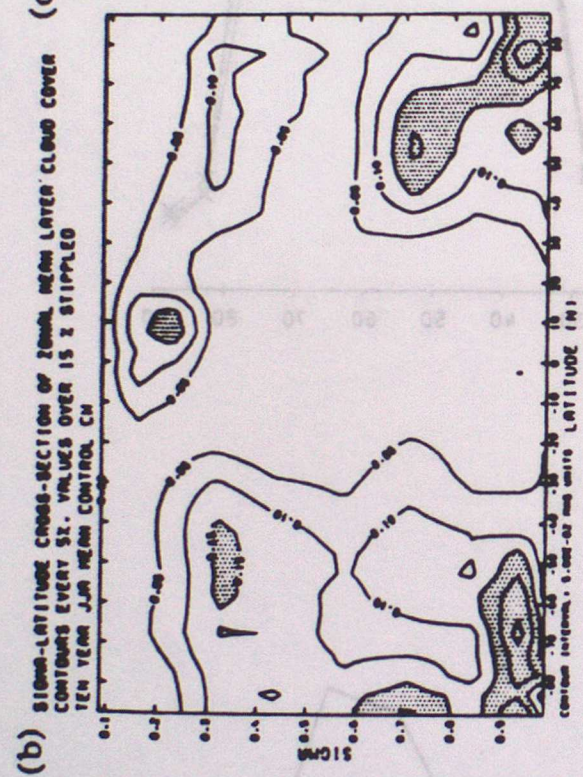
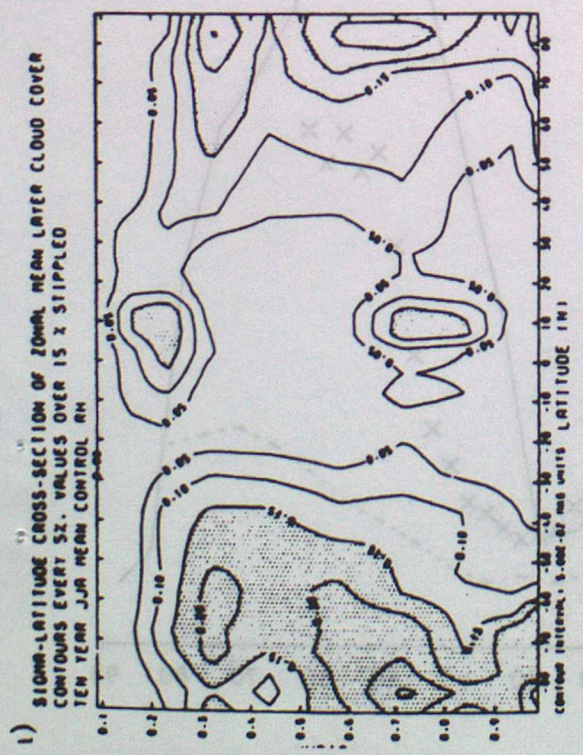


FIGURE 7



(e) HEIGHT-LATITUDE CROSS SECTION OF ZONAL MEAN LAYER CLOUD COVER
 CONTOURS EVERY 5%
 JJA CONTROL LMD

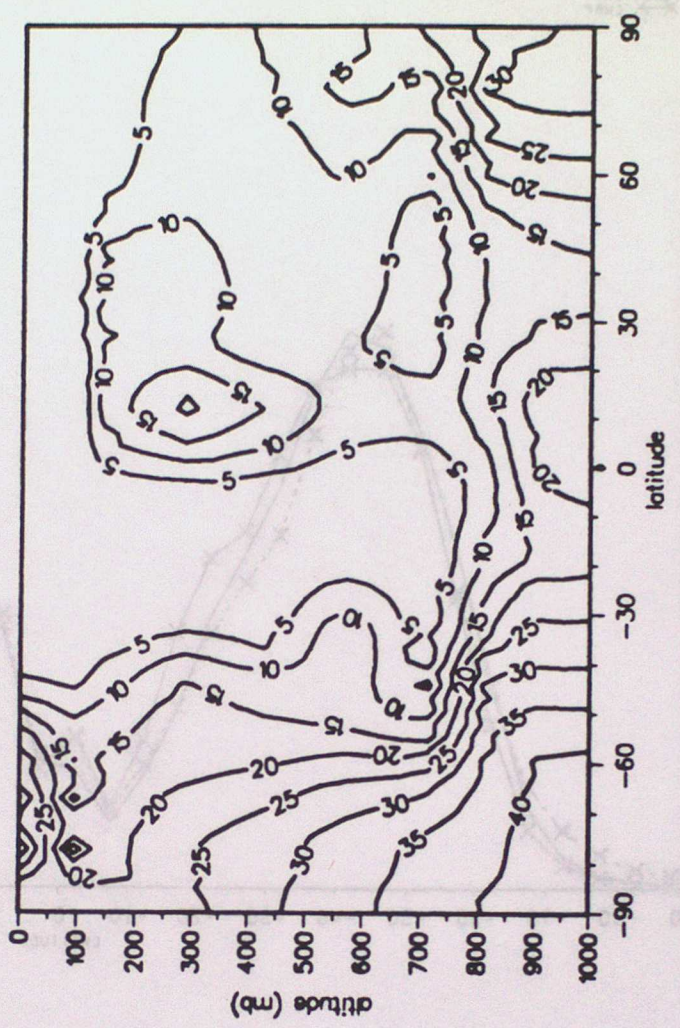
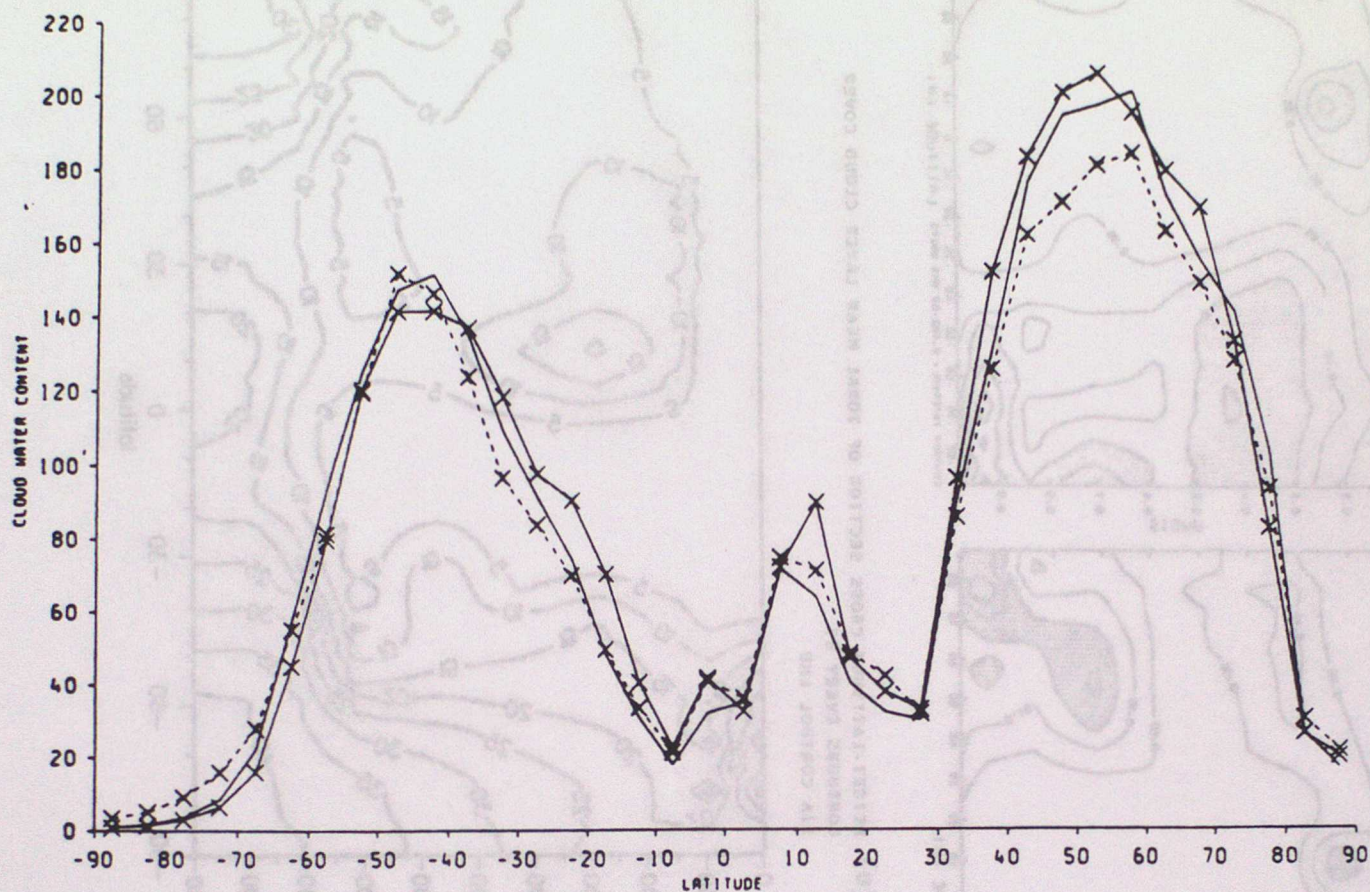


FIGURE 8

(a) VERTICAL INTEGRAL OF TOTAL WATER CONTENT
JJA 10 TEN YEAR MEAN

CM
CMRP

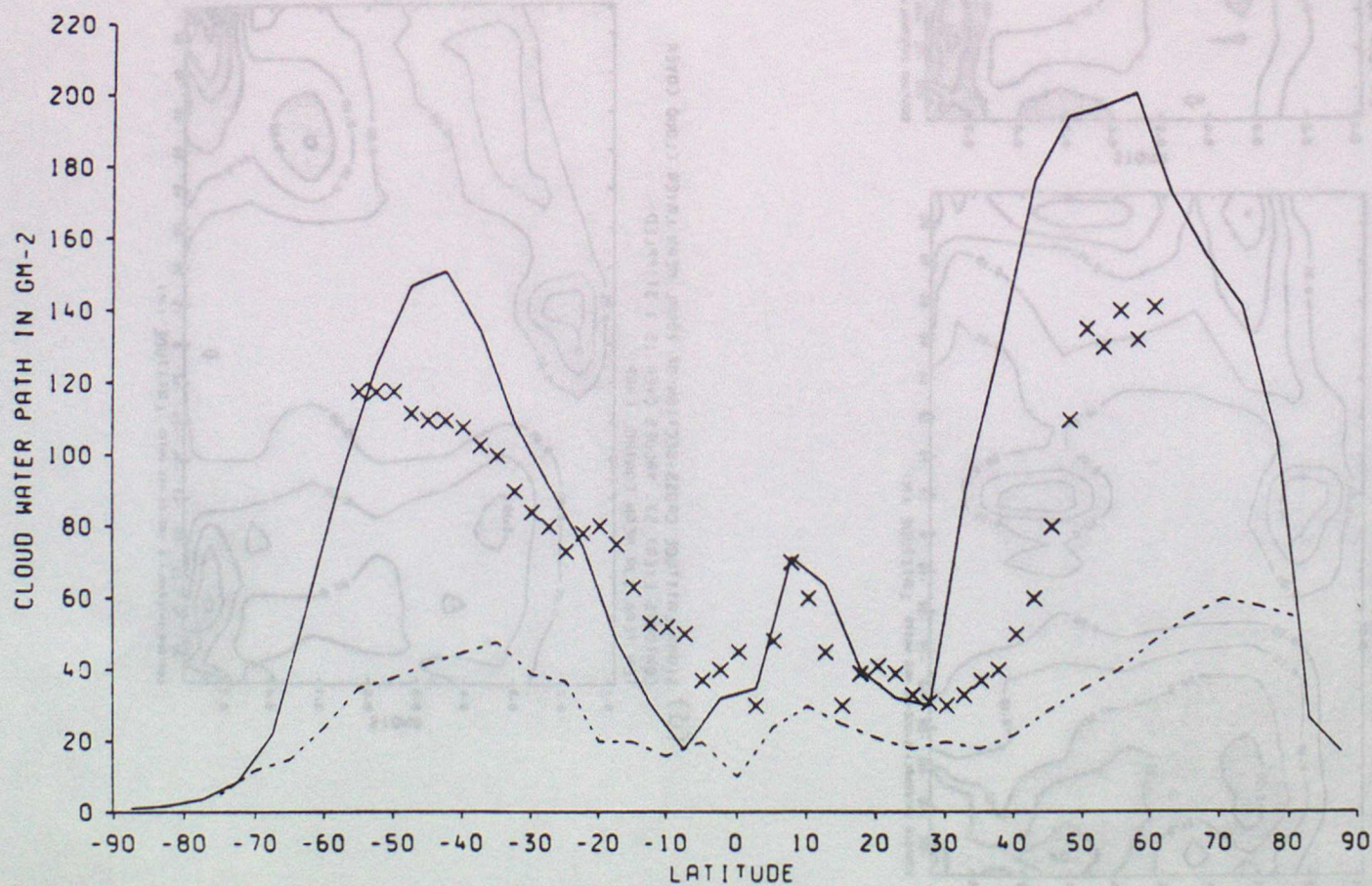
× × CMH



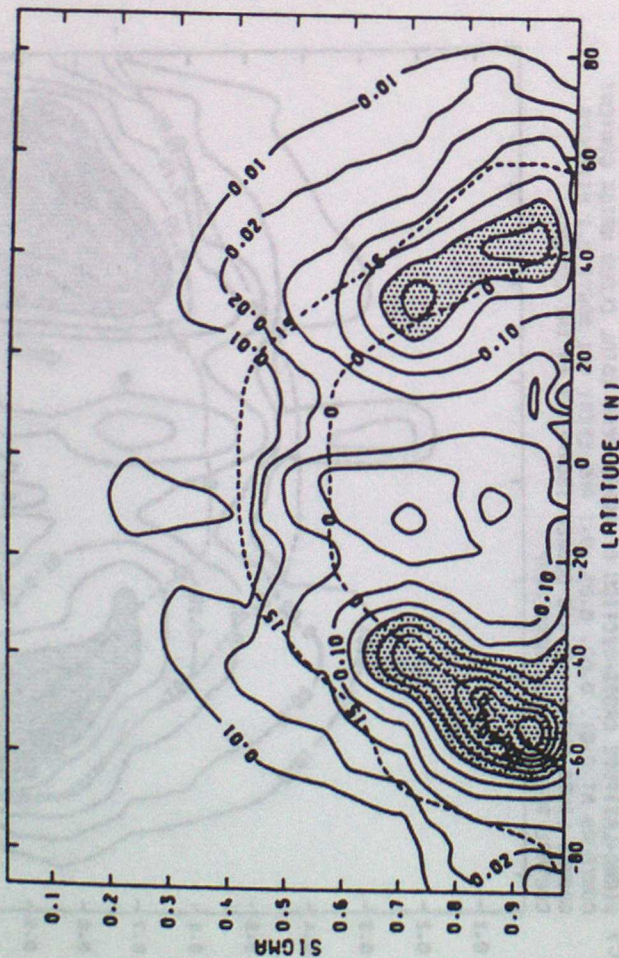
(b) VERTICAL INTEGRAL OF TOTAL WATER CONTENT
ANNUAL 10 TEN YEAR JJA MEAN

— CW
× × SMMR DATA FOR JULY 11 - AUG 10 1978

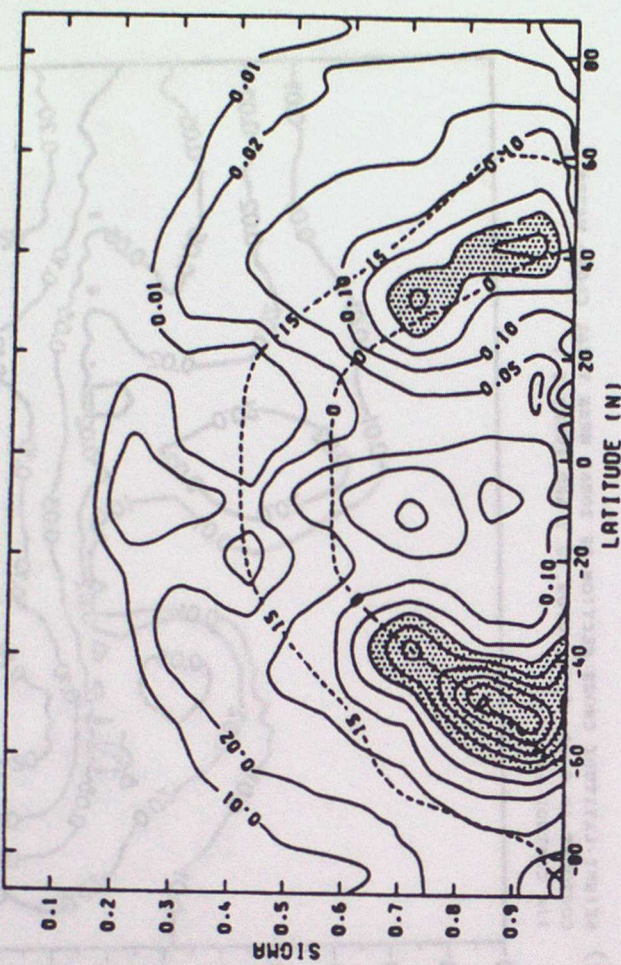
--- LMD



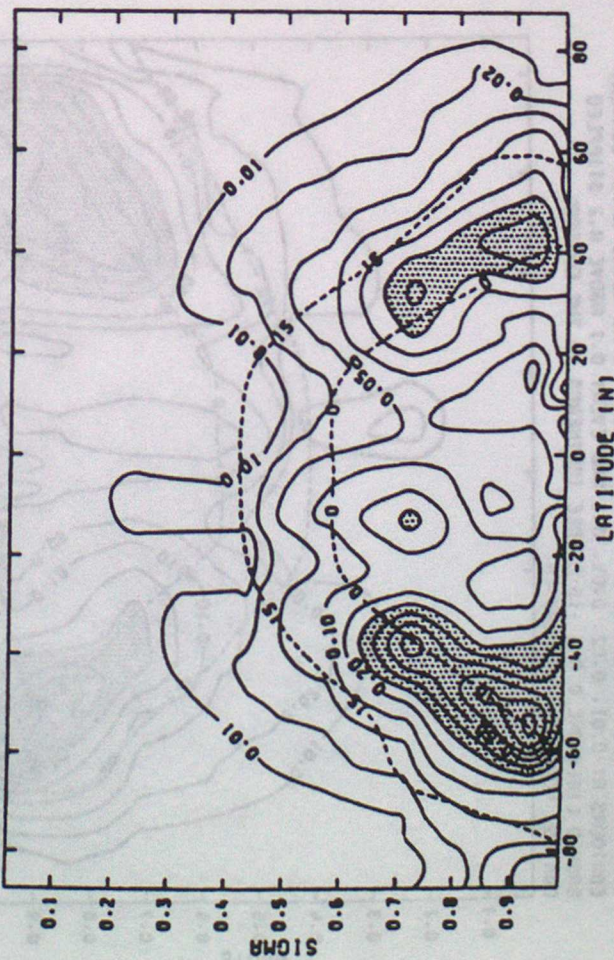
(a) SIGMA-LATITUDE CROSS-SECTION OF ZONAL MEAN TOTAL CLOUD WATER CONTENT
 CONTOURS AT 0.01, 0.02, 0.05, 0.1 AND EVERY 0.1 ABOVE 0.2 STIPPLED
 DASHED LINES ARE 0 AND -15 DEGREE ISOTHERMS IN THE CONTROL
 CONTROL TEN YEAR DJF MEAN CM



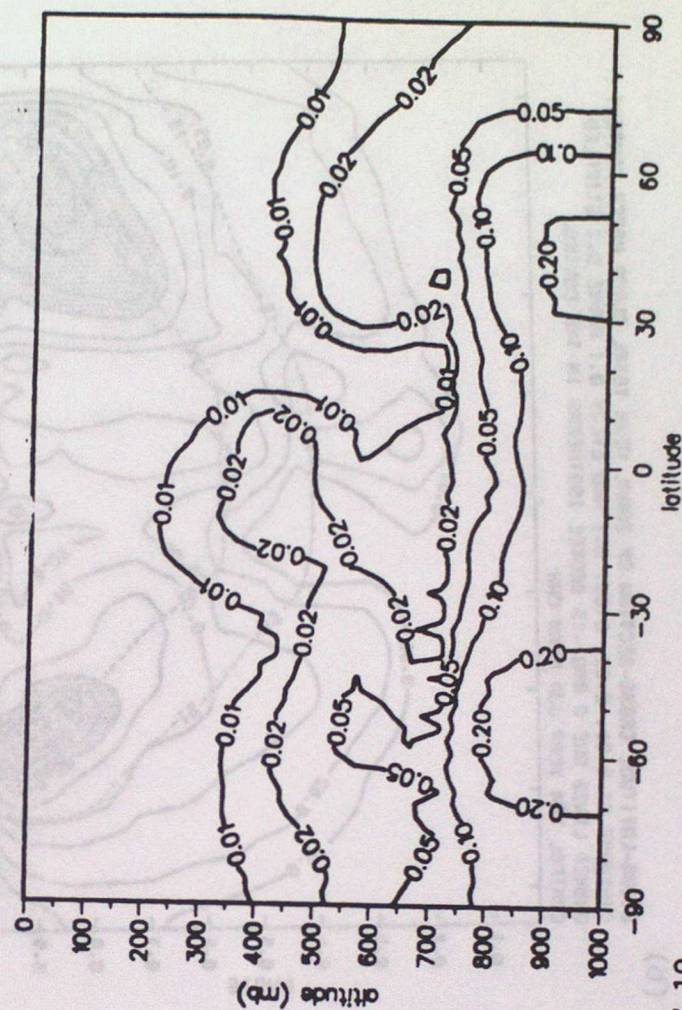
(b) SIGMA-LATITUDE CROSS-SECTION OF ZONAL MEAN TOTAL CLOUD WATER CONTENT
 CONTOURS AT 0.01, 0.02, 0.05, 0.1 AND EVERY 0.1 ABOVE 0.2 STIPPLED
 DASHED LINES ARE 0 AND -15 DEGREE ISOTHERMS IN THE CONTROL
 CONTROL TEN YEAR DJF MEAN CMH



(c) SIGMA-LATITUDE CROSS-SECTION OF ZONAL MEAN TOTAL CLOUD WATER CONTENT
 CONTOURS AT 0.01, 0.02, 0.05, 0.1 AND EVERY 0.1 ABOVE 0.2 STIPPLED
 DASHED LINES ARE 0 AND -15 DEGREE ISOTHERMS IN THE CONTROL
 CONTROL TEN YEAR DJF MEAN CMRP



(d) HEIGHT-LATITUDE CROSS SECTION OF ZONAL MEAN TOTAL CLOUD WATER
 CONTOURS AT 0.01, 0.02, 0.05, 0.1 AND EVERY 0.1
 DJF CONTROL LMD



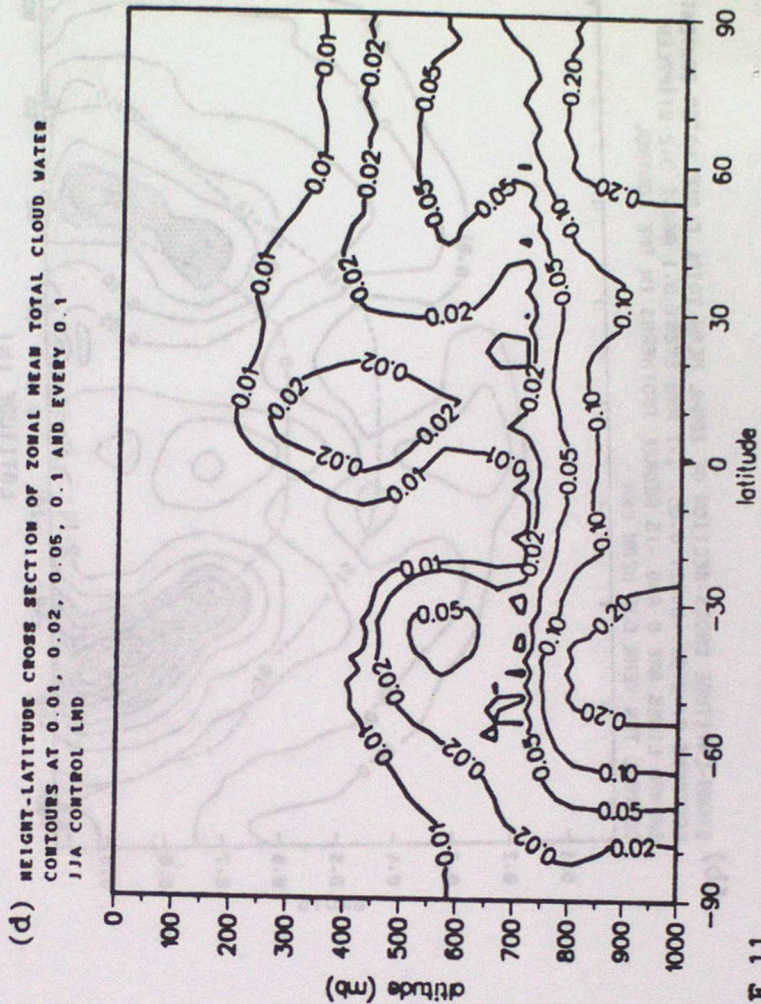
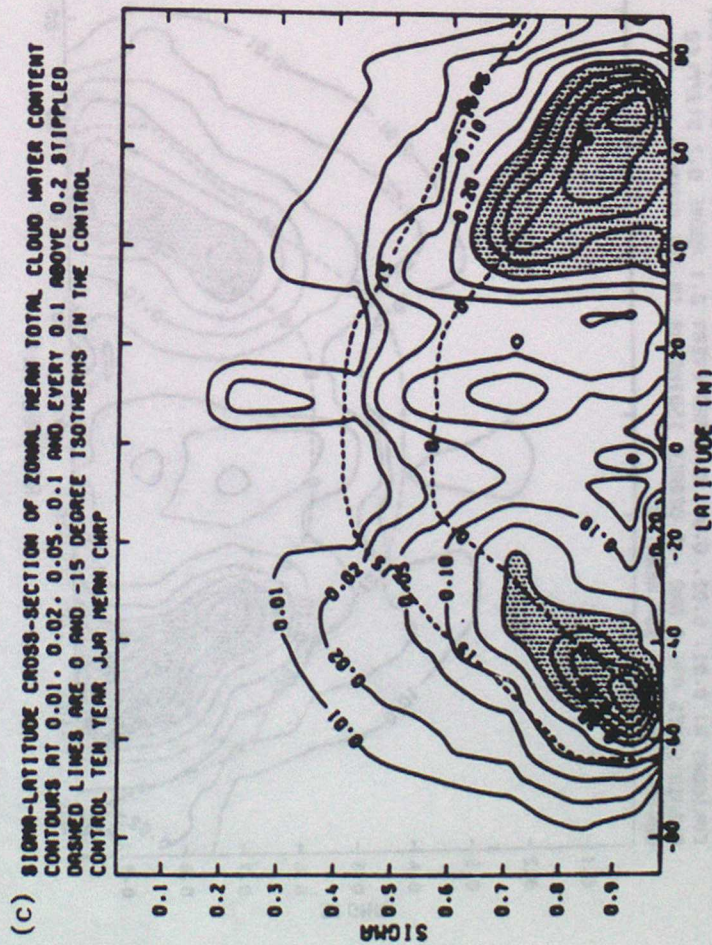
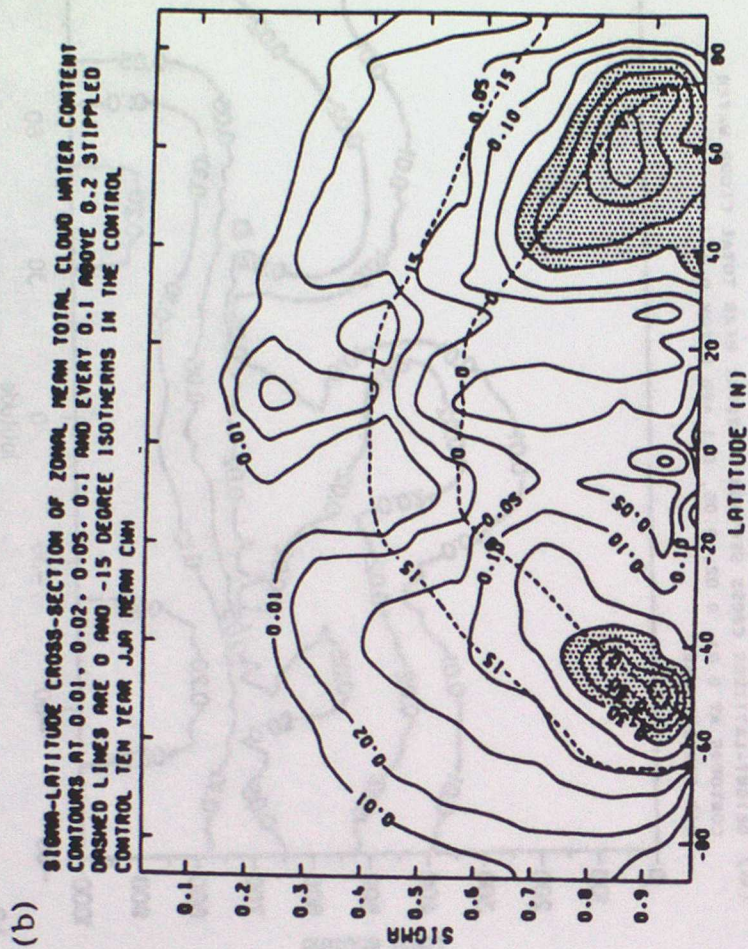
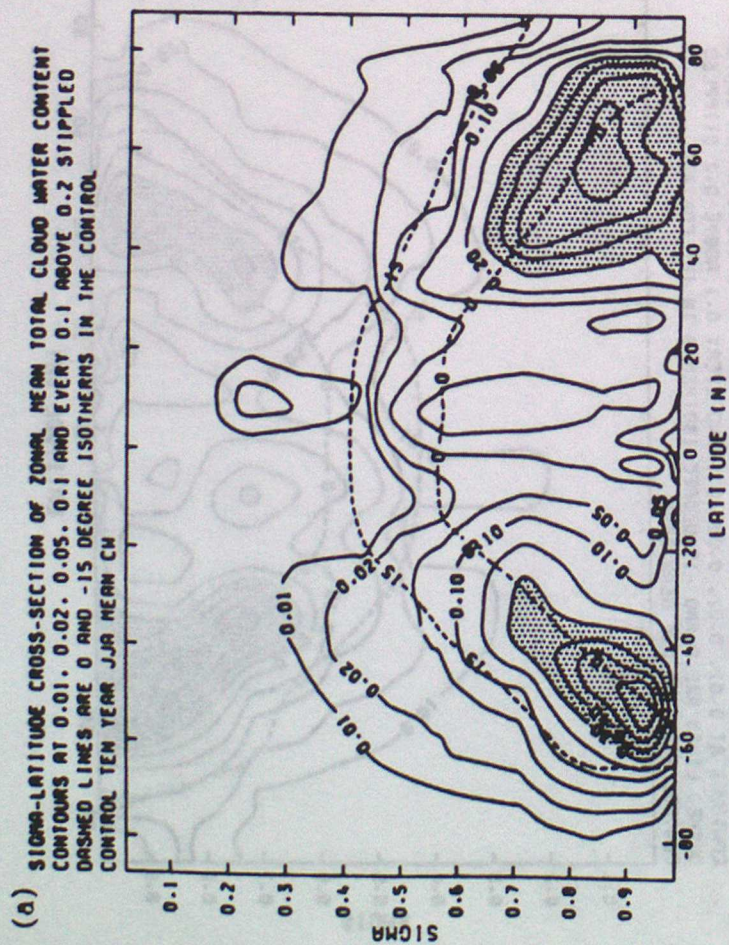
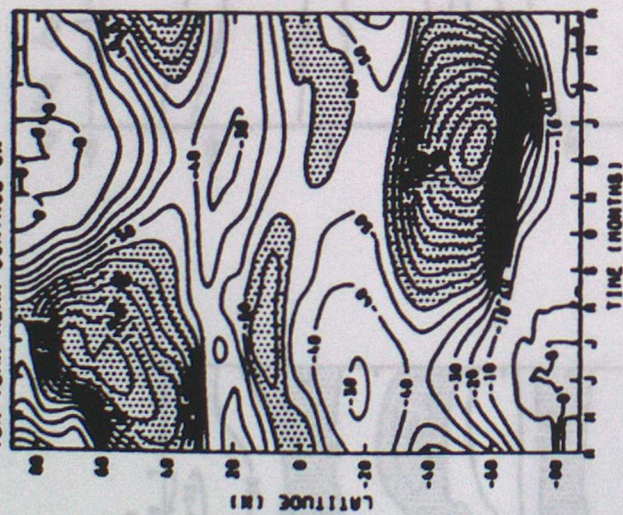
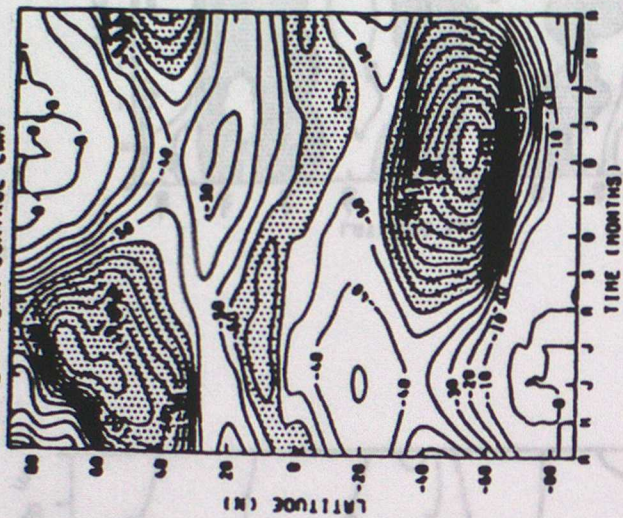


FIGURE 11

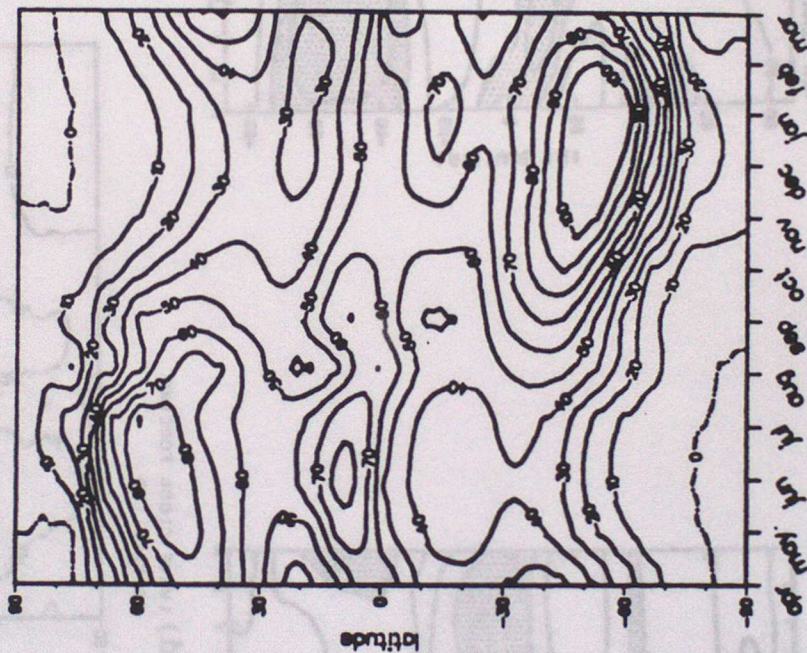
(a) SOLAR CLOUD FORCING
TEN YEAR MEAN CONTROL CM



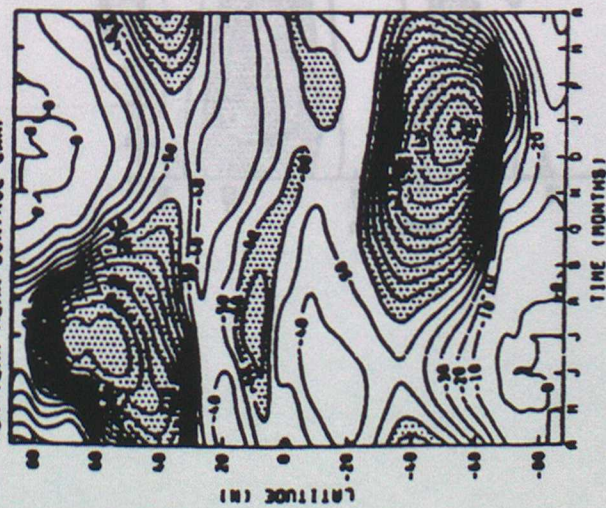
(b) SOLAR CLOUD FORCING
TEN YEAR MEAN CONTROL CM



(d) SOLAR CLOUD FORCING
CONTROL LND



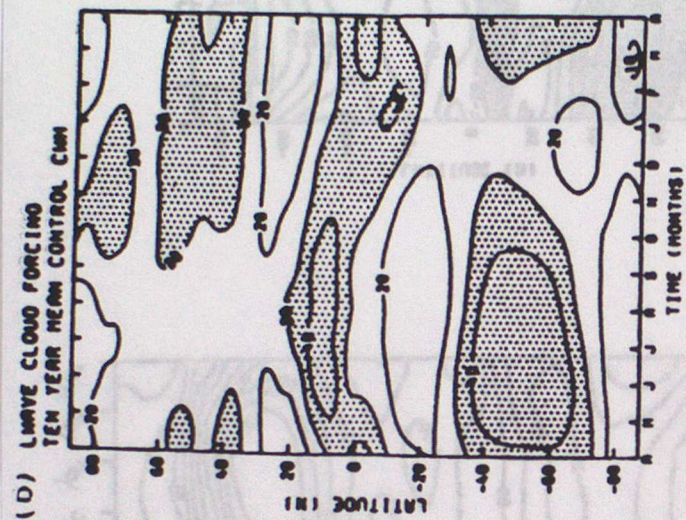
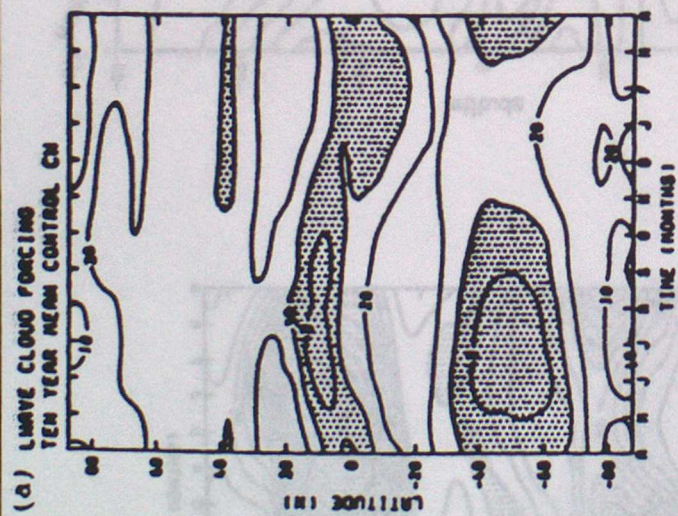
(c) SOLAR CLOUD FORCING
TEN YEAR MEAN CONTROL CM



(e)

SOLAR CLOUD FORCING
ERBE DATA FROM APR 85 TO APR 86





(d) LWAVE CLOUD FORCING
CONTROL LMD

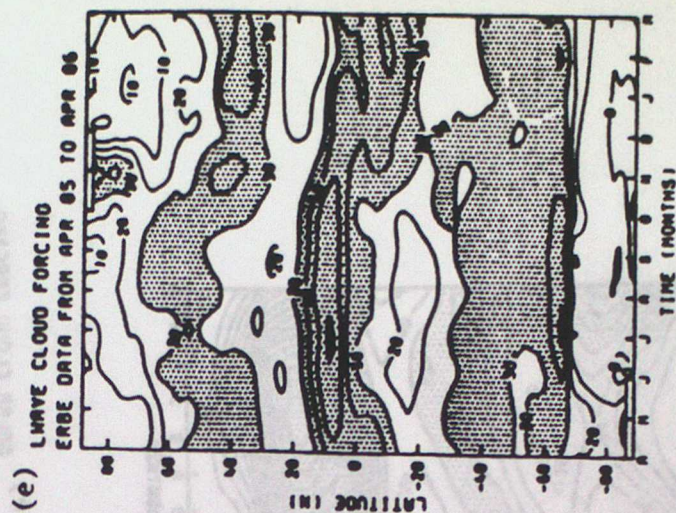
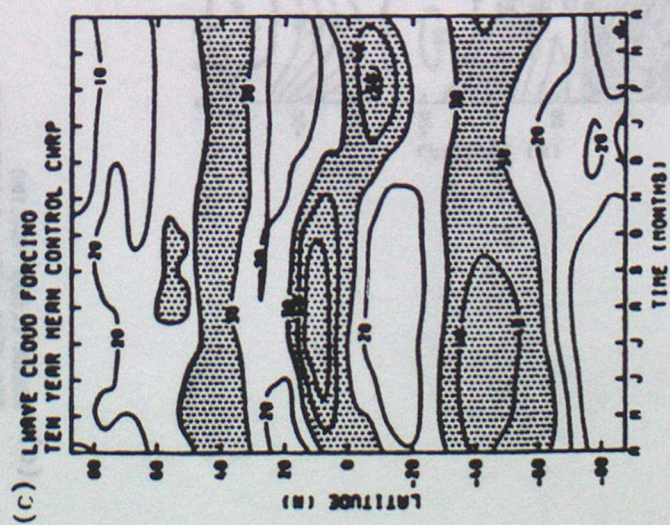
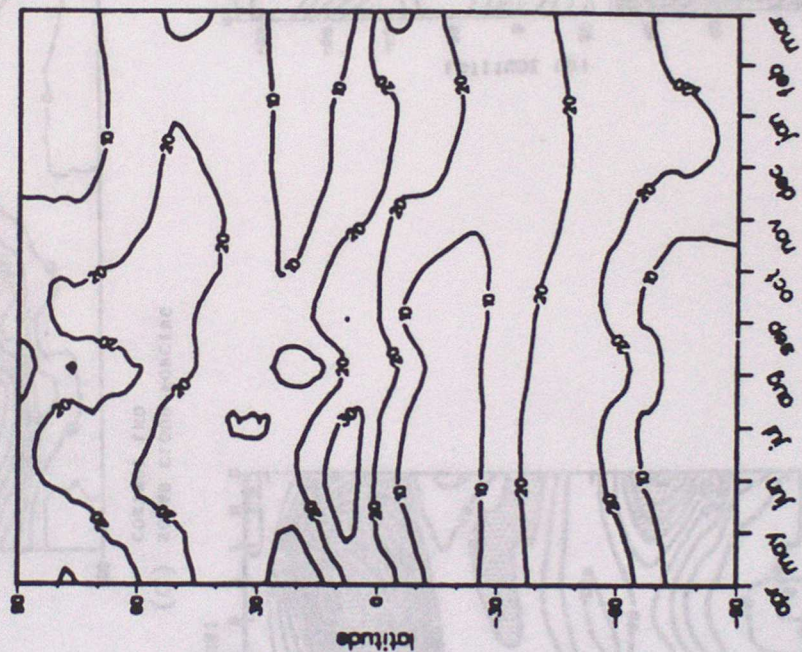
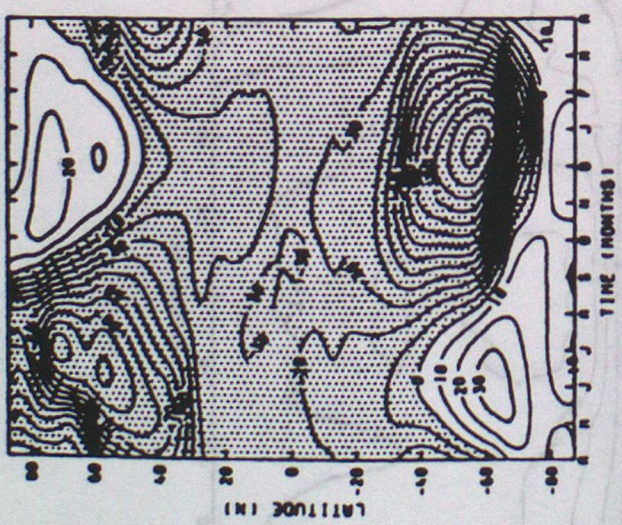
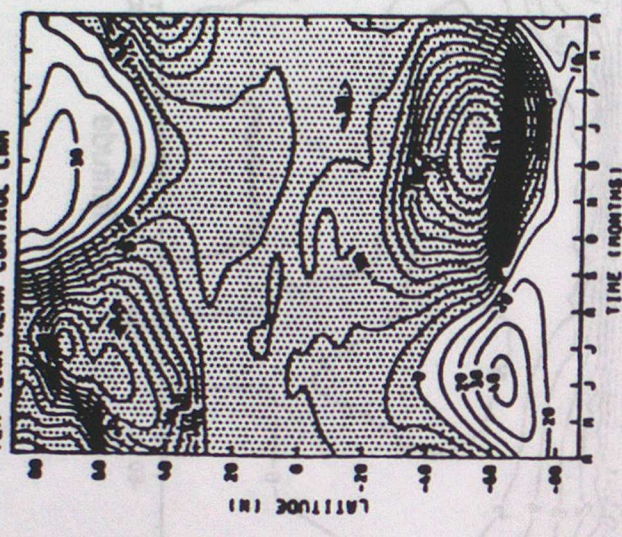


FIGURE 13

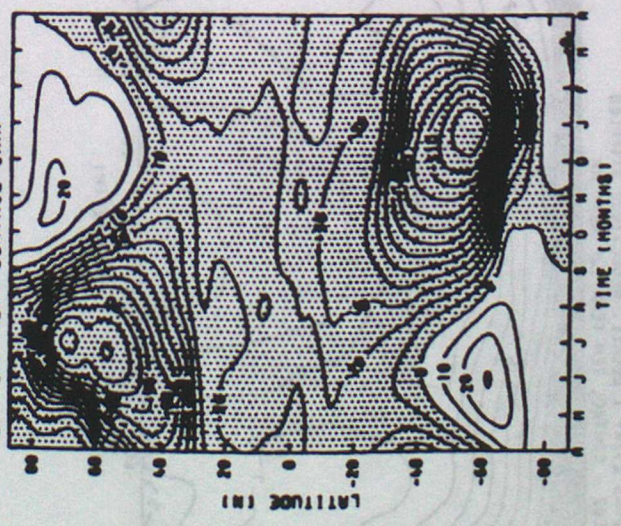
(a) NET CLOUD FORCING
TEN YEAR MEAN CONTROL CM



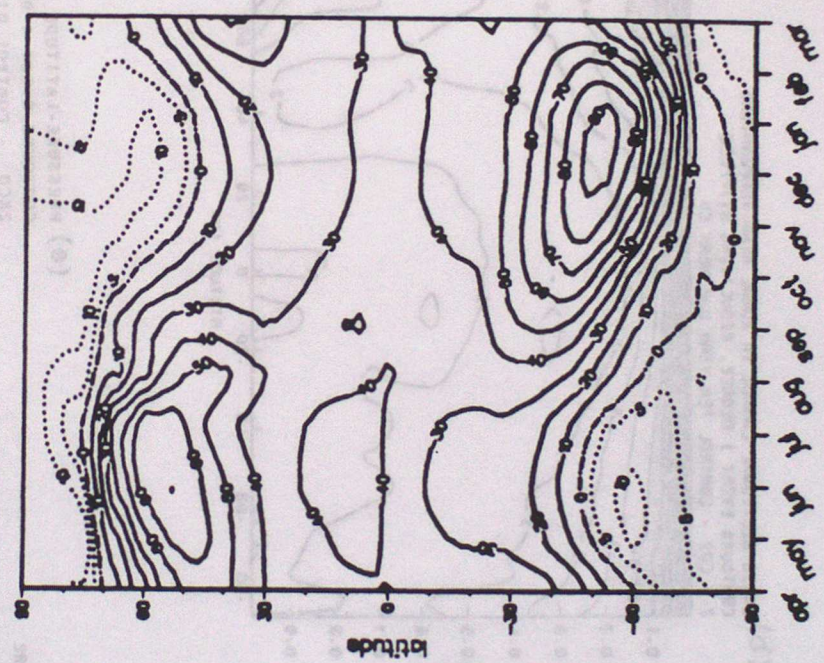
(b) NET CLOUD FORCING
TEN YEAR MEAN CONTROL CMM



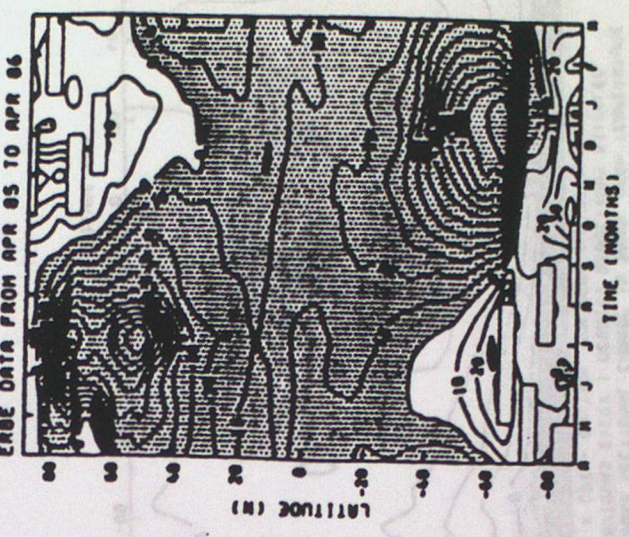
(c) NET CLOUD FORCING
TEN YEAR MEAN CONTROL CRRP



(d) NET CLOUD FORCING
CONTROL LMD



(e) DAY NETCF
ERBE DATA FROM APR 85 TO APR 86



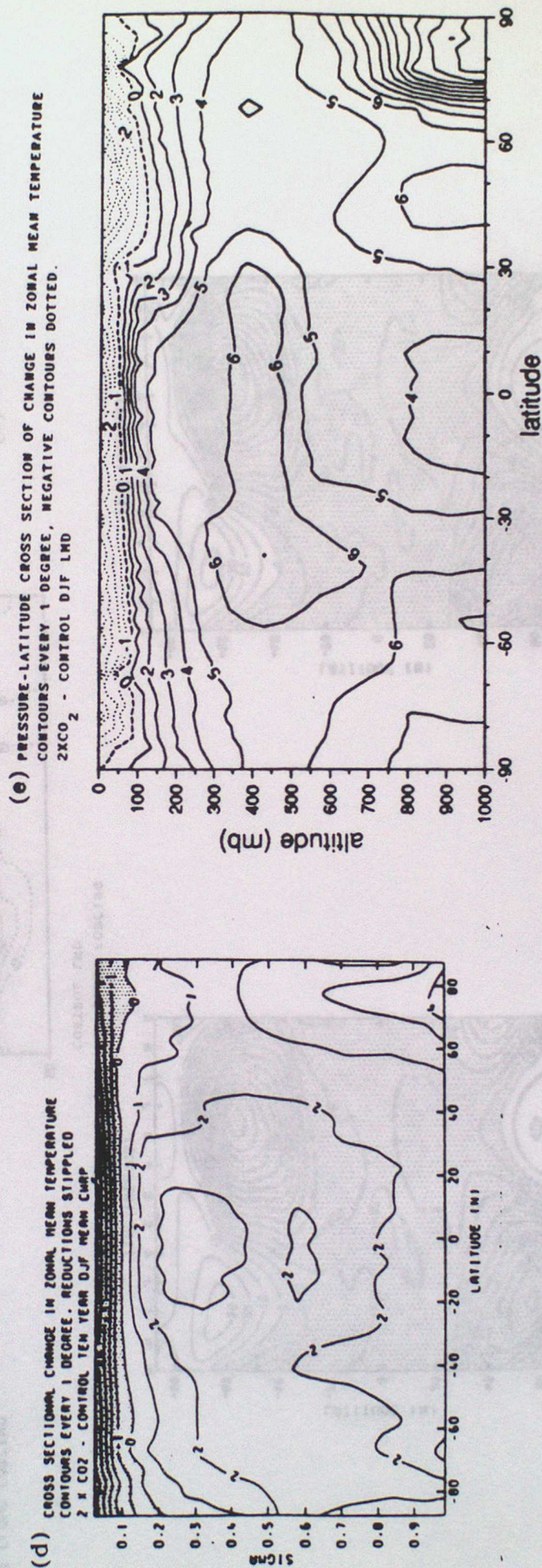
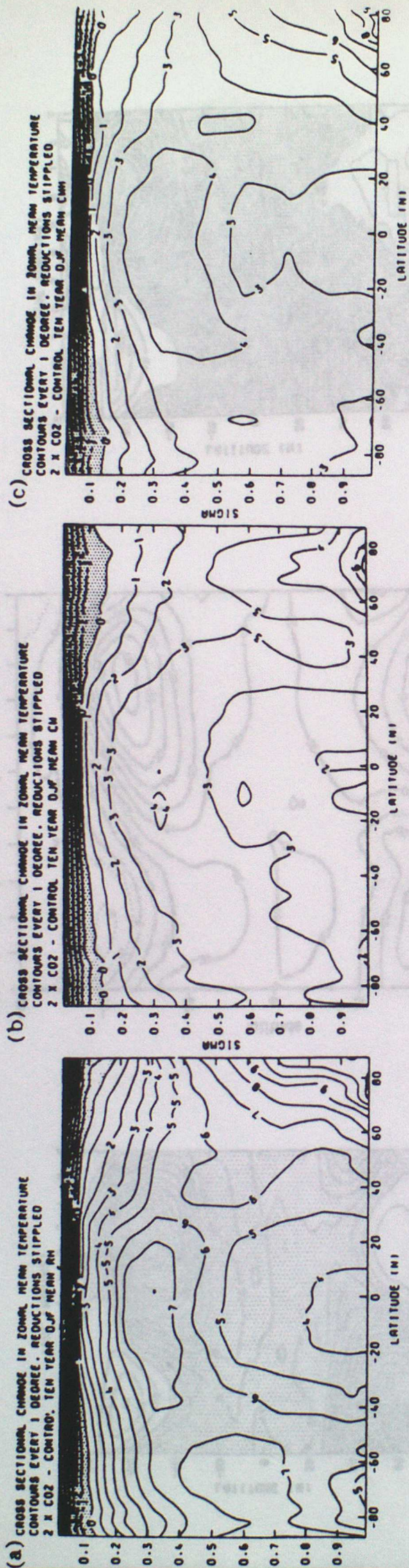


FIGURE 15

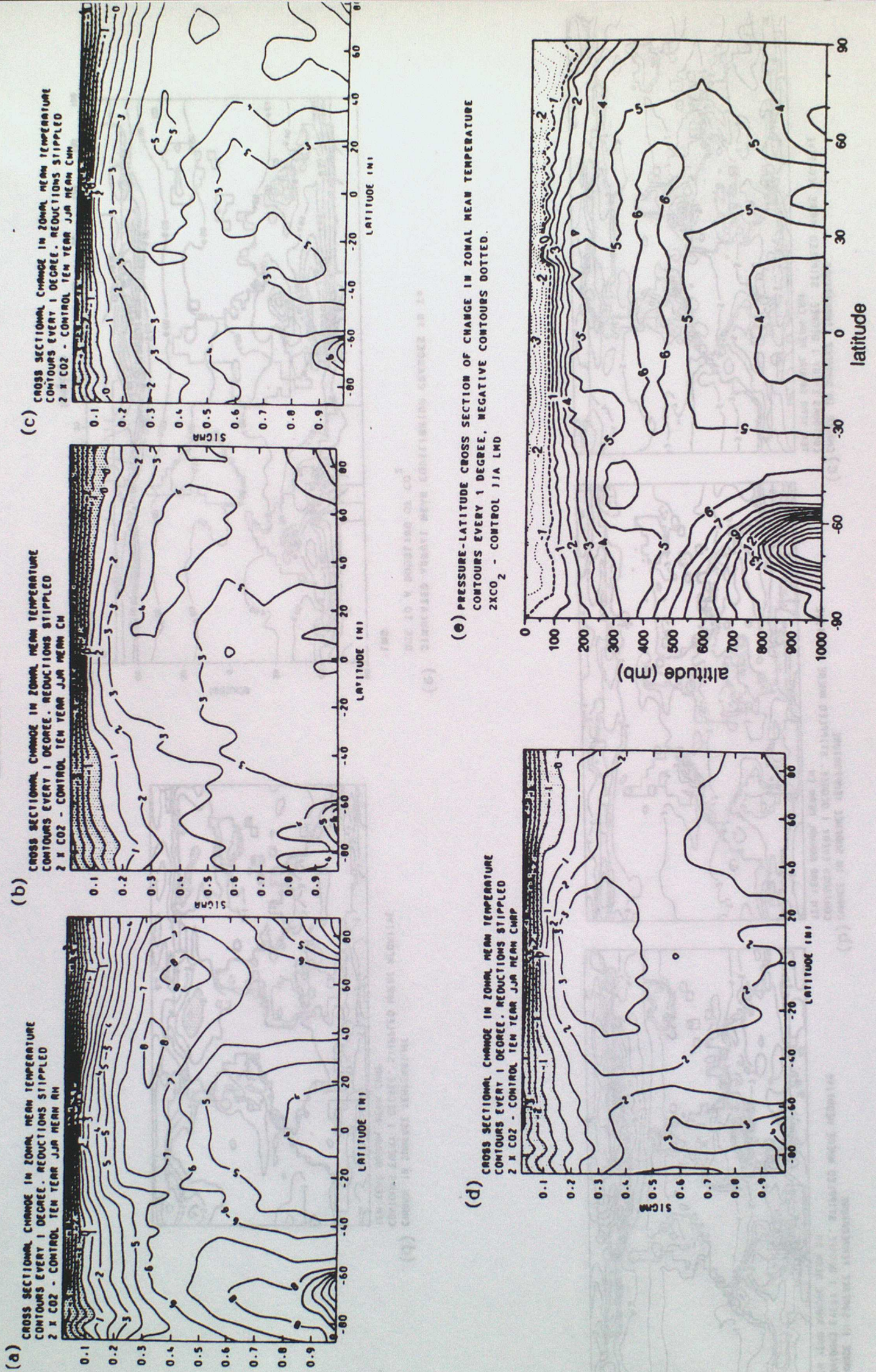
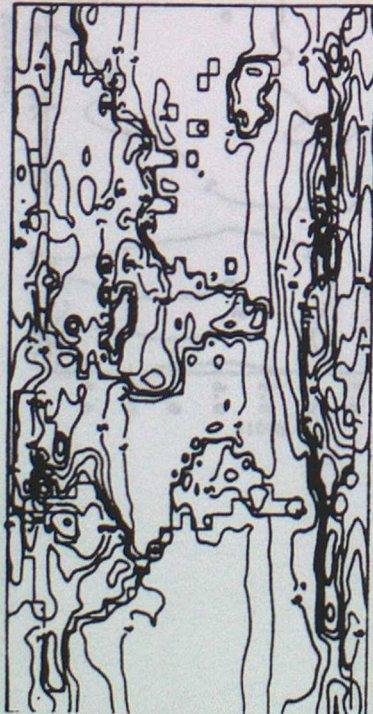


FIGURE 16

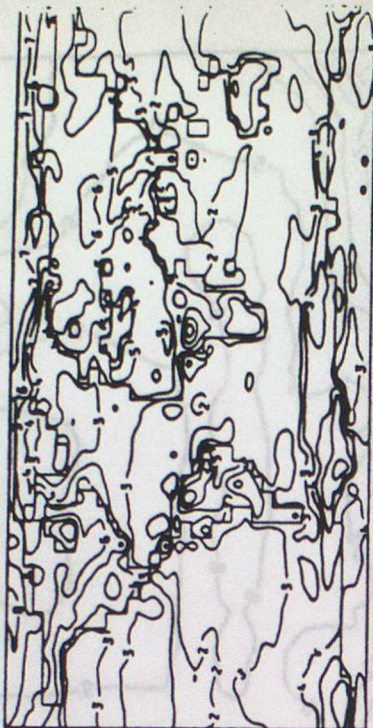
CHANGE IN SURFACE TEMPERATURE
 CONTOURS EVERY 1 DEGREE. STIPPLED WHERE NEGATIVE
 TEN YEAR ANNUAL MEAN RM



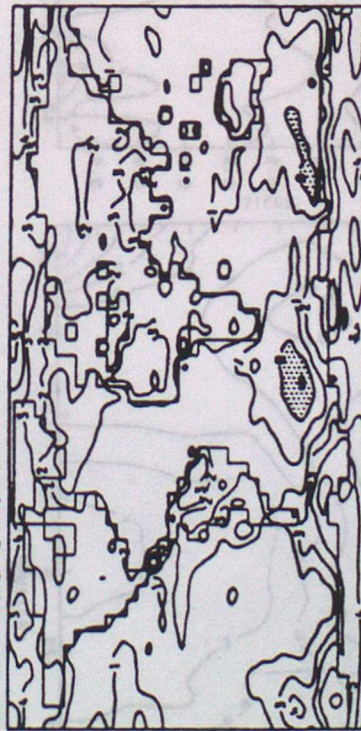
CHANGE IN SURFACE TEMPERATURE
 CONTOURS EVERY 1 DEGREE. STIPPLED WHERE NEGATIVE
 TEN YEAR ANNUAL MEAN CM



CHANGE IN SURFACE TEMPERATURE
 CONTOURS EVERY 1 DEGREE. STIPPLED WHERE NEGATIVE
 TEN YEAR ANNUAL MEAN CNH



CHANGE IN SURFACE TEMPERATURE
 CONTOURS EVERY 1 DEGREE. STIPPLED WHERE NEGATIVE
 TEN YEAR ANNUAL MEAN CNRP



SIMULATED ANNUAL MEAN EQUILIBRIUM CHANGES IN T_a
 DUE TO A DOUBLING OF CO_2
 LMD

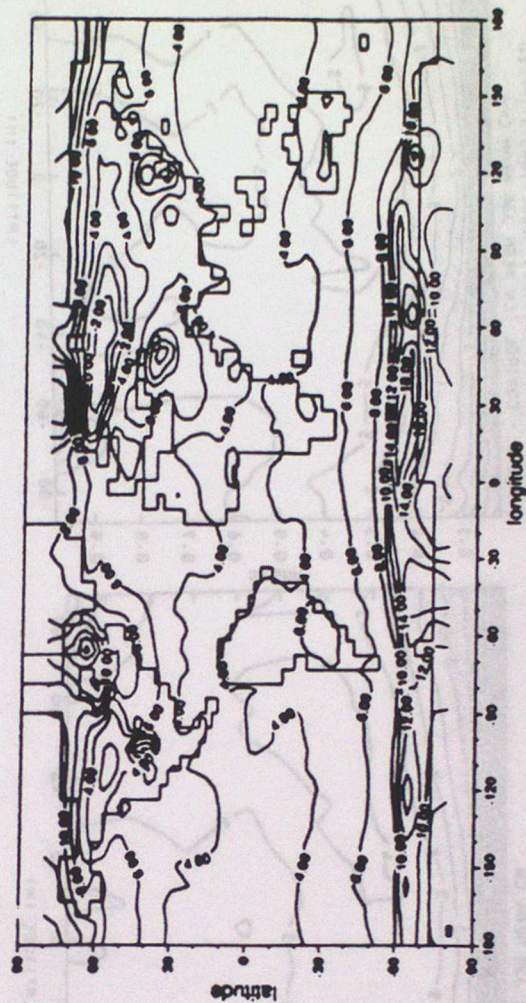
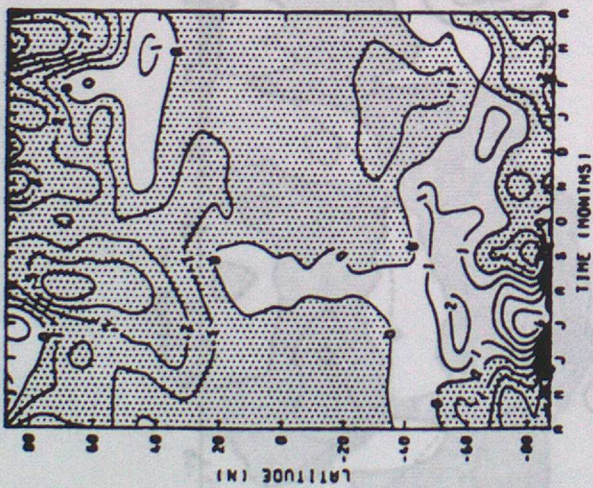
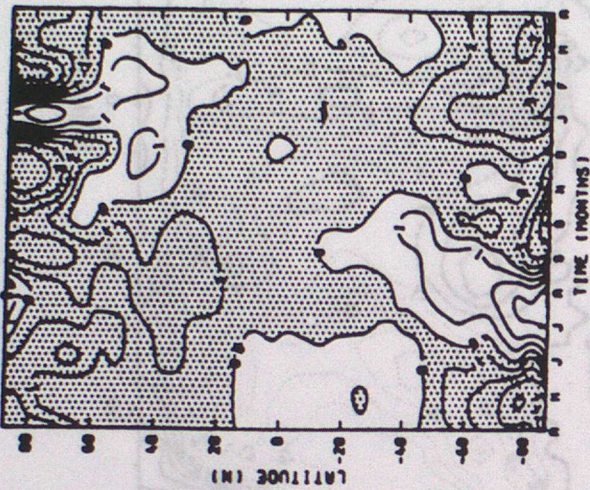


FIGURE 17

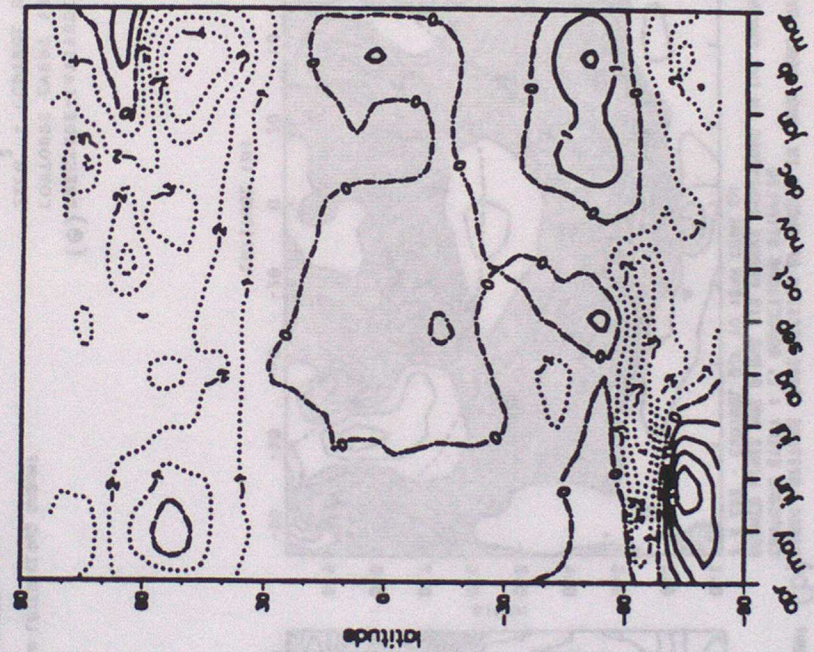
(a) DIFFERENCE IN PMSL
TEN YEAR MEAN RH



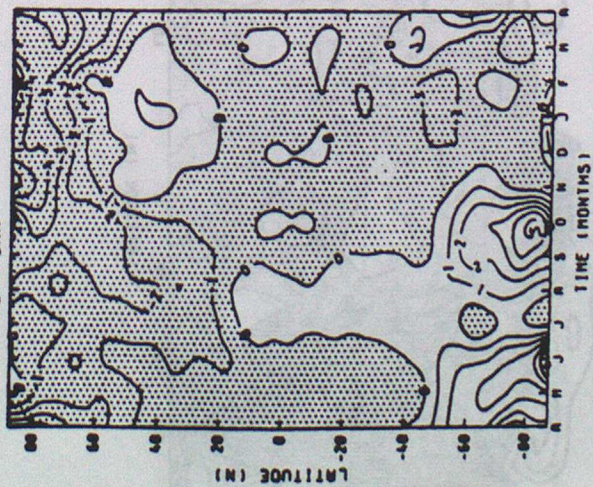
(b) DIFFERENCE IN PMSL
TEN YEAR MEAN CH



(d) DIFFERENCE IN PMSL
LND



(c) DIFFERENCE IN PMSL
TEN YEAR MEAN CHH



(e) DIFFERENCE IN PMSL
TEN YEAR MEAN CHRP

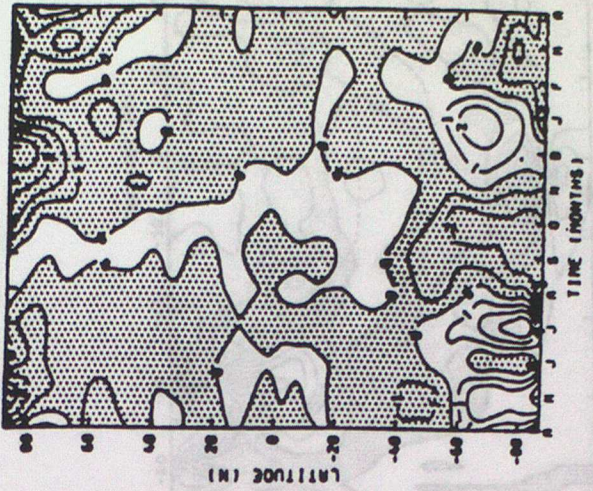
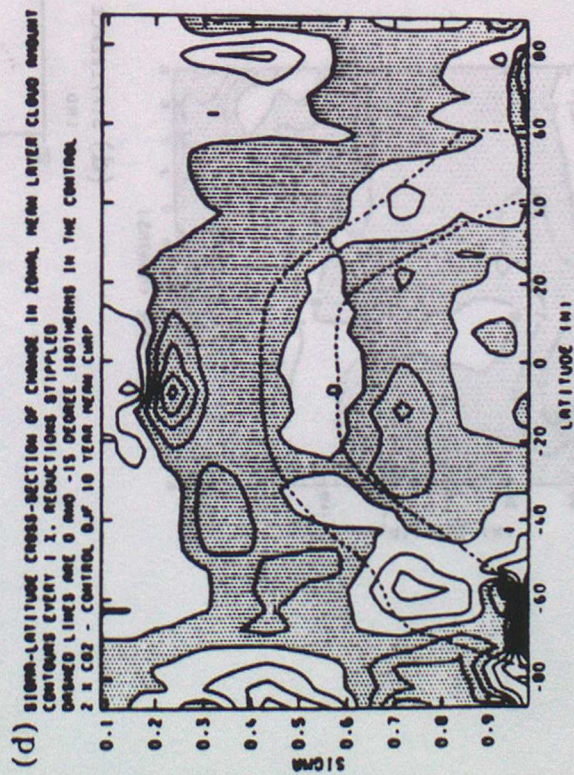
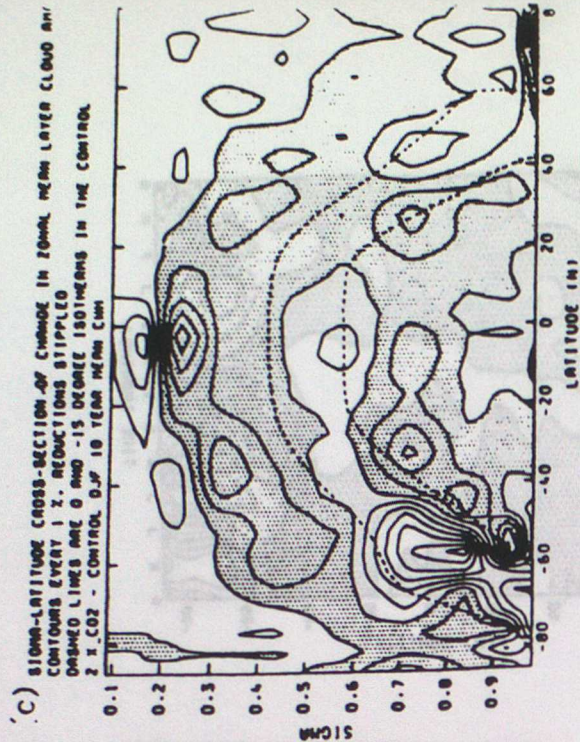
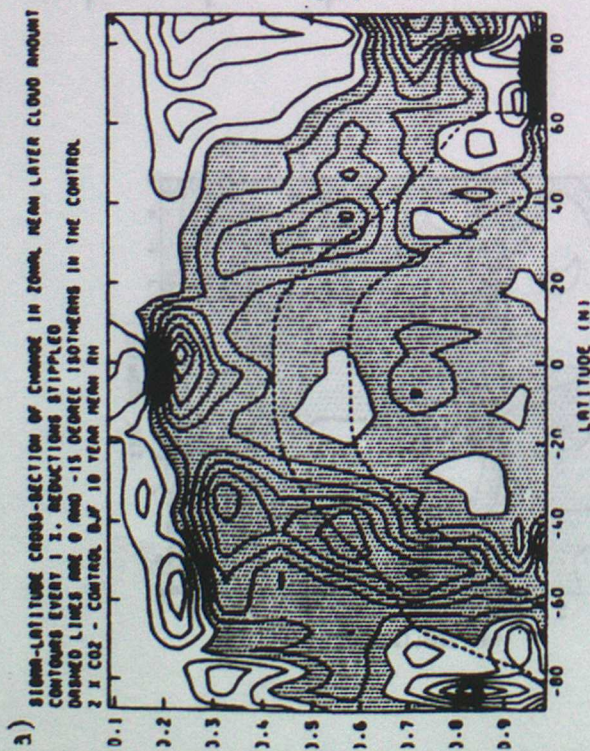


FIGURE 18



(e) PRESSURE-LATITUDE CROSS SECTION OF CHANGE IN ZONAL MEAN LAYER CLOUD AMOUNT
 CONTOURS EVERY 1%, NEGATIVE CONTOURS DOTTED.
 2XCO₂ - CONTROL DJF LMD

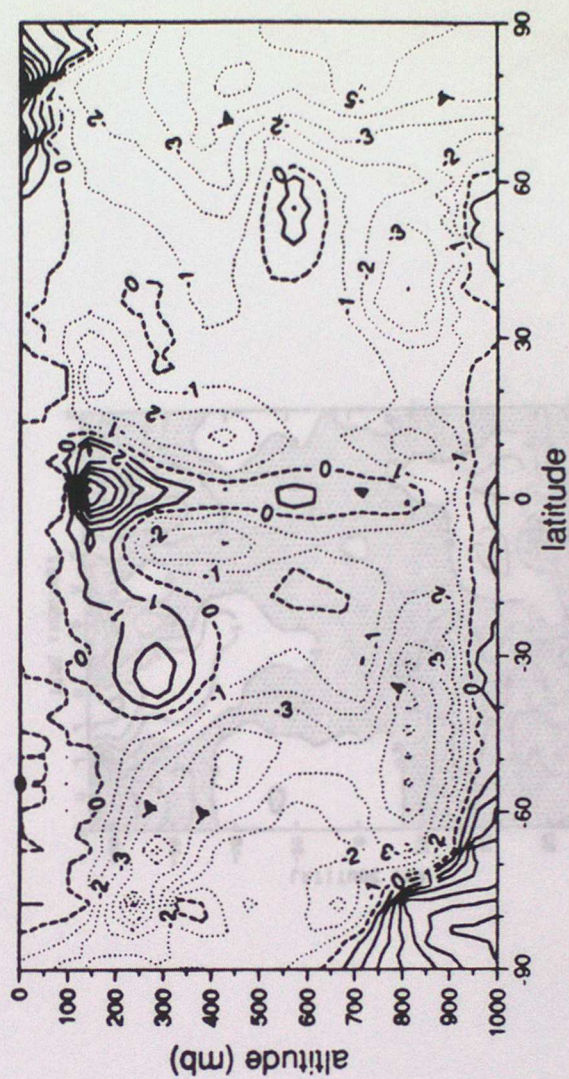


FIGURE 19

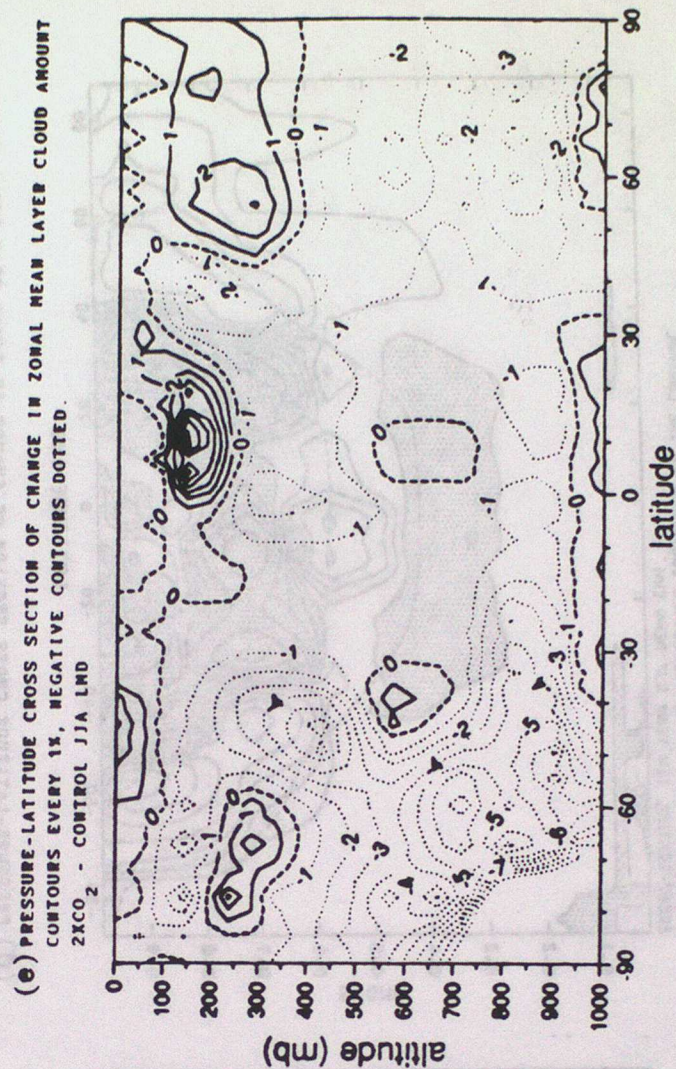
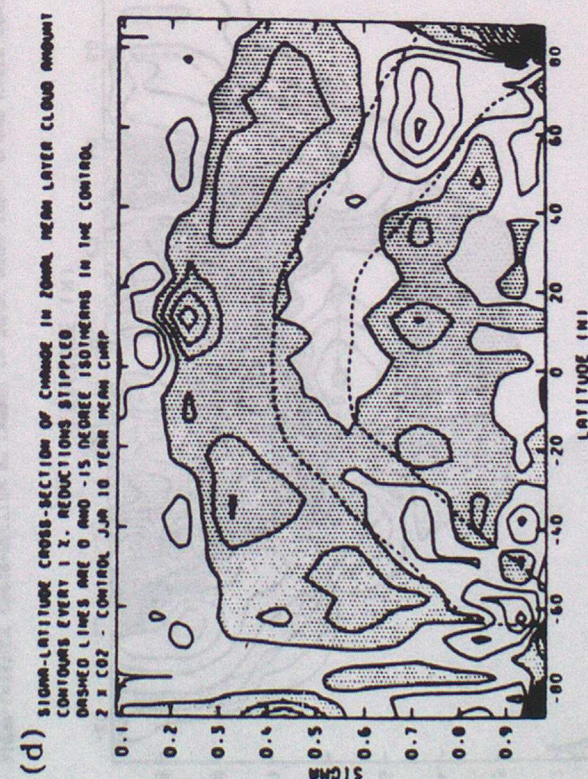
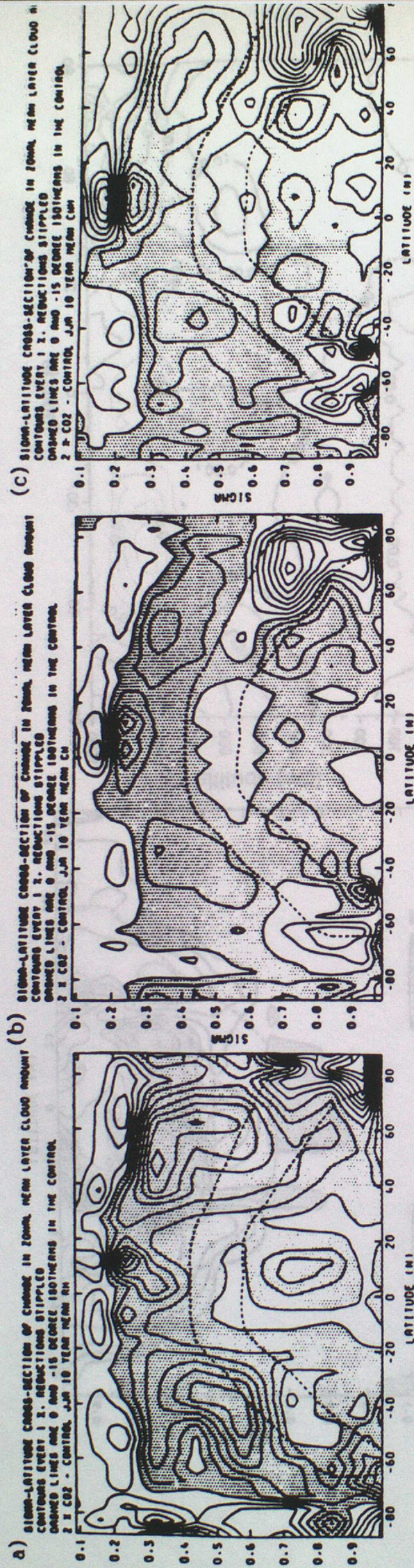


FIGURE 20

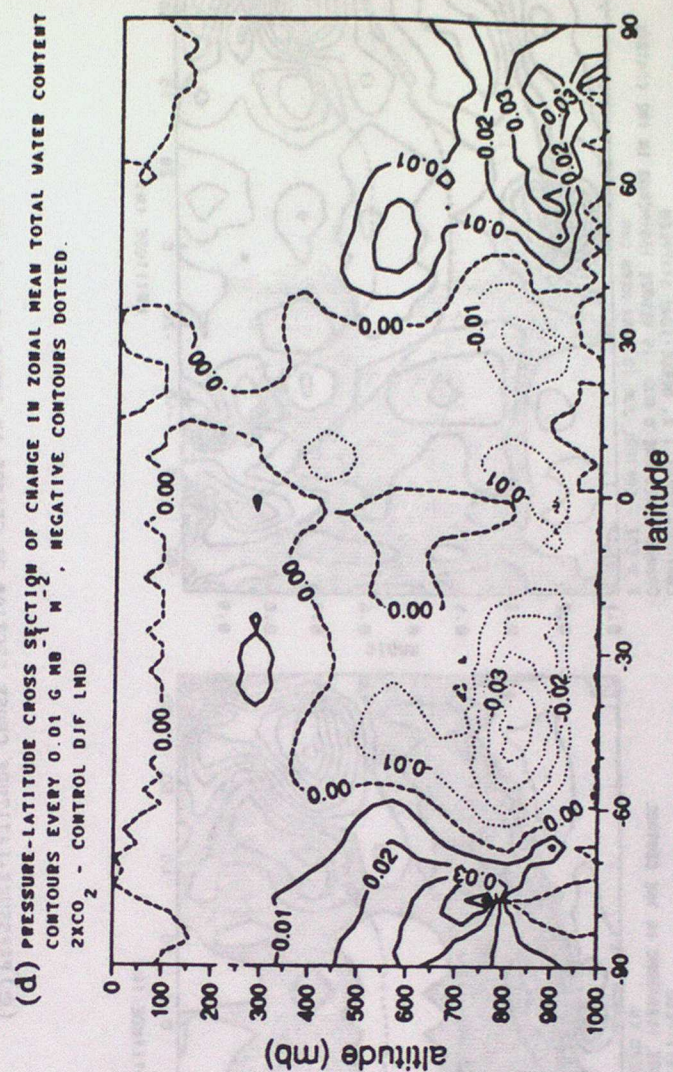
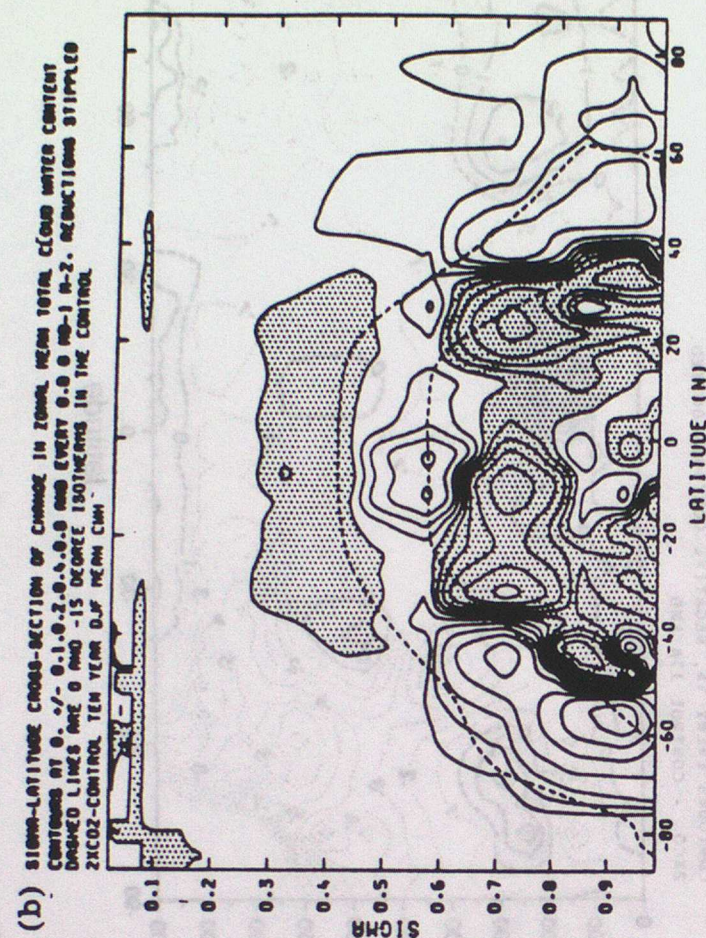
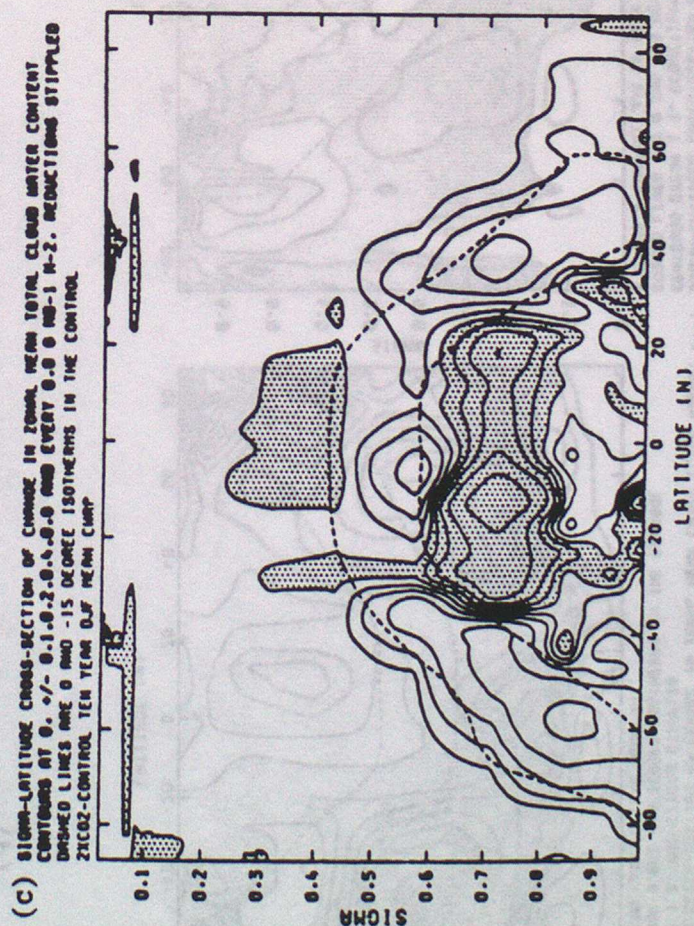
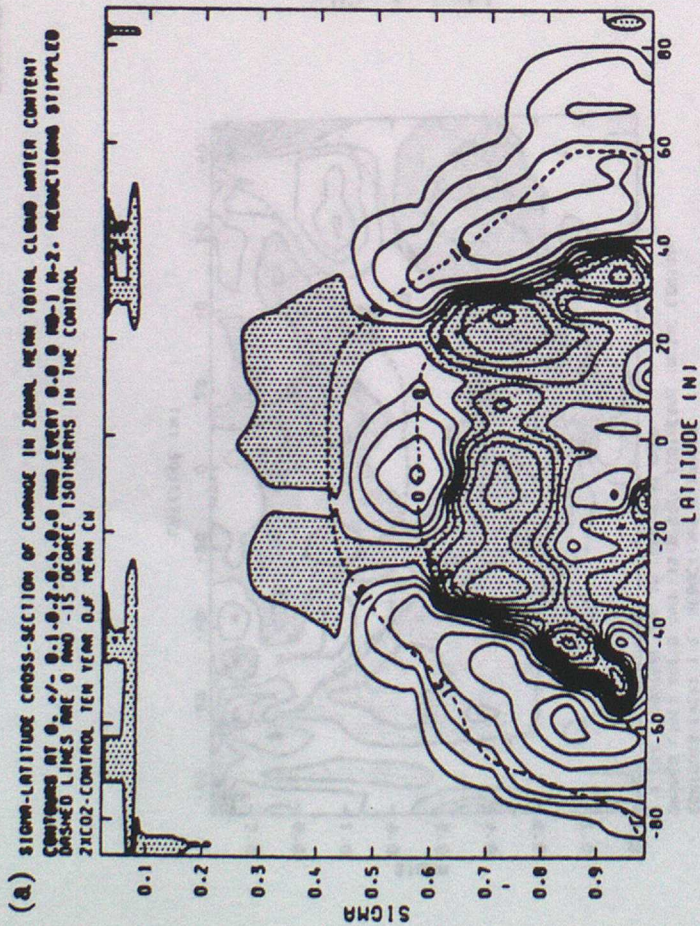


FIGURE 21

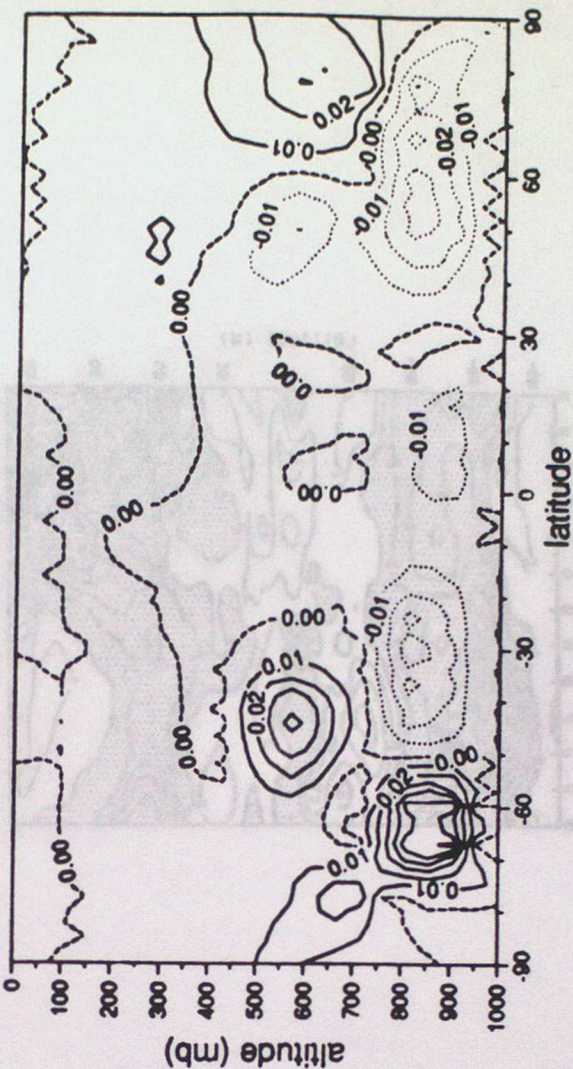
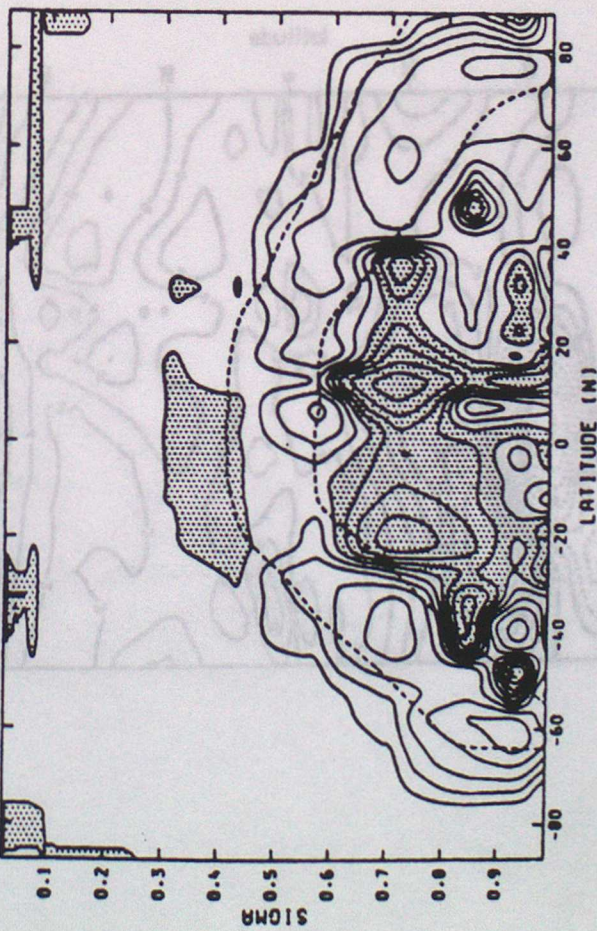
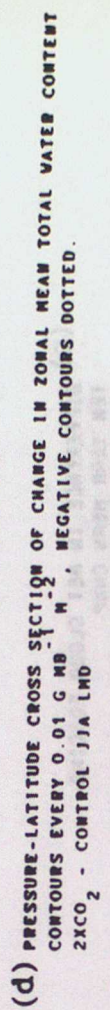
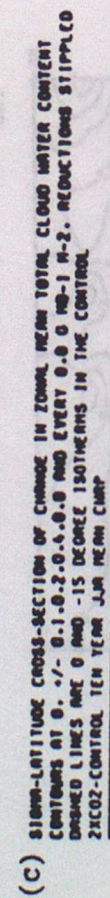
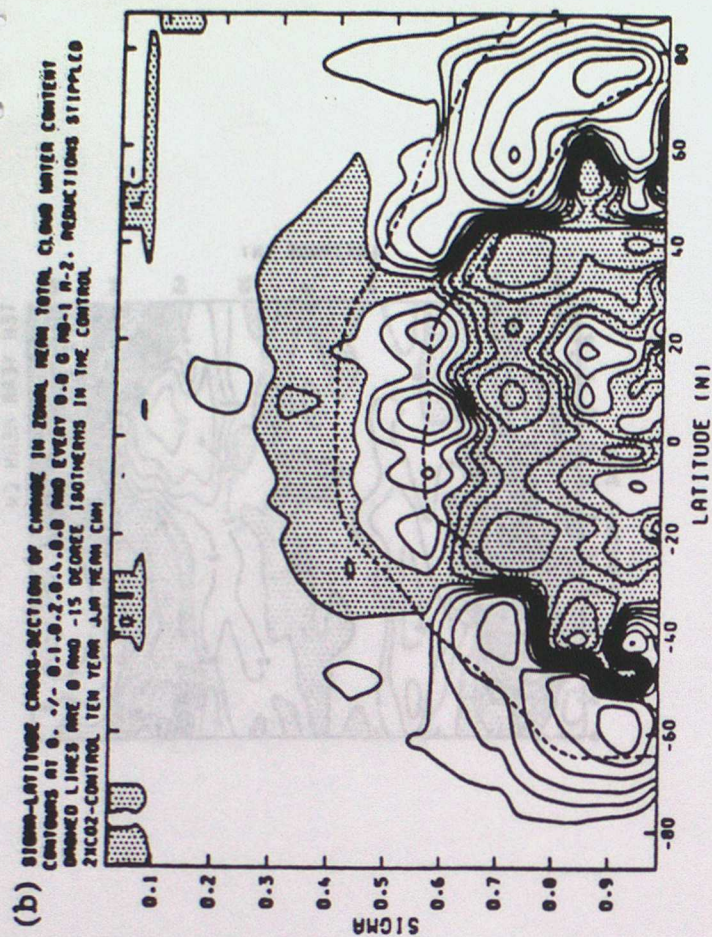
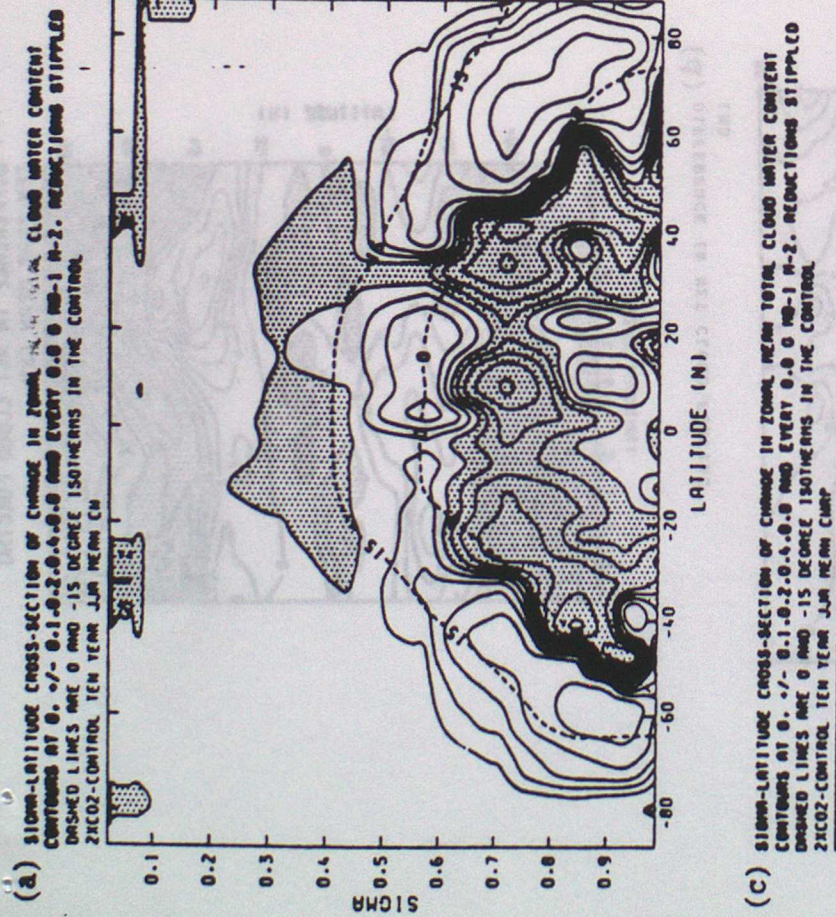
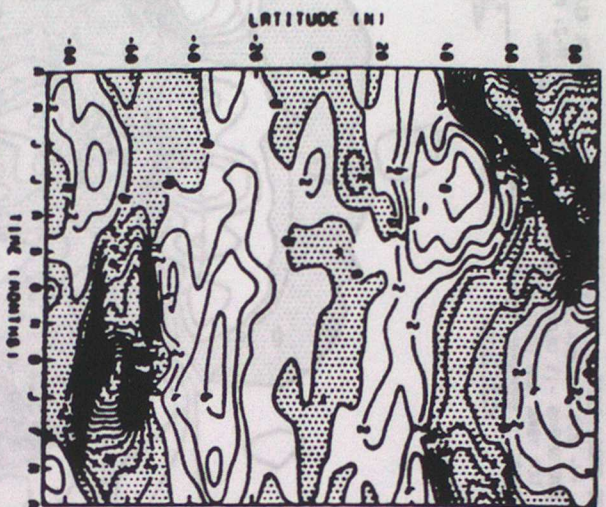
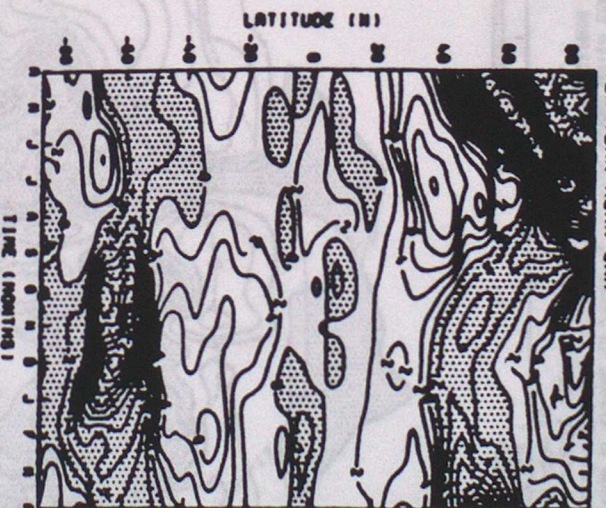


FIGURE 22

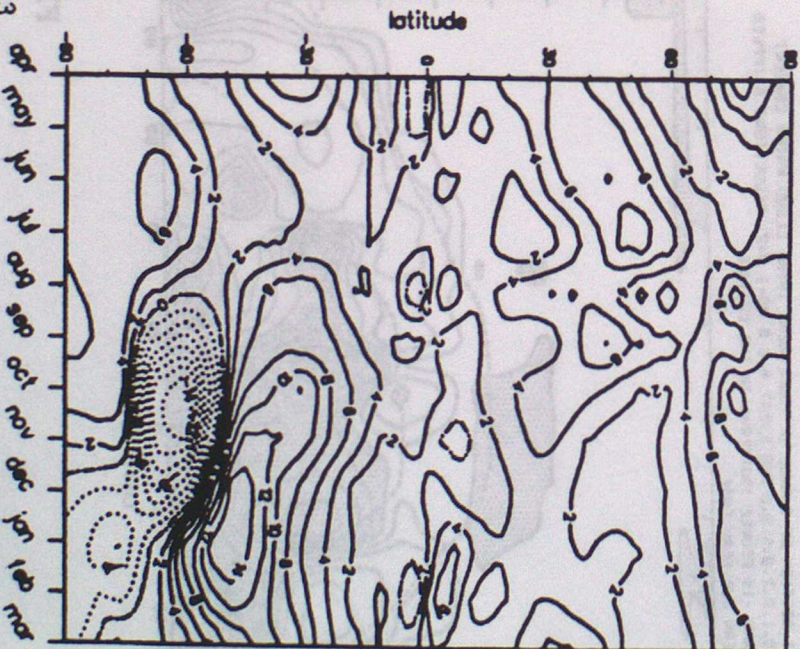
(b) DIFFERENCE IN NET CLOUD FORCING
TEN YEAR MEAN CM



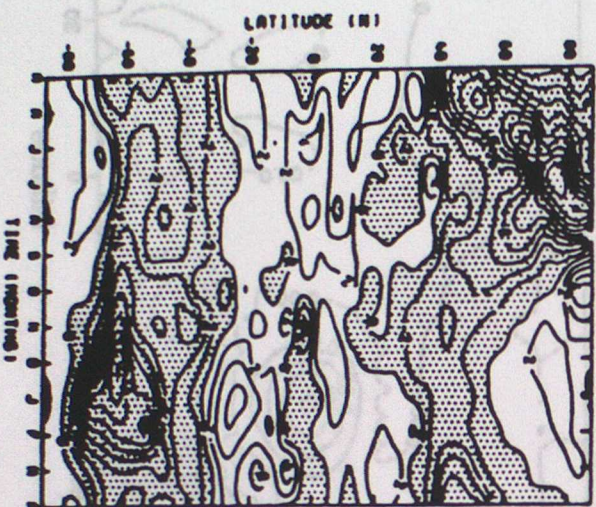
(c) DIFFERENCE IN NET CLOUD FORCING
TEN YEAR MEAN CM



(d) DIFFERENCE IN NET CLOUD FORCING
LND



(e) DIFFERENCE IN NET CLOUD FORCING
TEN YEAR MEAN CMRP



CHAPTER 4

THE IMPACT OF RESOLUTION ON THE SIMULATION OF CLOUD
AND RADIATION

BY

C A SENIOR

Introduction

Most contemporary models used for the simulation of climate and climate change have been limited to low resolution because of the lack of available computer power. It is thought that higher resolution models (grid spacing $< 4^\circ$) should be able to better simulate the small scale features of the general circulation. It is clearly of interest to consider the impact on the simulation of cloud forcing and feedback of moving from a resolution of more than 4° to one of less than 4° . A higher resolution version of CWH (Senior and Mitchell, this volume) has been run. The differences in cloud and cloud forcing in the present day climate and the cloud feedback produced for a doubling of CO_2 are considered below.

1. Models

A version of the UKMO AGCM coupled to a static 50m mixed layer ocean was run at two different horizontal resolutions, $5^\circ \times 7.5^\circ$ and $2.5^\circ \times 3.75^\circ$ Latitude/Longitude. The basic model is that described by Senior and Mitchell (this volume, referred to as CWH) with a cloud water content layer cloud scheme, fixed cloud radiative properties (Table 2, Senior and Mitchell, this volume) and a parametrization of cloud ice precipitation based on that by Heymsfield (1977).

The cloud scheme was tuned slightly for a lower horizontal resolution and a longer forward timestep in order to produce realistic cloud amounts. This involved lowering the relative humidity thresholds above which layer cloud is formed from 0.85 to 0.8 (all cloud layers except the lowest) and from 0.95 to 0.925 (in the lowest layer). A slight lowering of the threshold above which convective precipitation was initiated was also included. The two models were otherwise identical. Clearly any differences between the models in a comparison of resolution dependence is undesirable but it was felt that these changes were necessary to prevent unrealistically large amounts of cloud in the control version of the low resolution model. The $5^\circ \times 7.5^\circ$ and $2.5^\circ \times 3.75^\circ$ Latitude/Longitude resolutions will henceforth be referred to as CWH and HCWH respectively. The results shown are means for January and July from the final ten years of each experiment after reaching equilibrium for comparison with satellite data. To smooth the changes on doubling CO_2 , seasonal mean (December to February and June to August) difference charts will be shown.

1. Present Day Climate

(a) Cloud amount

The pattern of zonally averaged stratiform cloud is generally similar in both HCWH and CWH (Figure 1), with maxima in low cloud at high latitudes and high cloud at low latitudes, arising from areas of deep convection. On average the cloud amount is rather greater in HCWH than in CWH. This is especially true at mid-latitudes in the Southern Hemisphere, because of the much deeper simulation of the Southern Hemisphere circumpolar trough in this model (not shown) and in the sub-tropical boundary layer. The greater amount of tropical high cloud may be more realistic but the increased cloud at high latitudes is excessive when compared to a ground based climatology (Warren et al 1986, 1988).

The seasonal cycle of cloud (Figure 2) is again similar at both resolutions. The tendency for increased summer cloud amounts in the Northern Hemisphere is more noticeable in HCWH although the seasonal cloud changes at high latitudes in the Southern Hemisphere are less pronounced than in CWH. The Northward shift of the ITCZ in JJA, marked by cloud amounts greater than 50%, is similar at both resolutions.

(b) Cloud Radiative Forcing

Below, we consider comparisons of cloud forcing (Ramanathan et al 1989) from the two model resolutions with cloud forcing data from the Earth Radiation Budget Experiment (ERBE) (Barkstrom et al 1984). For brevity, only the July simulations and satellite data will be shown but the model errors are similar in January.

(i) Cloud Shortwave Forcing

In July both models simulate the strongest forcing over Northern mid-latitudes as in the ERBE data (Figure 3), however the magnitude is excessive especially in HCWH by as much as 25 Wm^{-2} and neither model simulates well the areas of much reduced CSF over North America and Eurasia although this is slightly better in CWH. HCWH simulates the largest peaks in CSF in the tropics rather better than CWH with a maximum further north over India, and stronger forcing over both South America and Africa. Both models simulate areas of weak forcing over land reasonably well but show overall

too strong a forcing particularly over the sub-tropical oceans.

The global mean values (Table 1) highlight the excessive strength of CSF in HCWH which may be due to too much cloud (especially at high latitudes as discussed above) or too high values of cloud albedo.

(ii) Cloud Longwave Forcing

In July both models show quite realistic maxima in CLF in the tropics especially over the bay of Bengal and the South China sea although the ERBE data suggests that the magnitude of the forcing is greater (Figure 4). The low resolution model has the largest forcing in the tropical west pacific, west of that observed and that in the high resolution model, illustrating the poor monsoon circulation in this model. HCWH shows a better structure and strength in the maximum over Africa and to some extent over South America than CWH. Each model has too great a CLF over the Southern ocean which may be associated with too much high cloud or too large a value of high cloud emissivity. In January (not shown) both models have quite a good representation of maximum CLF over the North Atlantic storm track but once again the tropical maxima are too weak.

The Global mean values of CLF (Table 1) show good agreement with ERBE data for both resolutions in both seasons.

2. Changes on doubling CO_2

A further experiment was performed with both versions of the model in which CO_2 amounts were doubled and the experiments were run for ten years after equilibrium was reached. All the charts are $2 \times \text{CO}_2$ - CONTROL mean differences over the periods December, January and February (DJF) and June, July and August (JJA) for the last ten years of each experiment at equilibrium.

(a). Zonally averaged Cloud

The patterns of change in zonally averaged cloud (Figure 5) are similar in both seasons in the two models with overall reductions in cloud amount but some localised increases in cloud, particularly in medium and low cloud at mid-high latitudes. The summer hemisphere increases are of similar magnitude in JJA but in DJF they are substantially larger in HCWH, where more cloud was present in the control. The changes in cloud in the low

resolution model with the cloud liquid water scheme (Smith 1990) have been discussed by Senior and Mitchell (this volume) and this is generally applicable to the higher resolution model as well. The largest increases occur between the 0°C and -15°C isotherms where cloud droplets change from cloud ice to cloud water as the atmosphere warms in response to increased CO_2 . The net change in low and medium level cloud is however a reduction and in HCWH there are marked changes in very high latitude cloud at mid levels in the Northern Hemisphere in JJA whereas in CWH these reductions are confined to latitudes equatorwards of 70°N . The upward shift of high tropical cloud is noticable at both resolutions but in HCWH, in JJA, the cloud increases occur on either side of the equator at around 10°N and S with a small net reduction in high cloud in between. The time-latitude diagrams of differences in total cloud amount (Figure 6) show that the largest increases occur at high latitudes. In CWH, the greatest increases occur in summer in both hemispheres, however in HCWH the largest increases are in spring and autumn in the Northern Hemisphere and summer in the Southern Hemisphere.

(b) Changes in Cloud radiative forcing

(i) Cloud Shortwave Forcing (CSF)

The zonally averaged changes in CSF (Figure 7) show a similar pattern in both seasons at both resolutions with a general reduction in the magnitude of CSF (as CSF is negative this appears as a positive change) in tropical and mid-latitudes where high albedo clouds at mid and low levels are reducing overall. This agreement reflects the similar cloud changes discussed above. At high latitudes in the summer hemisphere there is a large increase in CSF in both models where the net change in low and mid level cloud is positive. In DJF the increases in cloud are greater in HCWH and so the increase in CSF is equivalently greater and in JJA the increases in cloud and CSF are greater in CWH. The global mean annual mean changes in CSF (Table 2) are positive at both resolutions, leading to an enhancement of the warming which is slightly greater in HCWH.

(ii) Cloud Longwave Forcing (CLF)

The change in CLF is much smaller than the change in CSF at both resolutions and in both seasons and both resolutions show a similar pattern

outside of the tropics (Figure 7). Changes in CLF are dominated by changes in high cloud and there is an upward shift of high cloud at both resolutions (as described above), but an overall reduction in amount and so the CLF is reduced. In HCWH, in JJA, high cloud moves upwards and spreads out producing two new cloud maxima either side of the old maximum at around 5° S and this results in a large reduction in CLF at this latitude which is not seen in CWH. Similarly in DJF, the upward movement of high cloud is accompanied by a slight northward shift which results in a increase in CLF at the latitude of the new maximum and a reduction just to the south of this. The global mean annual mean change in CLF is negative (Table 2) and is very similar at both resolutions and tends to offset the enhancement of the warming arising from the changes in CSF.

(c) Climate Sensitivity analysis

The change in CSF dominates over the change in CLF and so the overall effect of cloud is to enhance the warming, ie a positive cloud feedback. Using the notation of Cess et al (1990) an estimation of the cloud feedback can be calculated as λ/λ_C (Table 3), where λ and λ_C are the total and 'clear-sky' climate sensitivity parameters respectively (See Senior and Mitchell, this volume, for further details) and where values greater than 1 indicate a positive cloud feedback. This shows that there is a small positive cloud feedback at both resolutions, which is slightly larger in HCWH. It should also be noted that the clear-sky sensitivity λ_C is slightly larger in CWH.

3. Summary

The cloud and cloud radiative forcings are similar at both resolutions although there is some improvement in cloud and cloud forcing especially in the tropics with increasing resolution, when compared to ERBE data. The changes in cloud and cloud forcing on doubling CO_2 are also similar. Those differences that do occur are at least partly related to differences in the climatology of the model at different resolutions. This implies that the 'change of phase' cloud feedback found in the low resolution model and reported by Senior and Mitchell (this volume) is not resolution dependent.

Table 1 Global mean cloud forcing

FORCING	JULY			JANUARY		
	ERBE	HCWH	CWH	ERBE	HCWH	CWH
LW	29.8	30.4	30.6	29.7	27.6	28.7
SW	-48.4	-60.5	-57.2	-51.8	-63.3	-59.3
NET	-17.7	-30.1	-26.6	-21.7	-35.7	-30.7

Table 2 Change in annual mean cloud forcing

FORCING	HCWH	CWH
ΔLW	-1.87	-1.54
ΔSW	2.85	2.27
ΔNET	0.98	0.73

Table 3 Climate Sensitivity Analysis

MODEL	ΔT	λ	ΔC_F	λ_C	λ/λ_C
HCWH	3.4	0.85	0.98	0.68	1.25
CWH	3.3	0.84	0.73	0.71	1.18

References

- Barkstrom, B.R., 1984. The earth radiation budget experiment (ERBE). *Bull. Am. Met. Soc.*, 65, 1170-1185.
- Cess, R.D., G.L. Potter, J.P. Blanchet, G.J. Boer, A.D. Del Genio, M. Deque, V. Dymnikov, V. Galin, W.L. Gates, S.J. Ghan, J.T. Kiehl, A.A. Lacis, H. Le Treut, Z.-X. Li, X.-Z. Liang, B.J. McAvaney, V.P. Meleshko, J.F.B. Mitchell, J.J. Morcrette, D.A. Randall, L. Rikus, E. Roeckner, J.F. Royer, U. Schlese, D.A. Sheinin, A. Slingo, A.P. Sokolov, K.E. Taylor, W.M. Washington, R.T. Wetherald, I. Yagai and M.-H. Zhang, 1990. Intercomparison and interpretation of climate feedback processes in 19 atmospheric general circulation models. *J. Geophys. Res.*, 95, 16601-16615.
- Heymsfield, A.J., 1977. Precipitation development in stratiform ice clouds: A microphysical and dynamical study. *J. Atmos. Sci.*, 34, 367-381.
- Ramanathan, V, R.D. Cess, E.F. Harrison, P. Minnis, B.R. Barkstrom, E. Ahmad, D. Hartmann, 1989. Cloud-radiative forcing and Climate: Results from the Earth Radiation Budget Experiment. *Science*, 243, 57-63.
- Senior, C.A. and J.F.B. Mitchell, 1991. CO₂ and Climate: The impact of cloud parametrization. This Volume
- Smith, R.N.B., 1990. A scheme for predicting layer cloud and their water content in a general circulation model. *Q. J. R. Meteorol. Soc.*, 116, 435-460.
- Warren, S.G, C.J. Hahn, J. London, R.M. Chervin and R.L Jenne, 1988. Global distribution of total cloud cover and cloud type amounts over land, NCAR Tech.Note NCAR/TN-273+STR, Nat. Cent. for Atmos. Res., Boulder, Colo.
- Warren, S.G, C.J. Hahn, J. London, R.M. Chervin and R.L Jenne, 1988. Global distribution of total cloud cover and cloud type amounts over the ocean, NCAR Tech. Note NCAR/TN-273+STR, Nat. Cent. for Atmos. Res., Boulder, Colo.

Figure Captions

1. Height-latitude cross section of zonally averaged stratiform cloud cover. Contours every 5%, stippled above 15%.
 - (a) HCWH for January
 - (b) CWH for January
 - (c) HCWH for July
 - (d) CWH for July
2. Time-latitude diagrams of zonally averaged total cloud amount. Contours every 1%, Stippled above 50%.
 - (a) HCWH
 - (b) CWH
3. Cloud shortwave forcing. Contours every 25 Wm^{-2} , stippled below 75 Wm^{-2} .
 - (a) HCWH for July
 - (b) CWH for July
 - (c) ERBE data for July 1985
4. Cloud longwave forcing. Contours every 20 Wm^{-2} , stippled above 40 Wm^{-2} .
 - (a) HCWH for July
 - (b) CWH for July
 - (c) ERBE data for July 1985

5. Height-latitude cross section of changes in stratiform cloud amount on doubling CO_2 . Areas of reduction are stippled and the contours are every 1%. The dashed lines are the 0 and -15°C contours from the control simulation.

- (a) HCWH for DJF
- (b) CWH for DJF
- (c) HCWH for JJA
- (d) CWH for JJA

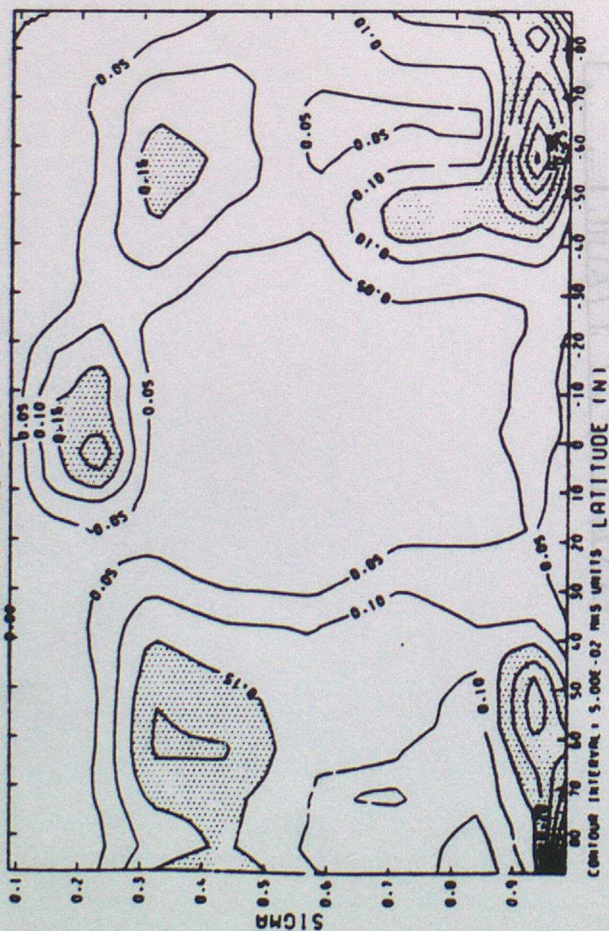
6. Time-Latitude diagrams of the change in total cloud amount on doubling CO_2 . Contours every 1 %, stippled where negative.

- (a) HCWH
- (b) CWH

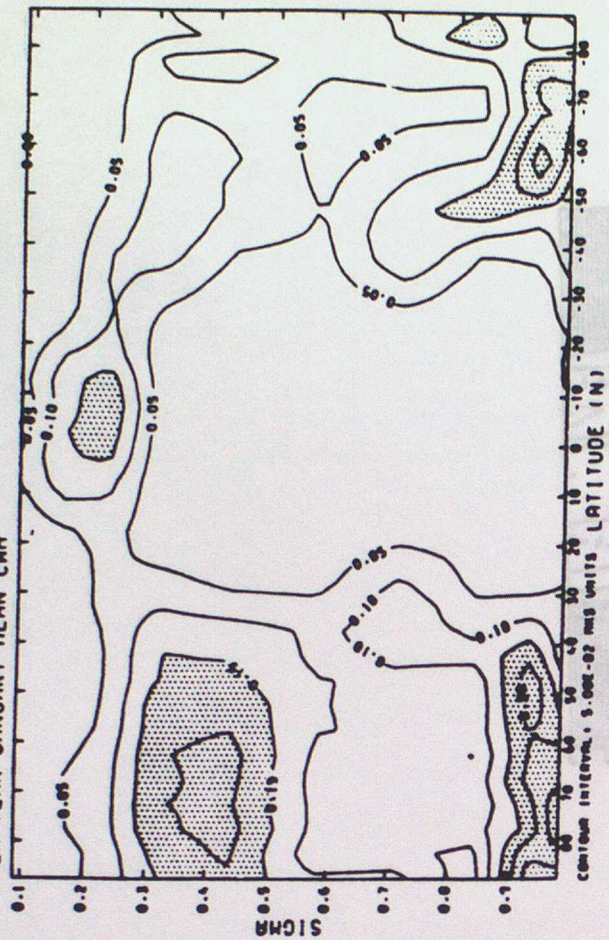
7. Zonally averaged graphs of change in cloud forcing in Wm^{-2} . Dashed line CWH, Solid line HCWH.

- (a) Shortwave Forcing for DJF
- (b) Shortwave Forcing for JJA
- (c) Longwave Forcing for DJF
- (d) Longwave Forcing for JJA

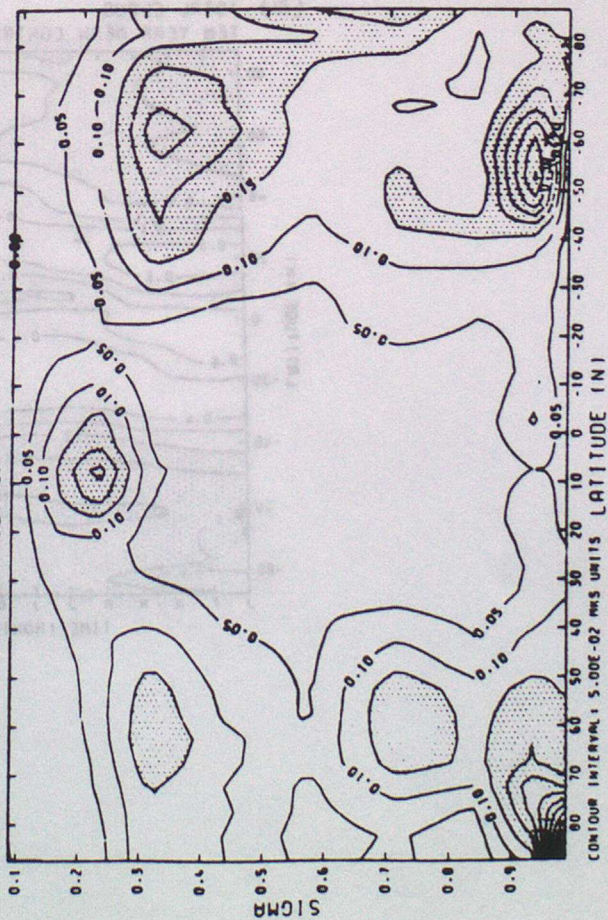
(a) SIGMA-LATITUDE CROSS-SECTION OF ZONAL MEAN LAYER CLOUD COVER
 CONTOURS EVERY 5%. VALUES OVER 15% STIPPLED
 TEN YEAR JANUARY MEAN CONTROL HCMH



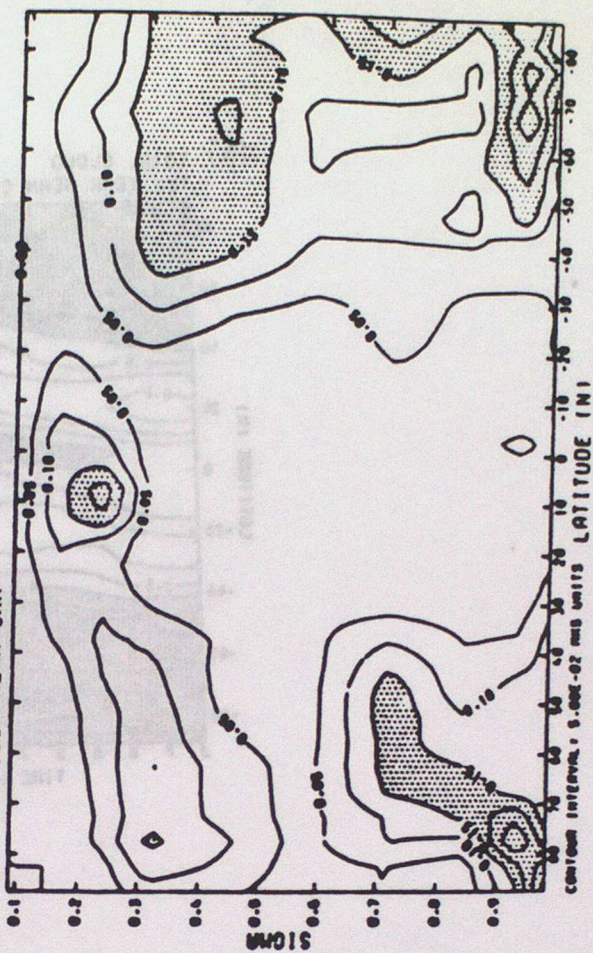
(b) SIGMA-LATITUDE CROSS-SECTION OF ZONAL MEAN LAYER CLOUD COVER
 CONTOURS EVERY 5%. VALUES OVER 15% STIPPLED
 TEN YEAR JANUARY MEAN CMH



(c) SIGMA-LATITUDE CROSS-SECTION OF ZONAL MEAN LAYER CLOUD COVER
 CONTOURS EVERY 5%. VALUES OVER 15% STIPPLED
 TEN YEAR JULY MEAN CONTROL HCMH



(d) SIGMA-LATITUDE CROSS-SECTION OF ZONAL MEAN LAYER CLOUD COVER
 CONTOURS EVERY 5%. VALUES OVER 15% STIPPLED
 TEN YEAR JULY MEAN CMH



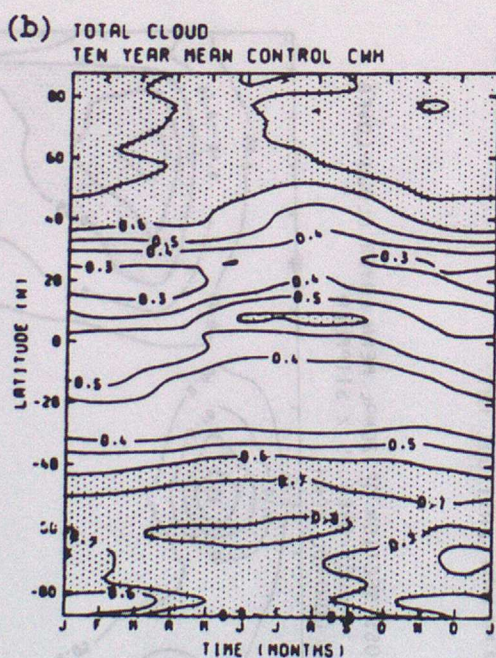


FIGURE 2

- (a) CLOUD SHORTWAVE FORCING
TEN YEAR JULY MEAN CWMH
CONTOURS EVERY 25 WM-2. STIPPLED BELOW -75 WM-2



- (b) CLOUD SHORTWAVE FORCING
TEN YEAR JULY MEAN CWMH
CONTOURS EVERY 25 WM-2. STIPPLED BELOW -75 WM-2



- (c) CLOUD SHORTWAVE FORCING
ERBE DATA FOR JULY 1985
CONTOURS EVERY 25 WM-2. STIPPLED BELOW -75 WM-2

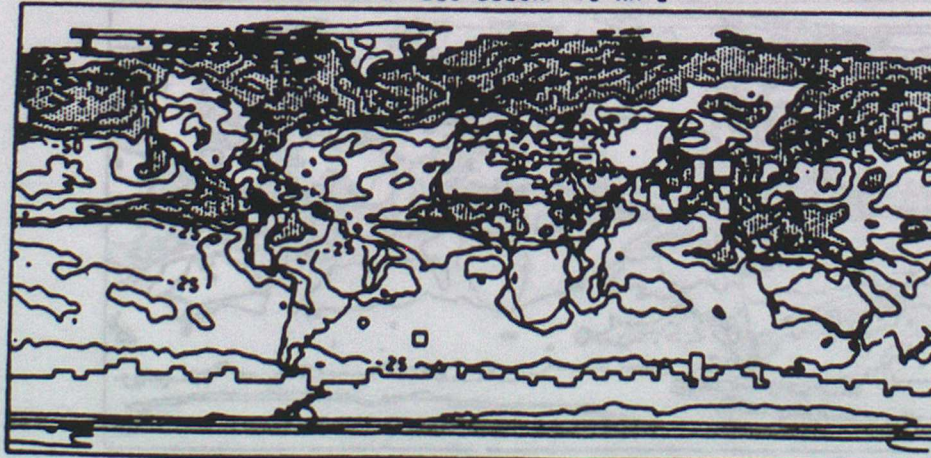
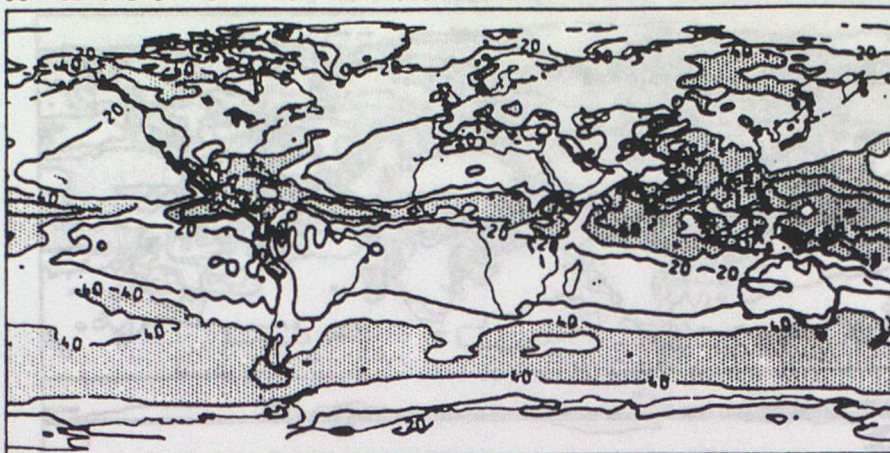
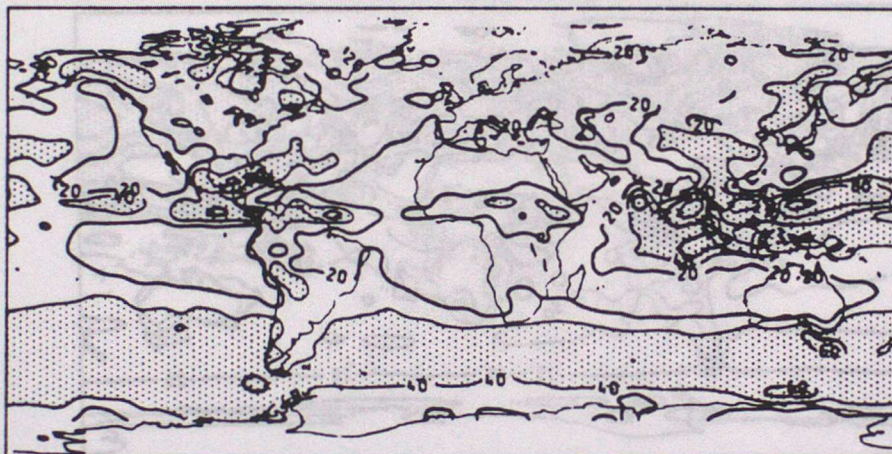


FIGURE 3

- (a) CLOUD LONGWAVE FORCING
TEN YEAR JULY MEAN MCWH
CONTOURS EVERY 20 WM-2. STIPPLED ABOVE 40 WM-2



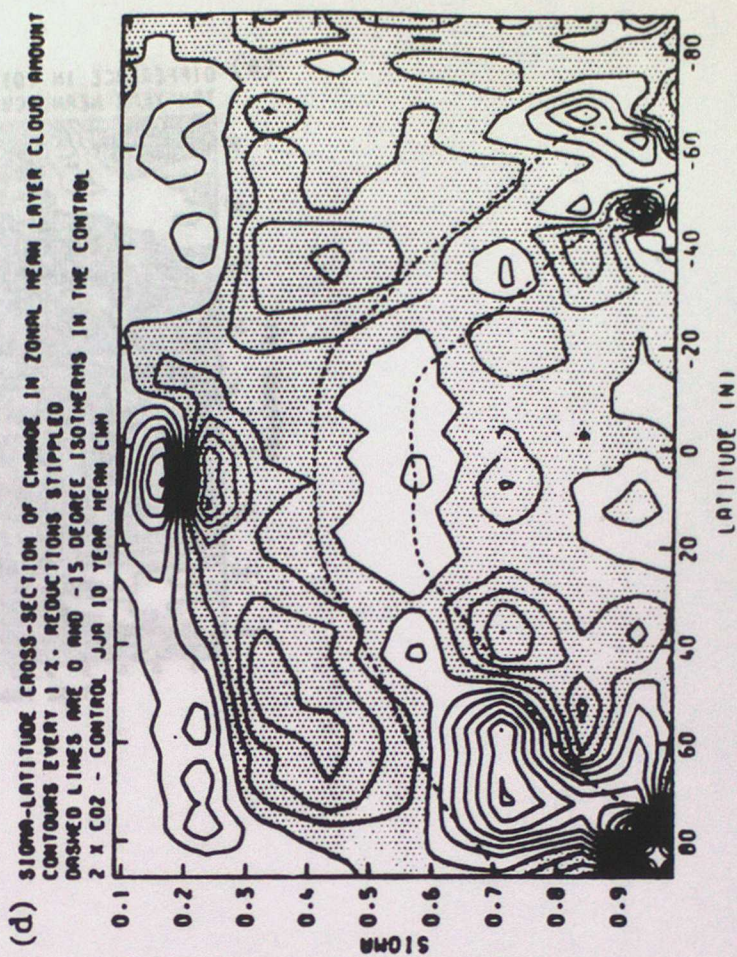
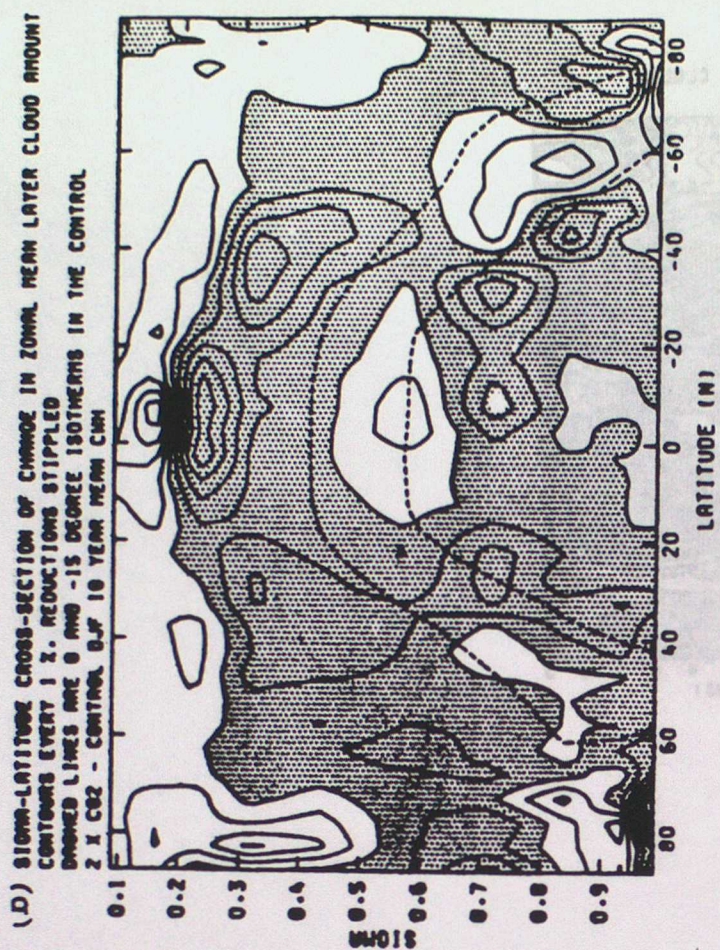
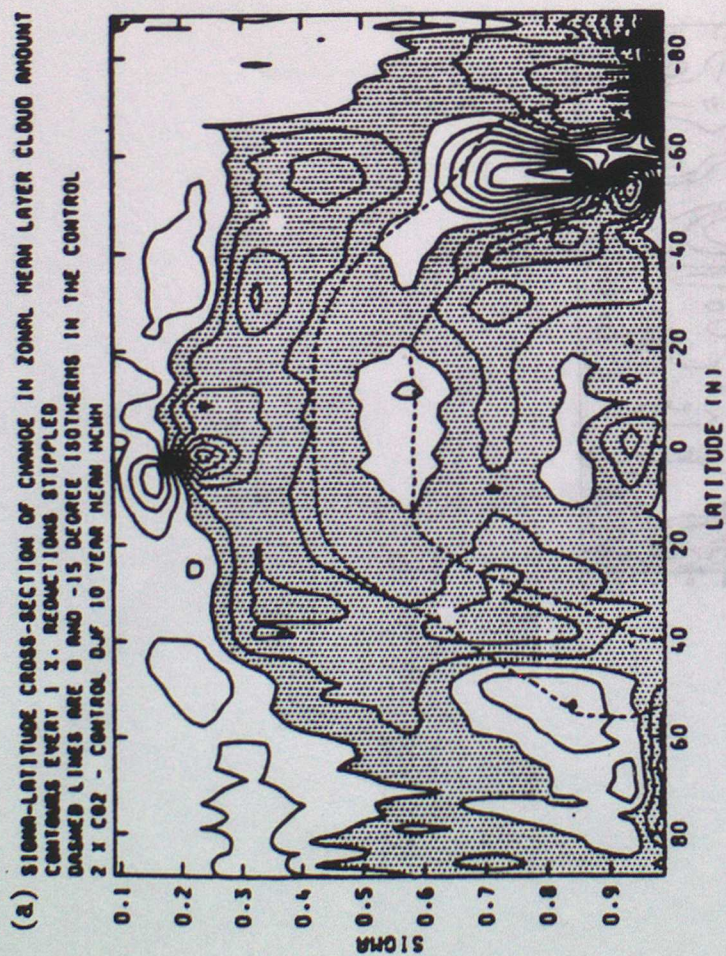
- (b) CLOUD LONGWAVE FORCING
TEN YEAR JULY MEAN CWH
CONTOURS EVERY 20 WM-2. STIPPLED ABOVE 40 WM-2



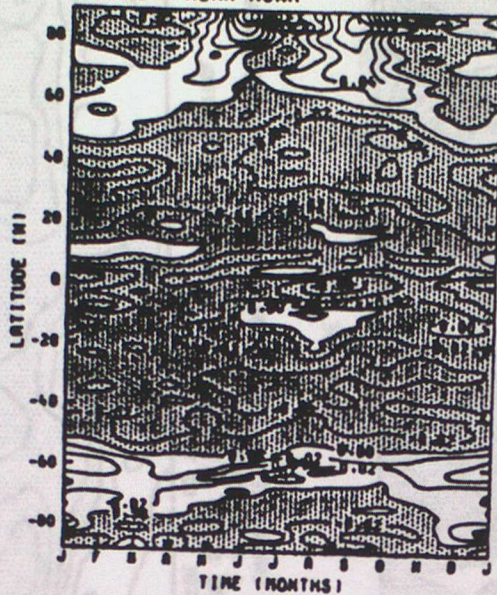
- (c) CLOUD LONGWAVE FORCING
ERBE DATA FOR JULY 1985
CONTOURS EVERY 20 WM-2. STIPPLED ABOVE 40 WM-2



FIGURE 4



(a) DIFFERENCE IN TOTAL CLOUD
TEN YEAR MEAN HCMH



(b) DIFFERENCE IN TOTAL CLOUD
TEN YEAR MEAN CMH

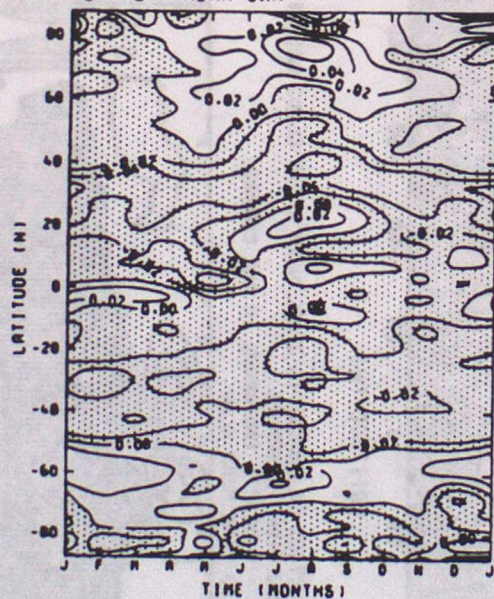
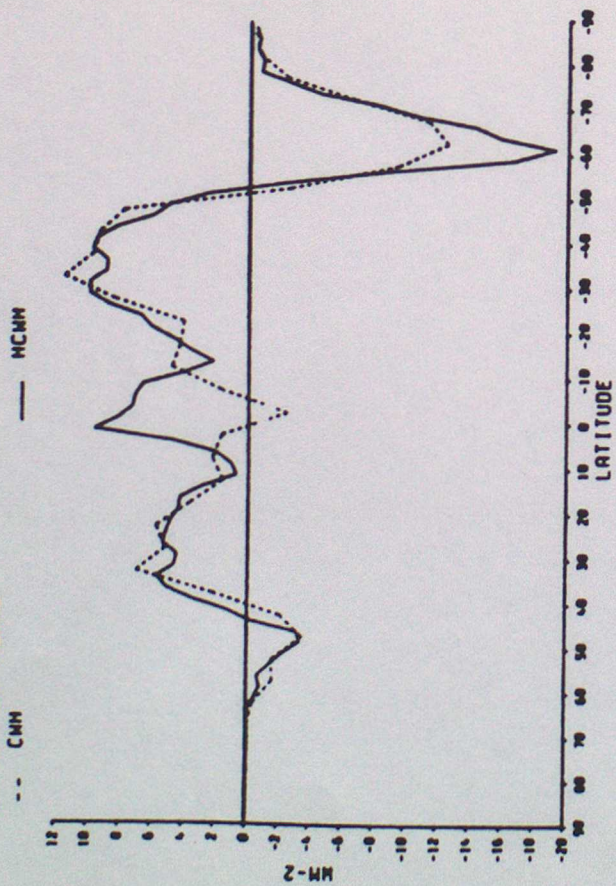
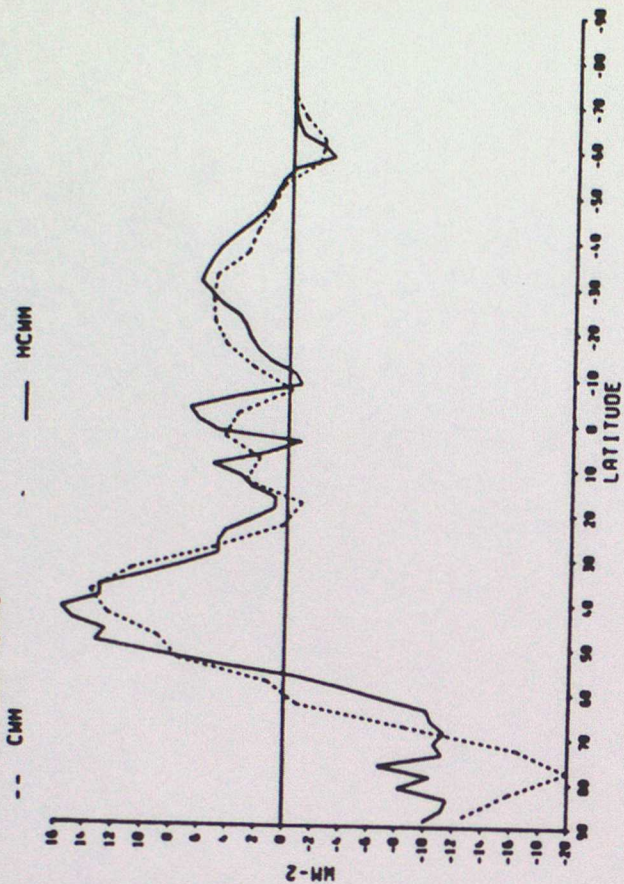


FIGURE 6

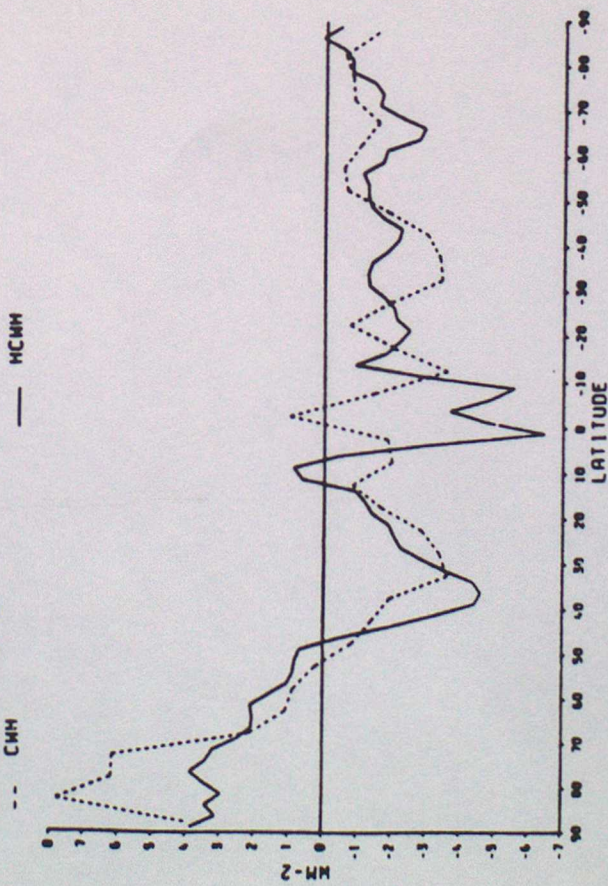
(a) ZONAL MEAN CHANGE IN CLOUD SHORTWAVE FORCING
TEN YEAR DJF MEANS



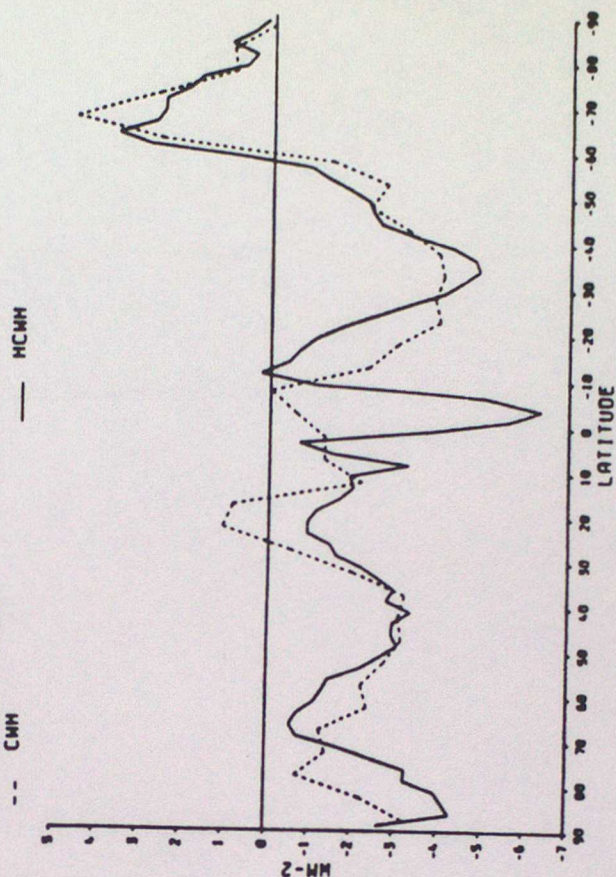
(b) ZONAL MEAN CHANGE IN CLOUD SHORTWAVE FORCING
TEN YEAR JJA MEANS



(c) ZONAL MEAN CHANGE IN CLOUD LONGWAVE FORCING
TEN YEAR DJF MEANS



(d) ZONAL MEAN CHANGE IN CLOUD LONGWAVE FORCING
TEN YEAR JJA MEANS



CLIMATE RESEARCH TECHNICAL NOTES

- | | | |
|---------|----------|---|
| CRTN 1 | Oct 1990 | Estimates of the sensitivity of climate to vegetation changes using the Penman-Monteith equation.
P R Rowntree |
| CRTN 2 | Oct 1990 | An ocean general circulation model of the Indian Ocean for hindcasting studies.
D J Carrington |
| CRTN 3 | Oct 1990 | Simulation of the tropical diurnal cycle in a climate model.
D P Rowell |
| CRTN 4 | Oct 1990 | Low frequency variability of the oceans.
C K Folland, A Colman, D E Parker and A Bevan |
| CRTN 5 | Dec 1990 | A comparison of 11-level General Circulation Model Simulations with observations in the East Sahel.
K Maskell |
| CRTN 6 | Dec 1990 | Climate Change Prediction.
J F B Mitchell and Qing-cun Zeng |
| CRTN 7 | Jan 1991 | Deforestation of Amazonia - modelling the effects of albedo change.
M F Mylne and P R Rowntree |
| CRTN 8 | Jan 1991 | The role of observations in climate prediction and research.
D J Carson |
| CRTN 9 | Mar 1991 | The greenhouse effect and its likely consequences for climate change.
D J Carson |
| CRTN 10 | Apr 1991 | Use of wind stresses from operational N.W.P. models to force an O.G.C.M. of the Indian Ocean.
D J Carrington |
| CRTN 11 | Jun 1991 | A new daily Central England Temperature series, 1772-1991.
D E Parker, T P Legg and C K Folland |
| CRTN 12 | Jul 1991 | Causes and predictability of Sahel rainfall variability.
D P Rowell, C K Folland, K Maskell, J A Owen, M N Ward |
| CRTN 13 | Jul 1991 | Modelling changes in climate due to enhanced CO ₂ , the role of atmospheric dynamics, cloud and moisture.
C A Senior, J F B Mitchell, H Le Treut and Z-X Li |